



HAL
open science

Extended general interfaces: Mori–Tanaka homogenization and average fields

Soheil Firooz, George Chatzigeorgiou, Paul Steinmann, Ali Javili

► **To cite this version:**

Soheil Firooz, George Chatzigeorgiou, Paul Steinmann, Ali Javili. Extended general interfaces: Mori–Tanaka homogenization and average fields. *International Journal of Solids and Structures*, 2022, 254-255, pp.111933. 10.1016/j.ijsolstr.2022.111933 . hal-03766531

HAL Id: hal-03766531

<https://hal.science/hal-03766531>

Submitted on 1 Sep 2022

HAL is a multi-disciplinary open access archive for the deposit and dissemination of scientific research documents, whether they are published or not. The documents may come from teaching and research institutions in France or abroad, or from public or private research centers.

L'archive ouverte pluridisciplinaire **HAL**, est destinée au dépôt et à la diffusion de documents scientifiques de niveau recherche, publiés ou non, émanant des établissements d'enseignement et de recherche français ou étrangers, des laboratoires publics ou privés.

Extended general interfaces: Mori–Tanaka homogenization and average fields

Soheil Firooz^a, George Chatzigeorgiou^b, Paul Steinmann^{a,c}, Ali Javili^{d,*}

^a*Institute of Applied Mechanics, Friedrich-Alexander-Universität Erlangen-Nürnberg, 91058 Erlangen, Germany*

^b*Arts et Metiers Institute of Technology, CNRS, Université de Lorraine, LEM3-UMR 7239, F-57070 Metz, France*

^c*Glasgow Computational Engineering Center, University of Glasgow, Glasgow G12 8QQ, United Kingdom*

^d*Department of Mechanical Engineering, Bilkent University, 06800 Ankara, Turkey*

Abstract

A well-established methodology to capture interphases in heterogeneous materials is to replace them by a zero-thickness interface model. Commonly accepted interface models intuitively assume that to satisfy the angular momentum balance, interfaces must coincide with the mid-layer of their corresponding interphases. Recently, via adopting weighted averages, an extended general interface model has been developed that allows for arbitrary interface positions while fulfilling the angular momentum balance. This manuscript incorporates this novel interface model into the Mori–Tanaka method within the framework of homogenization. Analytical solutions are developed to determine effective properties as well as average local fields for fiber-reinforced and particle-reinforced composites. Computational simulations using the finite element method (FEM) are carried out to compare with the analytical solutions. Through a set of numerical examples, the significance of the interface position on the overall response of heterogeneous materials is highlighted. Our extended framework clarifies various ambiguous observations originating from the trivial assumption of restricting the interface position to the mid-plane. One advantage of the current interface model is that it covers both the elastic and cohesive interface models at its limits and therefore the analytical solutions are widely applicable regardless of the interface type.

Keywords: Mori–Tanaka Homogenization, Composites, Extended general interface, Size effects

1. Introduction

In almost all heterogeneous materials, different factors such as manufacturing imprecisions, poor chemical adherence, coating or damage, give rise to the formation of imperfections between the constituents. As a result, when analyzing such media, an intermediate *interphase* region between the constituents shall be introduced to account for the imperfections. Interphases significantly influence the overall behavior of heterogeneous materials since they play a crucial

*Corresponding author.

Email address: ajavili@bilkent.edu.tr (Ali Javili)

role in force transfer between the constituents. Among the early works on the topic, the concept of an interphase in composites was introduced by Papanicolaou et al. [1, 2] where they investigated the thermomechanical properties of an interphase layer in various composites via comparing the experimental data against the results obtained from the rule of mixture.

1.1. Interphase models

The primary idea to study interphases in heterogeneous materials was to consider them as a homogeneous independent phase between the constituents [3–5]. A modified Mori–Tanaka method was proposed in [6, 7] where the elastic fields within the constituents of composites with coated fibers and particles were determined. Benveniste et al. [8, 9] employed the Mori–Tanaka method to obtain the effective moduli and the local stresses in the constituents of a composite with coated fibers. Duan et al. [10] developed a methodology to determine the stress and strain fields within arbitrarily oriented spheroidal inhomogeneities surrounded by interphases within an infinite heterogeneous medium. Further studies on the overall response of composites embedding homogeneous interphases can be found in [11–15]. A more generic model to study interphases is to assume the interphase to possess spatially variable properties. Examples of such interphases include inhomogeneous interphases, graded interphases, or multilayered interphases. A pioneering work on these interphase types was carried out on a fiber-reinforced polymer composite by Papanicolaou et al. [16] where they investigated the adhesion efficiency between the matrix and fiber in the presence of an inhomogeneous interphase. Inhomogeneous continuum modelling of functionally graded interphases has been developed by Ostaja-Starzewski et al. [17] where they accounted for local anisotropy and randomness of the constitutive laws. Theocaris et al. [18, 19] proposed a multi-cylinder model to determine the overall properties of fiber composites with variable interphase properties. Dasgupta and Bhandarkar [20] utilized the generalized self-consistent method and the Mori–Tanaka method to determine thermo-mechanical properties of composites with multiply coated cylindrical fibers, see [21] for a similar study on ellipsoidal fibers. Further studies on the overall response of composites embedding inhomogeneous or graded interphases include [22–28].

1.2. Interface models

A well-established methodology to capture finite-thickness interphases is to replace them by a zero-thickness interface model characterized by certain field jumps. Within the framework of elasticity, the pertinent interfacial field jumps are traction and displacement jumps. This idea was originally proposed by Sanchez-Palencia and Pham-Huy [29, 30] and later extended by Benveniste [31, 32], Karlbring [33, 34], Hashin [35–37] and Bövik [38]. There exist two main approaches to determine the correlation between the interphase and interface properties and jump conditions: the *asymptotic approach* and the *phenomenological approach*. This contribution mainly focuses on the latter.

The asymptotic approach is mainly based on exploiting the formal asymptotic expansion via Taylor series and imposing it on the displacement and traction fields within the finite-thickness interphase [32, 39–42]. The resulting expressions are then truncated, in many cases to first order with respect to the interphase thickness. Afterwards, via the transmission conditions at the interphase boundaries, a series of jump conditions at the interface are obtained in terms of the primal and secondary fields defined in the bulk neighbors [43–46]. Since the interfacial conditions are determined based on the interphase thickness-dependent quantities, no further assumptions are required to define the tangential or orthogonal behavior of the interface. As a result, the displacement or traction jump across the interface become a function of the displacement and traction fields in the bulk. While the majority of the contributions on asymptotic approach have studied flat interphases with first order expansions, only few took the interphase curvature into account and considered higher order jump conditions [47–50]. The phenomenological approach assumes the interface as an independent energetic lower dimension medium. Therefore, the interface possesses its own elastic parameters representing its tangential and orthogonal behavior. Among the well-established interface models based on the phenomenological approach, the elastic (stress-type or membrane type) interface model, the cohesive (spring-type) interface model and the general interface model are the most widely adopted ones. In the *elastic interface model* [51–53] the displacement remains continuous across the interface while the traction field experiences a jump due to the interface elasticity. In the *cohesive interface model* [54–56] a displacement jump occurs across the interface while the traction field remains continuous. In the *general interface model* [57, 58] both displacement and traction jumps across the interface are admissible. Note, the elastic and cohesive interface models can be interpreted as two limit cases of the general interface model. Table 1 gathers a selection of relevant contributions on interface models based on the phenomenological approach within the scope of mechanical problems.

Remark on the physical meaning of energetic surfaces and interfaces: Aside from capturing the interphase behavior, surfaces and interfaces play a crucial role in determining the overall behavior of materials at small scales. Several nano-structured materials exhibit qualitatively different physical, mechanical and chemical behavior due to their large area-to-volume ratio. For instance, it has been shown experimentally that the electric performance of a particle can be improved with surface modification at nano-scales [59], or it is observed that the melting temperature of particles is suppressed at nano-scales [60]. Such extraordinary behavior rendered by materials at small scales is rationalized by invoking the concept of surface/interface energy. Within the framework of elasticity, there exist two common strategies to formulate the surface/interface energy. First, to assume that the interface energy is a function of the interface strain/stress which gave rise to the development of the elastic interface model. Second, to assume that the interface energy is a function of the deformation jump across the interface which gave rise to the development of the cohesive interface model. While the elastic interface is a well-established model to account for surface tension, the

cohesive interface model is commonly adopted to tackle problems involving discontinuities, cracks or dislocations. The term “general” in the general interface model indicates that the interfacial energy depends on both deformation jump across the interface and interface strain/stress. For complex problems involving both interface elasticity and interfacial deformation discontinuity, the general interface has proven to be an accurate model. Thus, both the cohesive interface model and elastic interface model can be understood as two limits of the general interface model.

1.3. Significance of the interface position

As mentioned earlier, we substitute a non-zero thickness interphase with an interface of zero thickness which could be located at any positions throughout the thickness of the associated interphase. The interface could either coincide with the mid-plane of the corresponding interphase or be closer to any of the bulk constituents. While there exist numerous contributions in the literature investigating interface effects on the overall behavior of materials, only very few studies are available elaborating on interface position and its role on the material response. This, perhaps, stems from the fact that for the two most widely adopted interface models, cohesive and elastic interface models, the interface position does not play any role in determining the interfacial behavior. Classical *cohesive interface models* [56, 96, 97, 101–103] commonly adopt the standard traction-separation law in which the displacement jump across the interface determines the average cohesive tractions. For the *elastic interface model*, the interface is geometrically

Table 1: Selection of relevant contributions on interface models within the scope of mechanical problems.

cohesive interface	Barenblatt [55, 61], Dugdale [54], Mal and Bose [62], Theocaris et al. [63], Benveniste [31], Benveniste and Miloh [64], Aboudi [65, 66], Hashin [35, 36, 67, 68], Lipton and Vernescu [69] Gao [70], Zhao and Weng [71], Duan et al. [72–74], Ru [75, 76], Mura, Jasiuk and Tsuchida [77, 78], Zhong and Meguid [79], Huang et al. [80], Lee et al. [81], Benveniste and Aboudi [82], Jasiuk et al. [83, 84], Königsberger et al. [85, 86], He and Jiang [87], Qu et al. [88], He and Liu [89], Needleman [56], Xu and Needleman [90], Bisegna and Luciano [91], Wriggers et al. [92], Achenbach and Zhu [93, 94], Zhu et al. [95], Ortiz and Pandolfi [96], Gasser and Holzapfel [97], Mergheim and Steinmann [98], Hansbo and Hansbo [99, 100], van den Bosch et al. [101–103], Vossen et al. [104], Ottosen et al. [105, 106], Heitbreder et al. [107, 108], Ghosh et al. [109], Wells and Sluys [110], Guo et al. [111], Fagerström and Larsson [112], Ghosh et al. [113], Paggi and Wriggers [114, 115], Rezaei et al. [116, 117], Bayat et al. [118]
elastic interface	Gurtin and Murdoch [51, 52, 119], Gao et al. [120, 121], Caillerie [122], Benveniste and Miloh [32], Rubin and Benveniste [123], Rizzoni et al. [43], Fried and Gurtin [124], Dingreville and Qu [125, 126], Sharma et al. [127, 128], Yang [129], Sun et al. [130], Duan et al. [73, 74, 131–133], Huang and Wang [134], Monteiro et al. [135], Huang and Sun [136], He [137], Le-Quang and He [138–140], Mogilevskaya et al. [141–144], Kushch et al. [145–147], Muskhelishvili [148], Kushch and Sevostianov [149], Benveniste and Miloh [150], Gao et al. [121], Monchiet and Bonnet [151], Kushch [152] Sharma and Wheeler [153], Chen and Dvorak [154], Chen et al. [155], Fischer and Svoboda [156], Javili [157], Javili et al. [158] Nazarenko et al. [159], Chatzigeorgiou et al. [160–162], Steigmann and Ogden [53, 163], Zemlyanova and Mogilevskaya [164, 165], Han et al. [166], Yvonnet et al. [167], Javili et al. [168–170] Koutsawa et al. [171]
general interface	Hashin [57], Benveniste [58, 172, 173], Bövik [38], Monchiet and Bonnet [174], Gu and He [175], Gu et al. [176, 177], Serpilli et al. [46], Wang and Ye [178], Xu et al. [179], Firooz et al. [180, 181], Chatzigeorgiou et al. [182], Gu et al. [183], Javili et al. [184, 185], Kaessmair et al. [186], Javili [187], Saeb et al. [188–190], Pham et al. [191], Firooz and Javili [192], Firooz [193]

coherent by definition and therefore the interface position does not play a role in the interfacial behavior. For the *general interface model* though, due to admissible interface opening and interface elasticity, the interface position enters the governing equations and plays a significant role in the overall interfacial behavior. Commonly accepted general interface models [57, 58, 108, 183, 184, 194, 195] intuitively assume that the interface is located at the mid-plane of its associated interphase. This simplifying assumption has been essentially made to trivially satisfy the angular momentum balance on the interface [104–107]. Mergheim and Steinmann [98] and Hansbo and Hansbo [100] carried out further investigations on the interface position when dealing with weak discontinuities. Recently, Saeb et al. [196] revisited this issue via employing weighted averages and demonstrated that *the interface is allowed to take any arbitrary position between its bulk neighbors and yet satisfying the angular momentum balance*. They demonstrated that the trivial assumption of restricting the interface position to the mid-layer is only justifiable when capturing the behavior of uniform interphases. More complex interphase structures such as graded or inhomogeneous interphases can be accurately captured only if the interface is situated at a position other than the mid-plane, resulting in the notion of an *extended general interface model*, see Fig. 1. Firooz et al. [197] exploited this methodology within the framework of homogenization and developed analytical expressions for the overall behavior of fiber-reinforced and particle-reinforced composites using the composite cylinder assemblage (CCA), composite sphere assemblage (CSA) and the generalized self-consistent method (GSCM). This contribution completes [197] in that it introduces the Mori–Tanaka homogenization to study composites embedding extended general interfaces. Furthermore, in addition to numerical solutions using FEM, we compare our findings with those in [197].

Remark on the mathematical interpretation of interface position: The position of the interface, holds a *mathematical* interpretation rather than physical. Interface position indeed determines the contribution of its bulk neighbors in determining the balance laws and the interface conditions. In other words, unequal contributions from the bulk neighbors become possible if the general interface model is furnished with an additional feature, called interface position. For instance, Saeb et al. [196] demonstrated that when using the general interface model to replace a graded interphase in a heterogeneous medium, the interface shall be located at the stiffer part of the interphase so as to capture interphase effects more accurately.

1.4. Objectives and key features

The main objective of this manuscript is to propose a modified Mori–Tanaka homogenization approach to account for extended general interfaces with an arbitrary interface position for both fiber-reinforced and particle-reinforced composites. In order to establish a stand-alone contribution, a brief overview is provided first to introduce the notation, elaborating the kinematics of the problem, balance equations, material modeling, micro-to-macro transition and step-by-step Mori–Tanaka homogenization. Our developed methodology not only obtains the overall elastic moduli of

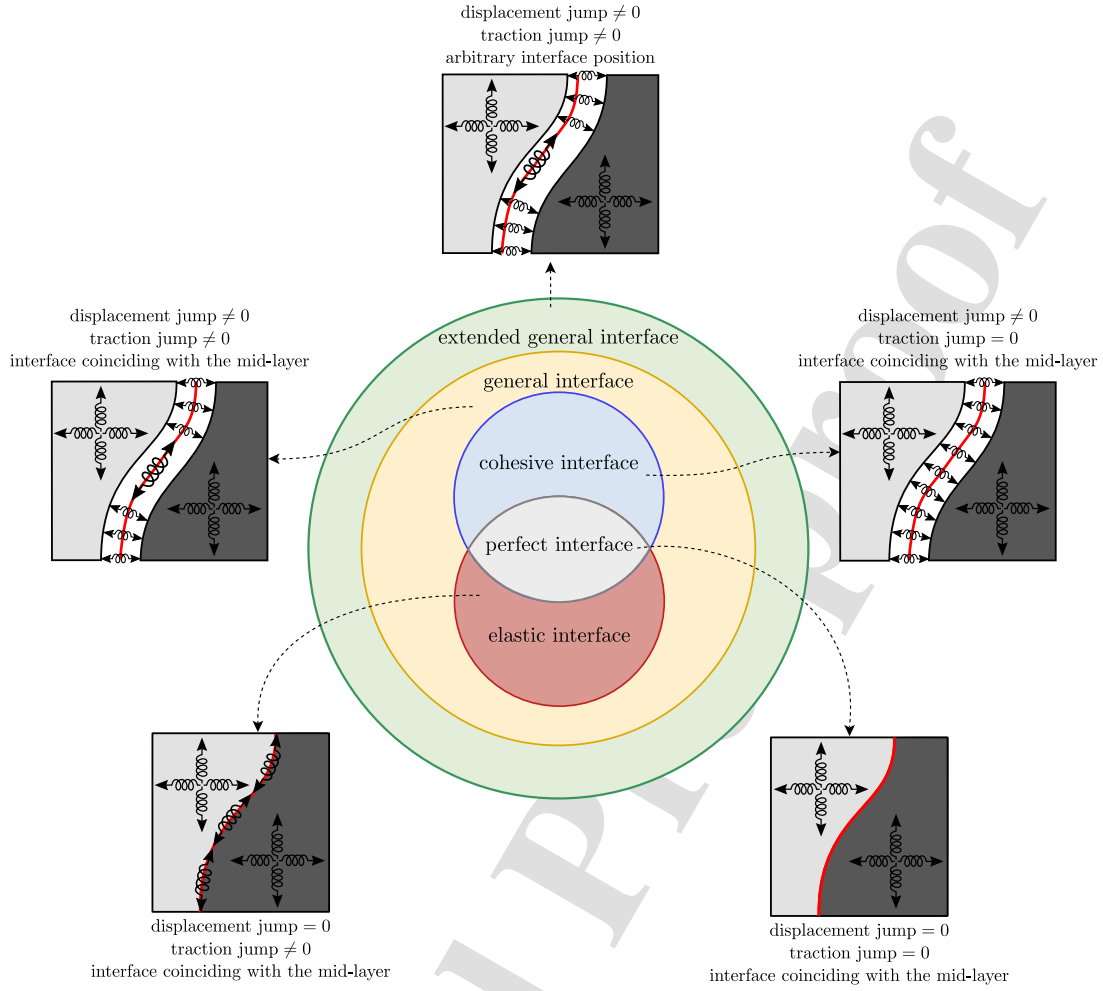


Figure 1: Classification of interface models based on the continuity of the displacement and traction fields and interface position. All the classical interface models assume that the interface coincides with the mid-layer whereas the extended general interface model accommodates arbitrary interface positions.

composites, but also determines the concentration tensors in each phase of the medium. The primary advantage of the concentration tensors is that they enable determination of the average of stress or strain fields within the constituents of the medium, hence, furnishing better insights into the material micro-structural response. Through a set of examples, the influence of different interface properties on the overall response of heterogeneous materials will be examined and the notion of *smaller-stronger* and *smaller-weaker* responses will be critically revisited when the extended general interface model is accounted for.

Remark on accounting for damage and softening: Our proposed *extended general interface model* recovers anything that a *cohesive interface model* or an *elastic interface model* can capture, but it can also do a lot more than that, See Fig. 3. The extended general interface model here can, in principle, account for damage mechanism via

introducing more complex traction-separation laws through a different interface constitutive model. More precisely, the interface out-of-plane response, commonly referred to as traction-separation law, can be nonlinear and it may as well include damage or softening. In the extended general interface model, since the interface has both in-plane and out-of-plane response, accounting for interface damage requires further elaboration to distinguish between orthogonal damage and tangential damage on the interface. Saeb et al. [190] carried out a comprehensive study on modeling of damage using the general interface model. However, in this contribution, we have limited the discussion to the kinematics and kinetics of the problem within the framework of linear elasticity as well as the homogenization using the Mori–Tanaka method. Leaving out “damage” in the discussion here is not a shortcoming of the model but it is rather an assumption to obtain analytical expressions. The interface model itself is generic enough to allow for debonding, softening and damage.

1.5. Notations and definitions

Throughout this manuscript, macroscopic quantities are distinguished from microscopic quantities by a left superscript “M”. For instance, $^M\{\bullet\}$ is a macroscopic quantity with $\{\bullet\}$ being its microscopic counterpart. Interface related quantities are distinguished from the bulk quantities by a bar placed on top them. That is, $\{\bar{\bullet}\}$ denotes an interface quantity with its bulk counterpart $\{\bullet\}$. The non-standard tensor products between two arbitrary second-order tensors \mathbf{A} and \mathbf{B} are defined as $[\bar{\mathbf{A}}\bar{\otimes}\mathbf{B}]_{ijkl} = [A]_{ik}[B]_{jl}$ and $[\mathbf{A}\bar{\otimes}\mathbf{B}]_{ijkl} = [A]_{il}[B]_{jk}$.

1.6. Organization of the manuscript

The remainder of this manuscript is organized as follows. Section 2 presents the governing equations for a continuum body embedding extended general interfaces. This is then followed by establishing the extended Mori–Tanaka method in Section 3 where analytical solutions for the effective properties of composites are obtained. Through a series of numerical examples in Section 5, the effects of the interface position on the overall behavior of composites are examined in detail. Section 6 summarizes this work and provides further outlooks.

2. Governing equations

This section elaborates on the governing equations of a continuum body embedding an extended general interface within the framework of linear elasticity. Here the position of the interface is no longer restricted to the mid-layer. Further details on the derivation of the equations are available in [196, 197]. The analysis carried out in this manuscript is based on the assumption that there exist a fictitious graded interphase whose response is fully captured via our proposed extended general interface model. Since the main objective of our contribution is to extend the Mori–Tanaka homogenization scheme to account for extended general interfaces with variable interface positions and elaborate the

pertinent kinetics and kinematics, we start our analysis from one step forward and do not detail on how interphase parameters and interface conditions/parameters are related. Undoubtedly, a comprehensive study investigating energy equivalence between interphase and interface aiming to obtain one-to-one correspondence between interphase and interface material parameters seems desirable and shall be considered as a separate contribution. See Saeb et al. [196]

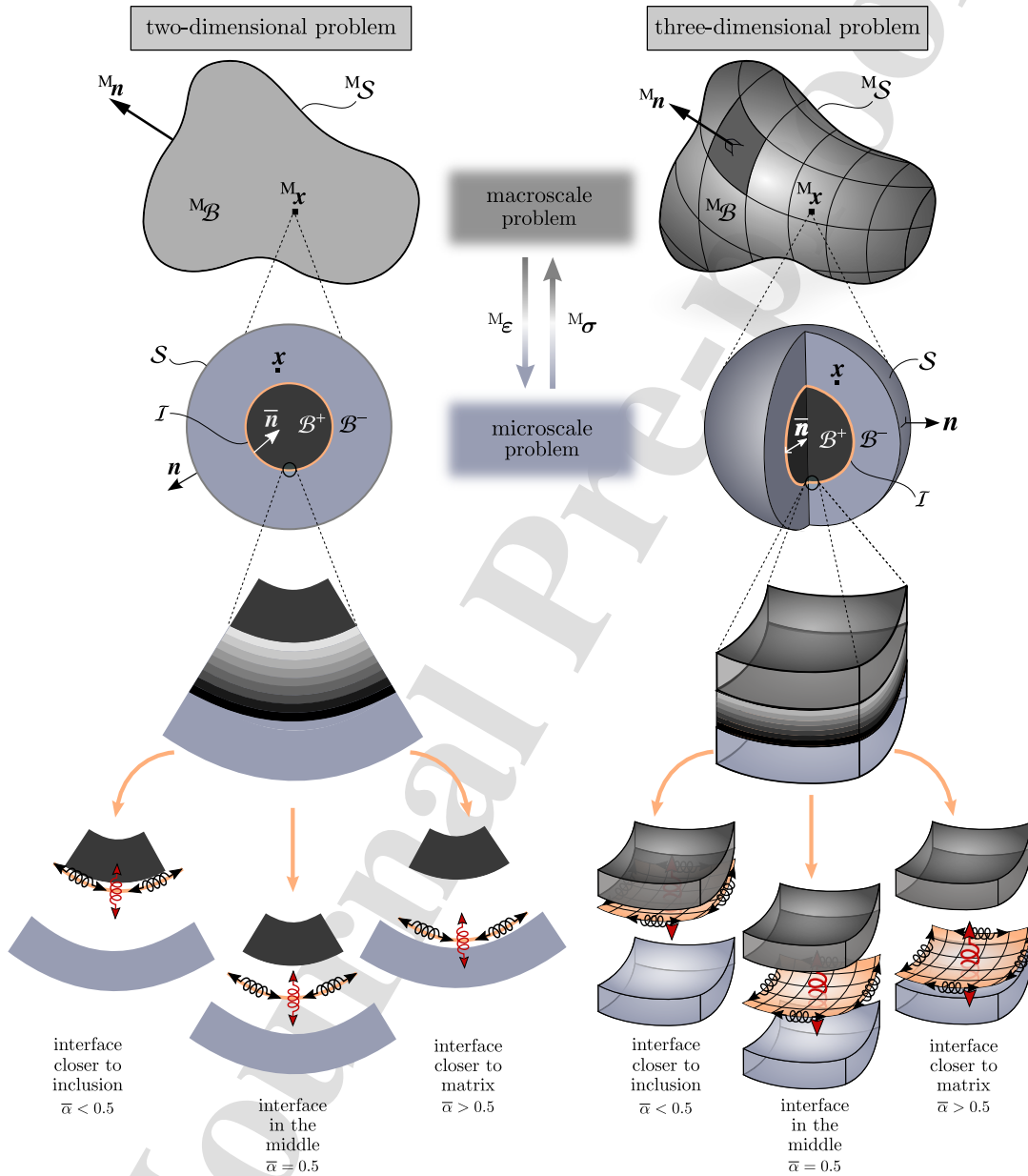


Figure 2: Problem definition for continuum bodies embedding an extended general interface within the homogenization framework. The macrostructures with their underlying RVE are shown for both two- and three-dimensional settings. A finite-thickness interphase is replaced with a zero-thickness extended general interface model with arbitrary interface position.

for a similar computational study at large deformations.

Figure 2 provides an illustrative definition of our problem in both two and three dimensional settings. Each of the two continuum bodies on top is assumed to occupy a configuration ${}^M\mathcal{B}$ representing a heterogeneous material at the macro-scale. At the micro-scale, the corresponding configurations are denoted as \mathcal{B} which indeed serve as the representative volume elements (RVE) that simply consist of an inhomogeneity surrounded by a matrix, see [195, 198–200]. In this contribution, to capture isotropy, the RVEs are considered to be circular for the two-dimensional setting and spherical for the three-dimensional setting. The interphase between the constituents is replaced by an extended general interface model. The extended general interface model is identified by three key features. First, it allows for interface opening associated with a displacement jump across the interface. Second, the interface displays elastic behavior which gives rise to a stress jump across the interface. Third, the interface can sit on any arbitrary layer between the constituents enabling unequal contributions from the neighbors to the interfacial response. As shown in Fig. 2, the interface \mathcal{I} splits the micro-structures into two disjoint subdomains, denoted as \mathcal{B}^+ and \mathcal{B}^- , corresponding to the plus and minus sides of the interface, respectively. The interface sides \mathcal{B}^+ and \mathcal{B}^- are allowed to detach/distance from each other. The unit vectors \mathbf{n} and $\bar{\mathbf{n}}$ signify the normals to the external boundary and the interface, respectively. The jump operator and the classical average operator on the interface read

$$\text{jump operator: } \llbracket \{\bullet\} \rrbracket = \{\bullet\}^+ - \{\bullet\}^-, \quad \text{average operator: } \{\{\bullet\}\} = \frac{1}{2}[\{\bullet\}^+ + \{\bullet\}^-], \quad (1)$$

with the superscripts indicating the interface sides. In this contribution, following the framework established in [196, 197], we employ an extended approach which employs the *weighted average operator* and *complementary weighted average operator* enabling unequal contributions from the plus and minus side of the interface as

$$\begin{aligned} \text{weighted average operator: } & \{\{\bullet\}\}_{\bar{\alpha}} = \bar{\alpha} \{\bullet\}^+ + [1 - \bar{\alpha}] \{\bullet\}^-, & \text{with } 0 \leq \bar{\alpha} \leq 1. & (2) \\ \text{complementary weighted average operator: } & \{\{\bullet\}\}_{[1-\bar{\alpha}]} = [1 - \bar{\alpha}] \{\bullet\}^+ + \bar{\alpha} \{\bullet\}^-, & & \end{aligned}$$

The parameter $\bar{\alpha}$ defines the interface position which plays a crucial role in determining the kinematics of the extended general interface model. As shown in Fig. 2, when $\bar{\alpha} < 0.5$ the interface is closer to the inhomogeneity, when $\bar{\alpha} > 0.5$ the interface is closer to the matrix and when $\bar{\alpha} = 0.5$ the interface coincides with the mid-plane. Note, $\bar{\alpha} = 0.5$ recovers the classical definition of the general interface model. Let \mathbf{u}^+ and \mathbf{u}^- define the displacement fields in the plus and minus sides of the interface, respectively. Exploiting the weighted average operator defined in Eq. (2), one

can define a generic form for the interface displacement $\bar{\mathbf{u}}$ which reads

$$\bar{\mathbf{u}} := \llbracket \mathbf{u} \rrbracket_{\bar{\alpha}} = \bar{\alpha} \mathbf{u}^+ + [1 - \bar{\alpha}] \mathbf{u}^-. \quad (3)$$

The strain fields in the bulk and on the interface accordingly read

$$\boldsymbol{\varepsilon} = \frac{1}{2} [\mathbf{I} \cdot \text{Grad} \mathbf{u} + [\text{Grad} \mathbf{u}]^T \cdot \mathbf{I}] \quad \text{in } \mathcal{B}, \quad \bar{\boldsymbol{\varepsilon}} = \frac{1}{2} [\bar{\mathbf{I}} \cdot \overline{\text{Grad}} \bar{\mathbf{u}} + [\overline{\text{Grad}} \bar{\mathbf{u}}]^T \cdot \bar{\mathbf{I}}] \quad \text{on } \mathcal{I}, \quad (4)$$

where \mathbf{I} is the second-order identity tensor and $\bar{\mathbf{I}} := \mathbf{I} - \bar{\mathbf{n}} \otimes \bar{\mathbf{n}}$. The interface operators $\overline{\text{Grad}} \{\bullet\}$ and $\overline{\text{Div}} \{\bullet\}$ are defined as

$$\overline{\text{Grad}} \{\bullet\} := \text{Grad} \{\bullet\} \cdot \bar{\mathbf{I}} \quad \text{and} \quad \overline{\text{Div}} \{\bullet\} := \text{Grad} \{\bullet\} : \bar{\mathbf{I}}. \quad (5)$$

Equipped with the kinematics definition of the problem, we proceed with the balance equations. Here, we limit our discussion to the micro-scale problem, thus body forces vanish from the governing equations. The linear momentum balance in the bulk and on the interface read [197]

$$\begin{cases} \text{Div} \boldsymbol{\sigma} = \mathbf{0} & \text{in } \mathcal{B}, \\ \mathbf{t} = \boldsymbol{\sigma} \cdot \mathbf{n} & \text{on } \partial \mathcal{B}, \end{cases} \quad \begin{cases} \overline{\text{Div}} \bar{\boldsymbol{\sigma}} + \llbracket \boldsymbol{\sigma} \rrbracket \cdot \bar{\mathbf{n}} = \mathbf{0} & \text{along } \mathcal{I}, \\ \bar{\mathbf{t}} = \llbracket \boldsymbol{\sigma} \rrbracket_{1-\bar{\alpha}} \cdot \bar{\mathbf{n}} = [1 - \bar{\alpha}] [\boldsymbol{\sigma}^+ \cdot \bar{\mathbf{n}}] + \bar{\alpha} [\boldsymbol{\sigma}^- \cdot \bar{\mathbf{n}}] & \text{across } \mathcal{I}, \end{cases} \quad (6)$$

with $\boldsymbol{\sigma}$ and $\bar{\boldsymbol{\sigma}}$ being the bulk and interface stresses and \mathbf{t} and $\bar{\mathbf{t}}$ being the bulk and interface tractions, respectively. The angular momentum balance equations can simply be obtained by writing the moments acting on the body with respect to an arbitrary reference point. For the bulk and the interface, one can write the angular momentum balance equation as [197]

$$\mathbf{e} : \boldsymbol{\sigma}^T = \mathbf{0} \quad \text{in } \mathcal{B}, \quad \llbracket \mathbf{x} \rrbracket \times \underbrace{\llbracket \boldsymbol{\sigma} \rrbracket_{1-\bar{\alpha}} \cdot \bar{\mathbf{n}}}_{\bar{\mathbf{t}}} + \mathbf{e} : \bar{\boldsymbol{\sigma}}^T + [\llbracket \mathbf{x} \rrbracket_{\bar{\alpha}} - \bar{\mathbf{x}}] \times \llbracket \boldsymbol{\sigma} \rrbracket \cdot \bar{\mathbf{n}} = \mathbf{0} \quad \text{on } \mathcal{I}, \quad (7)$$

with \mathbf{e} being the Levi–Civita permutation tensor and \mathbf{x} and $\bar{\mathbf{x}}$ being the bulk and interface position vectors, respectively. The bulk angular momentum balance is simply satisfied due to the symmetry of the Cauchy stress $\boldsymbol{\sigma} = \boldsymbol{\sigma}^T$. However, fulfilling the interface angular momentum balance is a more intricate task and can be sufficiently satisfied via imposing the three conditions $\llbracket \mathbf{x} \rrbracket \parallel \bar{\mathbf{t}}$, $\bar{\boldsymbol{\sigma}}^T = \bar{\boldsymbol{\sigma}}$ and $\bar{\mathbf{x}} = \llbracket \mathbf{x} \rrbracket_{\bar{\alpha}}$. The first two conditions can be guaranteed via proper definition of interface constitutive laws without any restriction on the interface position. However, the third condition $\bar{\mathbf{x}} = \llbracket \mathbf{x} \rrbracket_{\bar{\alpha}}$ is satisfied if the interface position is restricted by the weighted average of its two sides [196]. *Clearly, this definition of*

the interface position furnishes the interface with a new degree of freedom which significantly enhances the versatility of the extended general interface model towards capturing graded interphases.

To obtain the constitutive material behavior of the bulk and the interface, we utilize a variational approach based on the existence of a free energy density. The free energy density of the body contains the contribution from the bulk free energy density ψ and the interface free energy density $\bar{\psi}$ which read

$$\psi = \frac{1}{2} \boldsymbol{\varepsilon} : \mathbb{C} : \boldsymbol{\varepsilon} \quad \text{in } \mathcal{B}, \quad \bar{\psi} = \frac{1}{2} \bar{\boldsymbol{\varepsilon}} : \bar{\mathbb{C}} : \bar{\boldsymbol{\varepsilon}} + \frac{1}{2} \bar{\mathbb{C}} : [[\mathbf{u}]] \otimes [[\mathbf{u}]] \quad \text{on } \mathcal{I}, \quad (8)$$

with \mathbb{C} and $\bar{\mathbb{C}}$ being fourth-order constitutive tensors of the bulk and interface, respectively. The second-order tensor $\bar{\mathbb{C}}$ characterizes the interface orthogonal behavior. Note, the interface free energy density is composed of two parts associated with the interface tangential and orthogonal behavior. Using the free energy densities (8), the constitutive

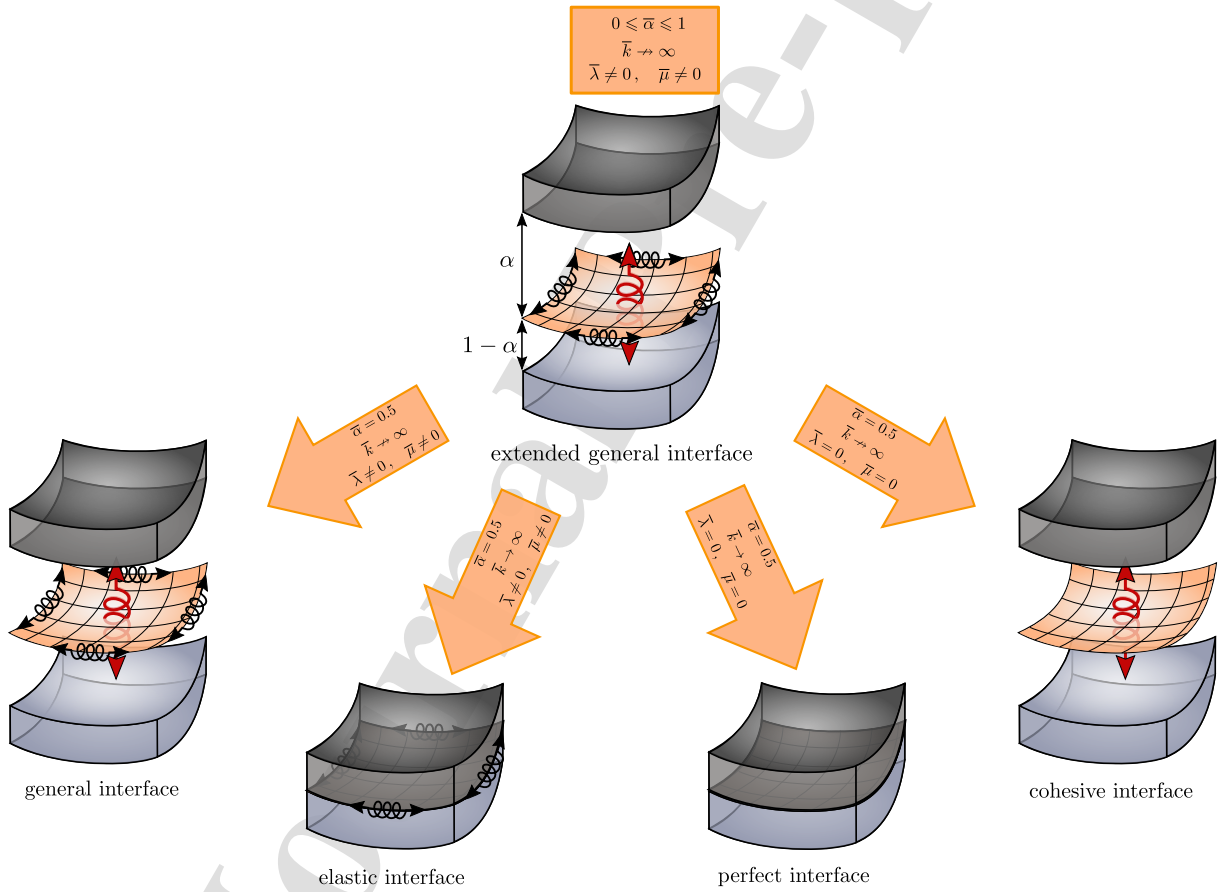


Figure 3: Illustration of recovering all the previously introduced interface models by the extended general interface model. The classical general interface model can be recovered by setting $\bar{\alpha} = 0.5$. The cohesive interface model is recovered when $\bar{\lambda} = \bar{\mu} = 0$ and $\bar{k} \rightarrow \infty$ and $\bar{\alpha} = 0.5$. The conditions $\bar{\lambda} \neq 0$, $\bar{\mu} \neq 0$ and $\bar{k} \rightarrow \infty$ and $\bar{\alpha} = 0.5$ recover the elastic interface model. Finally, the perfect interface model is recovered when $\bar{\lambda} = \bar{\mu} = 0$ and $\bar{k} \rightarrow \infty$ and $\bar{\alpha} = 0.5$.

relations for the bulk and the interface read

$$\boldsymbol{\sigma} = \frac{\partial \psi}{\partial \boldsymbol{\varepsilon}} \quad \text{in } \mathcal{B}, \quad \bar{\boldsymbol{\sigma}} = \frac{\partial \bar{\psi}}{\partial \bar{\boldsymbol{\varepsilon}}} \quad \text{and} \quad \bar{\boldsymbol{t}} := \frac{\partial \bar{\psi}}{\partial \llbracket \boldsymbol{u} \rrbracket} \quad \text{on } \mathcal{I}. \quad (9)$$

The bulk material response is assumed to be (linear) isotropic elastic while for the interface we additively decompose the material response into a tangential response along the interface and an orthogonal response across the interface.

That is

$$\begin{aligned} \mathbb{C} &= \mu [\mathbf{I} \otimes \mathbf{I} + \mathbf{I} \otimes \underline{\mathbf{I}}] + \lambda \mathbf{I} \otimes \mathbf{I} &\implies & \boldsymbol{\sigma} = \frac{\partial \psi}{\partial \boldsymbol{\varepsilon}} = 2\mu \boldsymbol{\varepsilon} + \lambda [\boldsymbol{\varepsilon} : \mathbf{I}] \mathbf{I} & \text{in } \mathcal{B}, \\ \bar{\mathbb{C}} &= \bar{\mu} [\bar{\mathbf{I}} \otimes \bar{\mathbf{I}} + \bar{\mathbf{I}} \otimes \bar{\underline{\mathbf{I}}}] + \bar{\lambda} \bar{\mathbf{I}} \otimes \bar{\mathbf{I}} &\implies & \bar{\boldsymbol{\sigma}} = \frac{\partial \bar{\psi}}{\partial \bar{\boldsymbol{\varepsilon}}} = 2\bar{\mu} \bar{\boldsymbol{\varepsilon}} + \bar{\lambda} [\bar{\boldsymbol{\varepsilon}} : \bar{\mathbf{I}}] \bar{\mathbf{I}} & \text{on } \mathcal{I}, \\ \bar{\mathbb{C}} &= \bar{k} \bar{\mathbf{I}} &\implies & \bar{\boldsymbol{t}} = \frac{\partial \bar{\psi}}{\partial \llbracket \boldsymbol{u} \rrbracket} = \bar{k} \llbracket \boldsymbol{u} \rrbracket & \text{on } \mathcal{I}, \end{aligned} \quad (10)$$

with λ and μ being the bulk Lamé parameters. The parameters $\bar{\lambda}$ and $\bar{\mu}$ are the interface Lamé parameters which represent interface tangential elasticity or resistance against in-plane stretch. The interface orthogonal resistance \bar{k} accounts for cohesive resistance or resistance against opening. It shall be underlined that the extended general interface parameters can recover any of the classical interface models such as general interface model, elastic interface model, cohesive interface model and perfect interface model. The conditions required to recover the classical interface models are illustrated in Figure 3 .

The final step to complete the homogenization framework is to bridge the micro- and macro-scales. At the micro-scale, the constitutive response is assumed to be known. Solving the associated boundary value problem and proper averaging over the RVE renders the macroscopic response [195, 197, 201–204]. The macroscopic stress and strain can be defined as

$${}^M \boldsymbol{\varepsilon} = \frac{1}{\mathcal{V}} \int_{\mathcal{B}} \boldsymbol{\varepsilon} \, dV + \frac{1}{\mathcal{V}} \int_{\mathcal{I}} \frac{1}{2} [\llbracket \boldsymbol{u} \rrbracket \otimes \bar{\boldsymbol{n}} + \bar{\boldsymbol{n}} \otimes \llbracket \boldsymbol{u} \rrbracket] \, dA, \quad \text{and} \quad {}^M \boldsymbol{\sigma} = \frac{1}{\mathcal{V}} \int_{\mathcal{B}} \boldsymbol{\sigma} \, dV + \frac{1}{\mathcal{V}} \int_{\mathcal{I}} \bar{\boldsymbol{\sigma}} \, dA. \quad (11)$$

Using the extended divergence theorem, one can write the above equations as surface integrals reading

$${}^M \boldsymbol{\varepsilon} = \frac{1}{\mathcal{V}} \int_{\partial \mathcal{B}} \frac{1}{2} [\boldsymbol{u} \otimes \boldsymbol{n} + \boldsymbol{n} \otimes \boldsymbol{u}] \, dA, \quad \text{and} \quad {}^M \boldsymbol{\sigma} = \frac{1}{\mathcal{V}} \int_{\partial \mathcal{B}} \boldsymbol{t} \otimes \boldsymbol{x} \, dA. \quad (12)$$

The incremental energy densities at micro- and macro-scales read

$$\text{micro-scale: } \begin{cases} \delta\psi = \boldsymbol{\sigma} : \delta\boldsymbol{\varepsilon} & \text{in } \mathcal{B}, \\ \delta\bar{\psi} = \bar{\boldsymbol{\sigma}} : \delta\bar{\boldsymbol{\varepsilon}} + \bar{\boldsymbol{t}} \cdot \llbracket \delta\boldsymbol{u} \rrbracket & \text{on } \mathcal{I}, \end{cases} \quad \text{macro-scale: } \begin{cases} \delta^M\psi = {}^M\boldsymbol{\sigma} : \delta^M\boldsymbol{\varepsilon} & \text{in } {}^M\mathcal{B}, \\ \delta^M\bar{\psi} \approx 0 & \text{on } {}^M\mathcal{I}. \end{cases} \quad (13)$$

Note that there is no interfacial energy at the macro-scale. Central to the homogenization is the Hill–Mandel condition which imposes an incremental energy equivalence between the micro- and macro-scales. The interface-enhanced Hill–Mandel condition reads

$$\delta^M\psi \stackrel{!}{=} \frac{1}{\mathcal{V}} \int_{\mathcal{B}} \delta\psi \, dV + \frac{1}{\mathcal{V}} \int_{\mathcal{I}} \delta\bar{\psi} \, dA, \quad (14)$$

with $\stackrel{!}{=}$ denoting that the equality is a condition. Inserting the microscopic and macroscopic incremental energy densities (13) into the Hill–Mandel condition yields

$$\frac{1}{\mathcal{V}} \int_{\mathcal{B}} \boldsymbol{\sigma} : \delta\boldsymbol{\varepsilon} \, dV + \frac{1}{\mathcal{V}} \int_{\mathcal{I}} [\bar{\boldsymbol{\sigma}} : \delta\bar{\boldsymbol{\varepsilon}} + \bar{\boldsymbol{t}} \cdot \llbracket \delta\boldsymbol{u} \rrbracket] \, dA - {}^M\boldsymbol{\sigma} : \delta^M\boldsymbol{\varepsilon} \stackrel{!}{=} 0. \quad (15)$$

Finally, via importing the macro strain and macro stress relations from Eq. (11) into Eq. (15), we arrive at the final form of the interface-enhanced Hill-Mandel condition reading

$$\int_{\partial\mathcal{B}} [\delta\boldsymbol{u} - \delta^M\boldsymbol{\varepsilon} \cdot \boldsymbol{x}] \cdot [\boldsymbol{t} - {}^M\boldsymbol{\sigma} \cdot \boldsymbol{n}] \, dA \stackrel{!}{=} 0. \quad (16)$$

Among all the boundary conditions satisfying the Hill–Mandel condition, the linear displacement boundary condition (DBC) and constant traction boundary condition (TBC) are of our interest here¹. See Firooz et al. [193] for a comprehensive study on the effects of the boundary condition and the RVE type on the overall behavior of heterogeneous materials in the computational homogenization framework. Note, Eqs. (12)–(16) hold for closed interfaces suitable to study composite with spherical particles and in-plane properties of composites with cylindrical fibers. For more general studies accounting for open interfaces, see [205].

Remark on the stress symmetry condition in the presence of surface tension Since the elastic response along the interface follows the surface elasticity theory of Gurtin–Murdoch, it is natural to scrutinize its validity in the presence of surface tension or other interface initial stresses. This discussion is particularly crucial because it is well established that the (linearized) stress along the interface loses its symmetry in the presence of a surface tension $\bar{\gamma}$. Via a consistent

¹Obviously, periodic boundary condition (PBC) is another viable choice which satisfies the Hill–Mandel condition. However, for circular and spherical RVEs, this boundary condition is not of particular interest.

linearization procedure, we argue that the non-symmetric structure of the linearized surface stress does not violate the angular momentum balance. Let $\bar{\mathbf{\Pi}}$ denotes the linearized interface stress at the reference configuration. That is

$$\bar{\mathbf{\Pi}} = \bar{\gamma} \bar{\mathbf{I}} + \bar{\mathbb{C}}_{\text{eff}} : \bar{\boldsymbol{\epsilon}} + \bar{\gamma} \overline{\text{Grad}} \bar{\mathbf{u}}, \quad (17)$$

with

$$\bar{\mathbb{C}}_{\text{eff}} = 2\bar{\mu}_{\text{eff}} \bar{\mathbb{I}}^{\text{sym}} + 2\bar{\lambda}_{\text{eff}} \bar{\mathbb{I}}^{\text{vol}} \quad \text{with} \quad \bar{\mathbb{I}}^{\text{vol}} := \frac{1}{2} [\bar{\mathbf{I}} \otimes \bar{\mathbf{I}}] \quad , \quad \bar{\mathbb{I}}^{\text{sym}} := \frac{1}{2} [\bar{\mathbf{I}} \otimes \bar{\mathbf{I}} + \bar{\mathbf{I}} \otimes \bar{\mathbf{I}}], \quad (18)$$

that immediately implies

$$\bar{\mathbf{\Pi}} = \bar{\gamma} \bar{\mathbf{I}} + [2\bar{\mu}_{\text{eff}} \bar{\mathbb{I}}^{\text{sym}} + 2\bar{\lambda}_{\text{eff}} \bar{\mathbb{I}}^{\text{vol}}] : \bar{\boldsymbol{\epsilon}} + \bar{\gamma} \overline{\text{Grad}} \bar{\mathbf{u}}, \quad (19)$$

or alternatively

$$\bar{\mathbf{\Pi}} = \bar{\gamma} \bar{\mathbf{I}} + 2[\bar{\mu} - \bar{\gamma}] \bar{\boldsymbol{\epsilon}} + [\bar{\lambda} + \bar{\gamma}] [\text{Tr} \bar{\boldsymbol{\epsilon}}] \bar{\mathbf{I}} + \bar{\gamma} \overline{\text{Grad}} \bar{\mathbf{u}} \quad \text{with} \quad \text{Tr} \bar{\boldsymbol{\epsilon}} = \bar{\boldsymbol{\epsilon}} : \bar{\mathbf{I}}, \quad (20)$$

which is precisely the interface stress as proposed by Gurtin and Murdoch [51]. Note that in the absence of surface tension, $\bar{\mathbf{\Pi}}$ coincides with $\bar{\boldsymbol{\sigma}}$ and its symmetry is trivially satisfied but the same cannot be said about $\bar{\mathbf{\Pi}}$ itself. However, as we show shortly, this “non-symmetry” is not in violation of the linearized angular momentum balance. To do so, we define the linearization operator \mathcal{L} on the interface as

$$\mathcal{L}\{\bullet\} = \{\bullet\}|_I + \frac{\partial\{\bullet\}}{\partial\bar{\mathbf{F}}}|_I : [\bar{\mathbf{F}} - \bar{\mathbf{I}}] = \{\bullet\}|_I + \frac{\partial\{\bullet\}}{\partial\bar{\mathbf{F}}}|_I : \overline{\text{Grad}} \bar{\mathbf{u}}, \quad (21)$$

where $\bar{\mathbf{u}}$ denotes the infinitesimal displacement on the interface, but not necessarily tangential to the interface, and $\bar{\mathbf{F}}$ is the deformation gradient along the interface. From definition (21), it follows that

$$\mathcal{L} \bar{\mathbf{F}} \equiv \bar{\mathbf{I}} + \overline{\text{Grad}} \bar{\mathbf{u}} \quad \text{and} \quad \bar{\mathbf{\Pi}} \equiv \mathcal{L} \bar{\mathbf{P}}, \quad (22)$$

with $\bar{\mathbf{P}}$ being the interface Piola stress. We omit the intermediate derivations for the sake of brevity. In order to obtain the linearized balance of angular momentum, we apply the identity

$$\mathcal{L}(\mathbf{A} \cdot \mathbf{B}) = \mathcal{L} \mathbf{A} \cdot \mathbf{B}|_I + \mathbf{A}|_I \cdot \mathcal{L} \mathbf{B} - (\mathbf{A} \cdot \mathbf{B})|_I, \quad (23)$$

on the interface angular momentum balance $\overline{\mathbf{P}} \cdot \overline{\mathbf{F}}^t = \overline{\mathbf{F}} \cdot \overline{\mathbf{P}}^t$ at finite deformations. The linearization of $\overline{\mathbf{P}} \cdot \overline{\mathbf{F}}^t$ reads

$$\mathcal{L}(\overline{\mathbf{P}} \cdot \overline{\mathbf{F}}^t) = \mathcal{L}\overline{\mathbf{P}} \cdot \overline{\mathbf{F}}^t|_I + \overline{\mathbf{P}}|_I \cdot \mathcal{L}\overline{\mathbf{F}}^t - (\overline{\mathbf{P}} \cdot \overline{\mathbf{F}}^t)|_I. \quad (24)$$

Using $\overline{\mathbf{F}}|_I = \overline{\mathbf{I}}$, $\overline{\mathbf{P}}|_I = \overline{\gamma}\overline{\mathbf{I}}$ and the symmetry property of $\overline{\gamma}\overline{\mathbf{I}}$ we obtain

$$\mathcal{L}(\overline{\mathbf{P}} \cdot \overline{\mathbf{F}}^t) = \overline{\gamma}\overline{\mathbf{I}} + \overline{\mathbb{C}}_{\text{eff}} : \overline{\boldsymbol{\epsilon}} + \overline{\gamma}[\overline{\text{Grad}}\overline{\mathbf{u}} + \overline{\text{Grad}}^t\overline{\mathbf{u}}], \quad (25)$$

which is indeed symmetric and fulfills the angular momentum balance a priori. Note that although we have elaborated on the symmetry condition for a surface tension $\overline{\gamma}$, an identical approach can also be employed to investigate this property for any symmetric initial stress $\overline{\boldsymbol{\sigma}}_0$. \square

3. Interface-enhanced Mori–Tanaka method

This section aims to establish an interface-enhanced Mori–Tanaka method for composites embedding extended general interfaces with arbitrary interface positions. *Our proposed framework not only determines the effective properties of composites but also provides global concentration tensors which link the macroscopic fields with the average fields, thus furnishing the state of stress and strain in each phase of the medium.* Chatzigeorgiou et al. [182] developed analytical estimates for the effective properties of fiber composites with general interfaces. Using energy principles, Duan et al. [206] proposed to substitute the inhomogeneity/interface system with an equivalent inhomogeneity to predict the overall behavior of the medium. Both methodologies provide reasonable estimates compared to full field homogenization strategies, like the periodic homogenization framework, but they cannot provide information about the local fields that are developed in various phases of the medium. Our proposed methodology here is similar to [206], but instead of looking for an equivalent inhomogeneity, we seek strain and stress dilute concentration tensors of the inhomogeneity/interface system, see also [180] and [181]. The idea of providing dilute concentration tensors is motivated by similar techniques in the literature for coated particles or fibers [8, 207–210]. Throughout this section, the superscripts (1) and (2) denote the properties associated with the inhomogeneity and the matrix, respectively.

Figure 4 shows the multi-scale representation of a heterogeneous continuum body for both two-dimensional and three-dimensional problems. Figure 4 (left) depicts the RVE consisting of multiple inhomogeneities occupying the domain \mathcal{B}_1 with the overall volume of \mathcal{V}_1 embedded in a matrix occupying the domain \mathcal{B}_2 with the volume \mathcal{V}_2 . Evidently, $\mathcal{B} = \mathcal{B}_1 \cup \mathcal{B}_2$ and $\mathcal{V} = \mathcal{V}_1 + \mathcal{V}_2$ and the inhomogeneities overall volume fraction is $f = \mathcal{V}_1/\mathcal{V}$. Figure 4 (right) shows a cutout of the RVE representing the Eshelby problem consisting of a heterogeneity occupying the domain Ω_1 with radius r_1 surrounded by an extended general interface \mathcal{I} which is embedded in an infinite matrix occupying

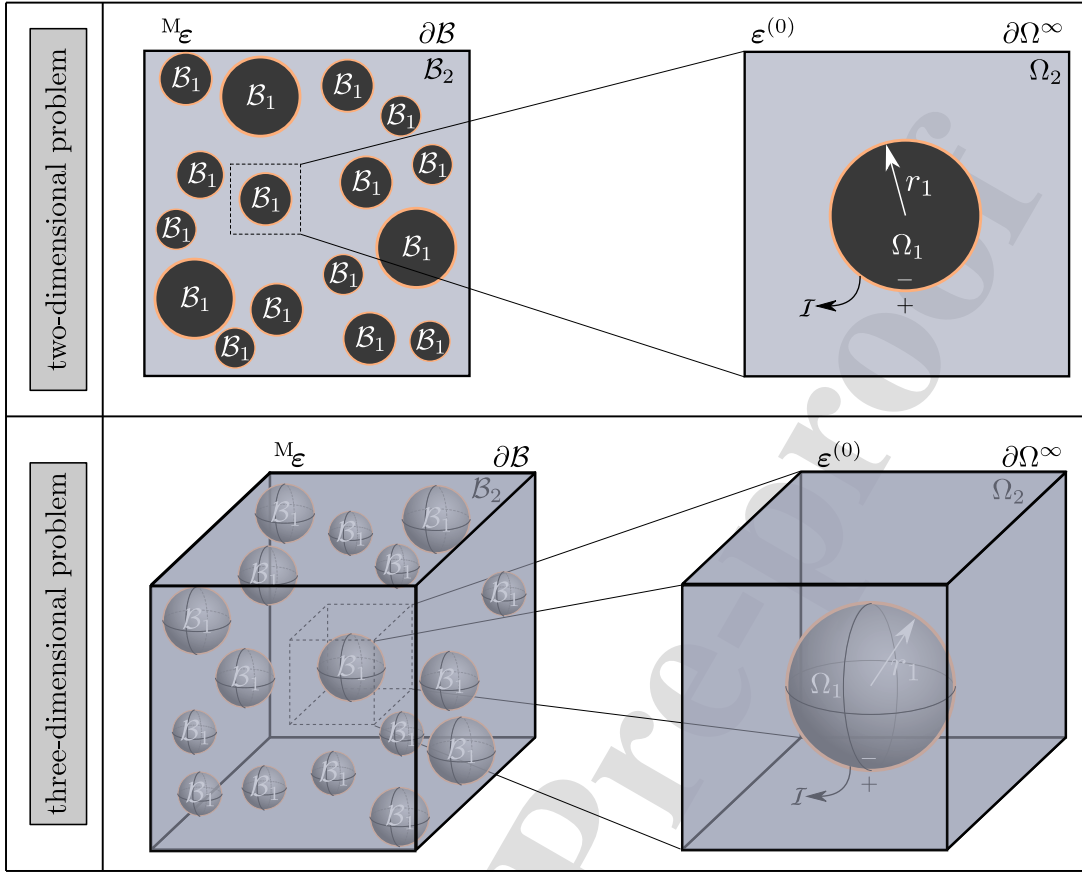


Figure 4: Inhomogeneity with extended general interface inside an infinite matrix (left) and the RVE consisting of the inhomogeneity with extended general interface inside a matrix material (right).

the domain Ω_2 with the boundary $\partial\Omega^\infty$. The inhomogeneity is considered to be the minus side of the interface with elasticity tensors $\mathbb{C}^{(1)}$ whereas the matrix is considered to be the plus side of the interface with the elasticity tensor $\mathbb{C}^{(2)}$. It is noteworthy that while the domains \mathcal{B}_1 and Ω_1 are identical, there is a subtle difference between the domains \mathcal{B}_2 and Ω_2 . The domain \mathcal{B}_2 corresponds to a finite matrix belonging to the RVE with the volume fraction $1 - f$ whereas the domain Ω_2 corresponds to an infinite matrix surrounding the inhomogeneity associated with the Eshelby problem. Here our objective is to determine the dilute strain concentration tensor and dilute stress-strain concentration tensor for the inhomogeneity and the inhomogeneity/interface system. Consider the RVE is subject to a macroscopic strain $\mathbb{M}\boldsymbol{\varepsilon}$. The macroscopic strain and stress can be written in terms of the average strains and stresses in the constituents of the RVE as

$$\begin{aligned} \mathbb{M}\boldsymbol{\varepsilon} &= \frac{1}{\mathcal{V}} \int_{\mathcal{B}} \boldsymbol{\varepsilon} \, dV + \frac{1}{2\mathcal{V}} \int_I [[\mathbf{u}]] \otimes \bar{\mathbf{n}} + \bar{\mathbf{n}} \otimes [[\mathbf{u}]] \, dA = [1 - f]\boldsymbol{\varepsilon}^{(2)} + f\boldsymbol{\varepsilon}^{(1)} + \widehat{\boldsymbol{\varepsilon}}, \\ \mathbb{M}\boldsymbol{\sigma} &= \frac{1}{\mathcal{V}} \int_{\mathcal{B}} \boldsymbol{\sigma} \, dV + \frac{1}{\mathcal{V}} \int_I \bar{\boldsymbol{\sigma}} \, dA = [1 - f]\boldsymbol{\sigma}^{(2)} + f\boldsymbol{\sigma}^{(1)} + \widehat{\boldsymbol{\sigma}} = [1 - f]\mathbb{C}^{(2)} : \boldsymbol{\varepsilon}^{(2)} + f\mathbb{C}^{(1)} : \boldsymbol{\varepsilon}^{(1)} + \widehat{\boldsymbol{\sigma}}, \end{aligned} \quad (26)$$

with

$$\begin{aligned}
 \boldsymbol{\varepsilon}^{(1)} &= \frac{1}{\mathcal{V}_1} \int_{\mathcal{B}_1} \boldsymbol{\varepsilon} \, dV, & \boldsymbol{\sigma}^{(1)} &= \frac{1}{\mathcal{V}_1} \int_{\mathcal{B}_1} \boldsymbol{\sigma} \, dV = \mathbb{C}^{(1)} : \boldsymbol{\varepsilon}^{(1)}, \\
 \boldsymbol{\varepsilon}^{(2)} &= \frac{1}{\mathcal{V}_2} \int_{\mathcal{B}_2} \boldsymbol{\varepsilon} \, dV, & \boldsymbol{\sigma}^{(2)} &= \frac{1}{\mathcal{V}_2} \int_{\mathcal{B}_2} \boldsymbol{\sigma} \, dV = \mathbb{C}^{(2)} : \boldsymbol{\varepsilon}^{(2)}, \\
 \widehat{\boldsymbol{\varepsilon}} &= \frac{1}{2\mathcal{V}} \int_I [\llbracket \mathbf{u} \rrbracket \otimes \bar{\mathbf{n}} + \bar{\mathbf{n}} \otimes \llbracket \mathbf{u} \rrbracket] \, dA, & \widehat{\boldsymbol{\sigma}} &= \frac{1}{\mathcal{V}} \int_I \bar{\boldsymbol{\sigma}} \, dA.
 \end{aligned} \tag{27}$$

In mean field homogenization approaches, an additional relation between the average strains and stresses can be identified through the so-called Eshelby problem (Figure 4 right). Accordingly, the infinite medium is subjected to a uniform strain $\boldsymbol{\varepsilon}^{(0)}$ and the resulting average strain and stress in the heterogeneity can be written as

$$\boldsymbol{\varepsilon}^{(1)} = \mathbb{T}^{(1)} : \boldsymbol{\varepsilon}^{(0)} = \frac{1}{2\mathcal{V}_1} \int_I [\mathbf{u}^- \otimes \bar{\mathbf{n}} + \bar{\mathbf{n}} \otimes \mathbf{u}^-] \, dA, \quad \text{and} \quad \boldsymbol{\sigma}^{(1)} = \mathbb{H}^{(1)} : \boldsymbol{\varepsilon}^{(0)} = \frac{1}{\mathcal{V}_1} \int_{\Omega_1} \boldsymbol{\sigma}^- \, dV, \tag{28}$$

with $\mathbb{T}^{(1)}$ being the dilute strain concentration tensor and $\mathbb{H}^{(1)}$ being the dilute stress-strain concentration tensor for the inhomogeneity. Note, \mathbf{u}^- and $\boldsymbol{\sigma}^-$ denote the displacement and stress on the minus side of the interface, respectively, which contain the contributions from the inhomogeneity alone. Similar to the work of Gu et al. [183], the inhomogeneity/interface system can be treated as an equivalent inhomogeneity with average strain and stress tensors defined as

$$\boldsymbol{\varepsilon}^{(\text{eq})} = \mathbb{T}^{(\text{eq})} : \boldsymbol{\varepsilon}^{(0)} = \frac{1}{2\mathcal{V}} \int_I [\mathbf{u}^+ \otimes \bar{\mathbf{n}} + \bar{\mathbf{n}} \otimes \mathbf{u}^+] \, dA, \quad \text{and} \quad \boldsymbol{\sigma}^{(\text{eq})} = \mathbb{H}^{(\text{eq})} : \boldsymbol{\varepsilon}^{(0)} = \frac{1}{\mathcal{V}_1} \int_{\Omega_1} \boldsymbol{\sigma}^- \, dV + \frac{1}{\mathcal{V}_1} \int_I \bar{\boldsymbol{\sigma}} \, dA, \tag{29}$$

with $\mathbb{T}^{(\text{eq})}$ being the dilute strain concentration tensor and $\mathbb{H}^{(\text{eq})}$ being the dilute stress-strain concentration tensor for the equivalent inhomogeneity. Returning back to the RVE problem, the Mori–Tanaka approach assumes that the far-field strain $\boldsymbol{\varepsilon}^{(0)}$ coincides with the average strain in the matrix $\boldsymbol{\varepsilon}^{(2)}$, therefore $\boldsymbol{\varepsilon}^{(0)} \equiv \boldsymbol{\varepsilon}^{(2)}$. Exploiting Eqs. (27)–(28), one could write

$$\begin{aligned}
 f \boldsymbol{\varepsilon}^{(\text{eq})} &= f \mathbb{T}^{(\text{eq})} : \boldsymbol{\varepsilon}^{(2)} = \frac{1}{2\mathcal{V}} \int_I [\mathbf{u}^+ \otimes \bar{\mathbf{n}} + \bar{\mathbf{n}} \otimes \mathbf{u}^+] \, dA = \underbrace{\frac{1}{2\mathcal{V}} \int_I [\mathbf{u}^- \otimes \bar{\mathbf{n}} + \bar{\mathbf{n}} \otimes \mathbf{u}^-] \, dA}_{f \mathbb{T}^{(1)} : \boldsymbol{\varepsilon}^{(2)} = f \boldsymbol{\varepsilon}^{(1)}} + \underbrace{\frac{1}{2\mathcal{V}} \int_I [\llbracket \mathbf{u} \rrbracket \otimes \bar{\mathbf{n}} + \bar{\mathbf{n}} \otimes \llbracket \mathbf{u} \rrbracket] \, dA}_{\widehat{\boldsymbol{\varepsilon}}} \\
 f \boldsymbol{\sigma}^{(\text{eq})} &= f \mathbb{H}^{(\text{eq})} : \boldsymbol{\varepsilon}^{(2)} = \underbrace{\frac{1}{\mathcal{V}} \int_{\mathcal{B}} \boldsymbol{\sigma}^- \, dV}_{f \mathbb{H}^{(1)} : \boldsymbol{\varepsilon}^{(2)} = f \boldsymbol{\sigma}^{(1)}} + \underbrace{\frac{1}{\mathcal{V}} \int_I \bar{\boldsymbol{\sigma}} \, dA}_{\widehat{\boldsymbol{\sigma}}},
 \end{aligned} \tag{30}$$

which lead to the interface-enhanced Mori–Tanaka relations

$$\boldsymbol{\varepsilon}^{(1)} = \mathbb{T}^{(1)} : \boldsymbol{\varepsilon}^{(2)}, \quad \boldsymbol{\varepsilon}^{(1)} + \frac{1}{f} \widehat{\boldsymbol{\varepsilon}} = \mathbb{T}^{(\text{eq})} : \boldsymbol{\varepsilon}^{(2)}, \quad \mathbb{C}^{(1)} : \boldsymbol{\varepsilon}^{(1)} + \frac{1}{f} \widehat{\boldsymbol{\sigma}} = \mathbb{H}^{(\text{eq})} : \boldsymbol{\varepsilon}^{(2)}. \quad (31)$$

Thus, Eq. (26) yields

$$\mathbb{M}_{\boldsymbol{\varepsilon}} = \left[[1-f]\mathbb{I} + f\mathbb{T}^{(\text{eq})} \right] : \boldsymbol{\varepsilon}^{(2)}, \quad \mathbb{M}_{\boldsymbol{\sigma}} = \left[[1-f]\mathbb{C}^{(2)} + f\mathbb{H}^{(\text{eq})} \right] : \boldsymbol{\varepsilon}^{(2)}, \quad (32)$$

where \mathbb{I} is the fourth order identity tensor. Accordingly, one could write $\boldsymbol{\varepsilon}^{(2)} = \left[[1-f]\mathbb{I} + f\mathbb{T}^{(\text{eq})} \right]^{-1} : \mathbb{M}_{\boldsymbol{\varepsilon}}$ resulting in the macroscopic stress-strain relationship

$$\mathbb{M}_{\boldsymbol{\sigma}} = \left[[1-f]\mathbb{C}^{(2)} + f\mathbb{H}^{(\text{eq})} \right] : \left[[1-f]\mathbb{I} + f\mathbb{T}^{(\text{eq})} \right]^{-1} : \mathbb{M}_{\boldsymbol{\varepsilon}}. \quad (33)$$

Consequently, the macroscopic stiffness tensor can be defined as

$$\mathbb{M}_{\mathbb{C}} = \left[[1-f]\mathbb{C}^{(2)} + f\mathbb{H}^{(\text{eq})} \right] : \left[[1-f]\mathbb{I} + f\mathbb{T}^{(\text{eq})} \right]^{-1}, \quad (34)$$

whose components are indeed the effective properties of the composite medium. Note, the properties of the equivalent particle in [183] can be recovered according to $\mathbb{C}^{(\text{eq})} = \mathbb{H}^{(\text{eq})} : \mathbb{T}^{(\text{eq})^{-1}}$. Finally, for a prescribed macroscopic strain $\mathbb{M}_{\boldsymbol{\varepsilon}}$, the average strain and stress in the constituents read

$$\begin{aligned} \boldsymbol{\varepsilon}^{(1)} &= \mathbb{T}^{(1)} : \left[[1-f]\mathbb{I} + f\mathbb{T}^{(\text{eq})} \right]^{-1} : \mathbb{M}_{\boldsymbol{\varepsilon}}, & \boldsymbol{\sigma}^{(1)} &= \mathbb{C}^{(1)} : \boldsymbol{\varepsilon}^{(1)} = \mathbb{C}^{(1)} : \mathbb{T}^{(1)} : \left[[1-f]\mathbb{I} + f\mathbb{T}^{(\text{eq})} \right]^{-1} : \mathbb{M}_{\boldsymbol{\varepsilon}}, \\ \boldsymbol{\varepsilon}^{(2)} &= \left[[1-f]\mathbb{I} + f\mathbb{T}^{(\text{eq})} \right]^{-1} : \mathbb{M}_{\boldsymbol{\varepsilon}}, & \boldsymbol{\sigma}^{(2)} &= \mathbb{C}^{(2)} : \boldsymbol{\varepsilon}^{(2)} = \mathbb{C}^{(2)} : \left[[1-f]\mathbb{I} + f\mathbb{T}^{(\text{eq})} \right]^{-1} : \mathbb{M}_{\boldsymbol{\varepsilon}}, \\ \widehat{\boldsymbol{\varepsilon}} &= f \left[\mathbb{T}^{(\text{eq})} - \mathbb{T}^{(1)} \right] : \left[[1-f]\mathbb{I} + f\mathbb{T}^{(\text{eq})} \right]^{-1} : \mathbb{M}_{\boldsymbol{\varepsilon}}, & \widehat{\boldsymbol{\sigma}} &= f \left[\mathbb{H}^{(\text{eq})} - \mathbb{C}^{(1)} : \mathbb{T}^{(1)} \right] : \left[[1-f]\mathbb{I} + f\mathbb{T}^{(\text{eq})} \right]^{-1} : \mathbb{M}_{\boldsymbol{\varepsilon}}. \end{aligned} \quad (35)$$

The final step to complete the homogenization framework is to determine the components of the dilute concentration tensors $\mathbb{H}^{(\text{eq})}$, $\mathbb{T}^{(\text{eq})}$ and $\mathbb{T}^{(1)}$. In doing so, we employ the Eshelby's inhomogeneity problem [211] for certain conditions suitable for fiber-reinforced and particle-reinforced composites. It is worthwhile to mention that the composite sphere assemblage and the composite cylinder assemblage approaches have been designed for uniform distribution of inhomogeneities and cannot be extended to more complex cases. On the other hand, the Mori–Tanaka approach is more flexible and non-uniform distributions of inhomogeneities can be adopted by proper modification of the relations (26) and (32), see for instance [212]. The relations in Eq. (35) provide implicitly the interactions between

inhomogeneities of different type or distributions.

3.1. Fiber-reinforced composites

To determine the components of the interaction tensors, the extended Eshelby's problem is solved analytically for four boundary value problems similar to those described by Hashin and Rosen [213] in the composite cylinders assemblage approach. Before proceeding with the elaboration of the boundary value problems, a brief introduction to preliminaries of fiber-reinforced composites seems desirable. According to Fig. 4, a cylindrical coordinate system proves to be convenient to analyze a fiber-reinforced composite medium. The constitutive material behavior for a transversely isotropic material, in Voigt notation, reads

Table 2: Summary of relevant relations in the bulk and on the interface for fiber-reinforced composites.

	bulk	interface
constitutive relations	$\begin{bmatrix} \sigma_{rr} \\ \sigma_{\theta\theta} \\ \sigma_{zz} \\ \sigma_{r\theta} \\ \sigma_{rz} \\ \sigma_{\theta z} \end{bmatrix} = \begin{bmatrix} \lambda + 2\mu_{tr} & \lambda & l & 0 & 0 & 0 \\ \lambda & \lambda + 2\mu_{tr} & l & 0 & 0 & 0 \\ l & l & m & 0 & 0 & 0 \\ 0 & 0 & 0 & \mu_{tr} & 0 & 0 \\ 0 & 0 & 0 & 0 & \mu_{ax} & 0 \\ 0 & 0 & 0 & 0 & 0 & \mu_{ax} \end{bmatrix} \begin{bmatrix} \varepsilon_{rr} \\ \varepsilon_{\theta\theta} \\ \varepsilon_{zz} \\ 2\varepsilon_{r\theta} \\ 2\varepsilon_{rz} \\ 2\varepsilon_{\theta z} \end{bmatrix}$	<p>tangential: $\begin{bmatrix} \bar{\sigma}_{\theta\theta} \\ \bar{\sigma}_{zz} \\ \bar{\sigma}_{\theta z} \end{bmatrix} = \begin{bmatrix} \bar{\lambda} + 2\bar{\mu}_{tr} & \bar{\lambda} & 0 \\ \bar{\lambda} & \bar{\lambda} + 2\bar{\mu}_{tr} & 0 \\ 0 & 0 & \bar{\mu}_{ax} \end{bmatrix} \begin{bmatrix} \bar{\varepsilon}_{\theta\theta} \\ \bar{\varepsilon}_{zz} \\ 2\bar{\varepsilon}_{\theta z} \end{bmatrix}$</p> <p>orthogonal: $\begin{bmatrix} \bar{i}_r \\ \bar{i}_\theta \\ \bar{i}_z \end{bmatrix} = \begin{bmatrix} \bar{k}_r [u_r] \\ \bar{k}_\theta [u_\theta] \\ \bar{k}_z [u_z] \end{bmatrix}$</p>
strain relations	$\varepsilon_{rr} = \frac{\partial u_r}{\partial r}$ $\varepsilon_{\theta\theta} = \frac{1}{r} \frac{\partial u_\theta}{\partial \theta} + \frac{u_r}{r}$ $\varepsilon_{zz} = \frac{\partial u_z}{\partial z}$ $2\varepsilon_{r\theta} = \frac{\partial u_\theta}{\partial r} + \frac{1}{r} \frac{\partial u_r}{\partial \theta} - \frac{u_\theta}{r}$ $2\varepsilon_{rz} = \frac{\partial u_z}{\partial r} + \frac{\partial u_r}{\partial z}$ $2\varepsilon_{\theta z} = \frac{1}{r} \frac{\partial u_z}{\partial \theta} + \frac{\partial u_\theta}{\partial z}$	$\bar{\varepsilon}_{rr} = 0$ $\bar{\varepsilon}_{\theta\theta} = \frac{1}{r_1} \frac{\partial \bar{u}_\theta}{\partial \theta} + \frac{\bar{u}_r}{r_1}$ $\bar{\varepsilon}_{zz} = \frac{\partial \bar{u}_z}{\partial z}$ $\bar{\varepsilon}_{r\theta} = 0$ $\bar{\varepsilon}_{rz} = 0$ $2\bar{\varepsilon}_{\theta z} = \frac{1}{r_1} \frac{\partial \bar{u}_z}{\partial \theta} + \frac{\partial \bar{u}_\theta}{\partial z}$
balance equations	$\frac{\partial \sigma_{rr}}{\partial r} + \frac{1}{r} \frac{\partial \sigma_{r\theta}}{\partial \theta} + \frac{\partial \sigma_{rz}}{\partial z} + \frac{\sigma_{rr} - \sigma_{\theta\theta}}{r} = 0$ $\frac{\partial \sigma_{r\theta}}{\partial r} + \frac{1}{r} \frac{\partial \sigma_{\theta\theta}}{\partial \theta} + \frac{\partial \sigma_{\theta z}}{\partial z} + \frac{2}{r} \sigma_{r\theta} = 0$ $\frac{\partial \sigma_{rz}}{\partial r} + \frac{1}{r} \frac{\partial \sigma_{\theta z}}{\partial \theta} + \frac{\partial \sigma_{zz}}{\partial z} + \frac{1}{r} \sigma_{rz} = 0$	$\frac{\bar{\sigma}_{\theta\theta}}{r_1} - \llbracket \sigma_{rr} \rrbracket = 0$ $\frac{1}{r_1} \frac{\partial \bar{\sigma}_{\theta\theta}}{\partial \theta} + \frac{\partial \bar{\sigma}_{\theta z}}{\partial z} + \llbracket \sigma_{r\theta} \rrbracket = 0$ $\frac{1}{r_1} \frac{\partial \bar{\sigma}_{\theta z}}{\partial \theta} + \frac{\partial \bar{\sigma}_{zz}}{\partial z} + \llbracket \sigma_{rz} \rrbracket = 0$

$$\begin{bmatrix} \sigma_{rr} \\ \sigma_{\theta\theta} \\ \sigma_{zz} \\ \sigma_{r\theta} \\ \sigma_{rz} \\ \sigma_{\theta z} \end{bmatrix} = \begin{bmatrix} \lambda + 2\mu_{tr} & \lambda & l & 0 & 0 & 0 \\ \lambda & \lambda + 2\mu_{tr} & l & 0 & 0 & 0 \\ l & l & m & 0 & 0 & 0 \\ 0 & 0 & 0 & \mu_{tr} & 0 & 0 \\ 0 & 0 & 0 & 0 & \mu_{ax} & 0 \\ 0 & 0 & 0 & 0 & 0 & \mu_{ax} \end{bmatrix} \begin{bmatrix} \varepsilon_{rr} \\ \varepsilon_{\theta\theta} \\ \varepsilon_{zz} \\ 2\varepsilon_{r\theta} \\ 2\varepsilon_{rz} \\ 2\varepsilon_{\theta z} \end{bmatrix}, \quad (36)$$

with five independent material constants. Note that in plane-strain linear elasticity, the bulk modulus κ relates to the Lamé parameters as $\kappa = \lambda + \mu_{tr}$. The strains in the bulk read

$$\begin{aligned} \varepsilon_{rr} &= \frac{\partial u_r}{\partial r}, & \varepsilon_{\theta\theta} &= \frac{1}{r} \frac{\partial u_\theta}{\partial \theta} + \frac{u_r}{r}, & \varepsilon_{zz} &= \frac{\partial u_z}{\partial z}, \\ 2\varepsilon_{r\theta} &= \frac{\partial u_\theta}{\partial r} + \frac{1}{r} \frac{\partial u_r}{\partial \theta} - \frac{u_\theta}{r}, & 2\varepsilon_{\theta z} &= \frac{1}{r} \frac{\partial u_z}{\partial \theta} + \frac{\partial u_\theta}{\partial z}, & 2\varepsilon_{rz} &= \frac{\partial u_z}{\partial r} + \frac{\partial u_r}{\partial z}, \end{aligned} \quad (37)$$

and the balance equations associated with the bulk (6)₁ expand to

$$\begin{aligned} \frac{\partial \sigma_{rr}}{\partial r} + \frac{1}{r} \frac{\partial \sigma_{r\theta}}{\partial \theta} + \frac{\partial \sigma_{rz}}{\partial z} + \frac{\sigma_{rr} - \sigma_{\theta\theta}}{r} &= 0, \\ \frac{\partial \sigma_{r\theta}}{\partial r} + \frac{1}{r} \frac{\partial \sigma_{\theta\theta}}{\partial \theta} + \frac{\partial \sigma_{\theta z}}{\partial z} + \frac{2}{r} \sigma_{r\theta} &= 0, \\ \frac{\partial \sigma_{rz}}{\partial r} + \frac{1}{r} \frac{\partial \sigma_{\theta z}}{\partial \theta} + \frac{\partial \sigma_{zz}}{\partial z} + \frac{1}{r} \sigma_{rz} &= 0. \end{aligned} \quad (38)$$

As mentioned before, for the interface, the constitutive behavior is decomposed into tangential and orthogonal behavior reading

$$\text{tangential: } \begin{bmatrix} \bar{\sigma}_{\theta\theta} \\ \bar{\sigma}_{zz} \\ \bar{\sigma}_{\theta z} \end{bmatrix} = \begin{bmatrix} \bar{\lambda} + 2\bar{\mu}_{tr} & \bar{\lambda} & 0 \\ \bar{\lambda} & \bar{\lambda} + 2\bar{\mu}_{tr} & 0 \\ 0 & 0 & \bar{\mu}_{ax} \end{bmatrix} \begin{bmatrix} \bar{\varepsilon}_{\theta\theta} \\ \bar{\varepsilon}_{zz} \\ 2\bar{\varepsilon}_{\theta z} \end{bmatrix}, \quad \text{orthogonal: } \begin{bmatrix} \bar{t}_r \\ \bar{t}_\theta \\ \bar{t}_z \end{bmatrix} = \begin{bmatrix} \bar{k}_r \llbracket u_r \rrbracket \\ \bar{k}_\theta \llbracket u_\theta \rrbracket \\ \bar{k}_z \llbracket u_z \rrbracket \end{bmatrix}. \quad (39)$$

Without loss of generality, one can demonstrate that the resistance along the interface for fiber-reinforced composites can be sufficiently captured with only one interface Lamé parameter and thus, we assume $\bar{\lambda} = 0$. The strains on the interface read

$$\bar{\varepsilon}_{\theta\theta} = \frac{1}{r_1} \frac{\partial \bar{u}_\theta}{\partial \theta} + \frac{\bar{u}_r}{r_1}, \quad \bar{\varepsilon}_{zz} = \frac{\partial \bar{u}_z}{\partial z}, \quad 2\bar{\varepsilon}_{\theta z} = \frac{1}{r_1} \frac{\partial \bar{u}_z}{\partial \theta} + \frac{\partial \bar{u}_\theta}{\partial z}, \quad (40)$$

and the interface balance equations (6)₂ expand to

$$\begin{aligned} \frac{\bar{\sigma}_{\theta\theta}}{r_1} - \llbracket \sigma_{rr} \rrbracket &= 0, \\ \frac{1}{r_1} \frac{\partial \bar{\sigma}_{\theta\theta}}{\partial \theta} + \frac{\partial \bar{\sigma}_{\theta z}}{\partial z} + \llbracket \sigma_{r\theta} \rrbracket &= 0, \\ \frac{1}{r_1} \frac{\partial \bar{\sigma}_{\theta z}}{\partial \theta} + \frac{\partial \bar{\sigma}_{zz}}{\partial z} + \llbracket \sigma_{rz} \rrbracket &= 0. \end{aligned} \quad (41)$$

Table 2 summarizes the relevant constitutive relations, strain relations and balance equations for the bulk and the interface for fiber-reinforced composites.

According to Eq. (36), the elasticity tensors for the fiber and the matrix, in Voigt notation, can be written as

$$\mathbb{C}^{(1)} = \begin{bmatrix} \lambda^{(1)} + 2\mu_{tr}^{(1)} & \lambda^{(1)} & l^{(1)} & 0 & 0 & 0 \\ \lambda^{(1)} & \lambda^{(1)} + 2\mu_{tr}^{(1)} & l^{(1)} & 0 & 0 & 0 \\ l^{(1)} & l^{(1)} & m^{(1)} & 0 & 0 & 0 \\ 0 & 0 & 0 & \mu_{tr}^{(1)} & 0 & 0 \\ 0 & 0 & 0 & 0 & \mu_{ax}^{(1)} & 0 \\ 0 & 0 & 0 & 0 & 0 & \mu_{ax}^{(1)} \end{bmatrix}, \quad \mathbb{C}^{(2)} = \begin{bmatrix} \lambda^{(2)} + 2\mu_{tr}^{(2)} & \lambda^{(2)} & l^{(2)} & 0 & 0 & 0 \\ \lambda^{(2)} & \lambda^{(2)} + 2\mu_{tr}^{(2)} & l^{(2)} & 0 & 0 & 0 \\ l^{(2)} & l^{(2)} & m^{(2)} & 0 & 0 & 0 \\ 0 & 0 & 0 & \mu_{tr}^{(2)} & 0 & 0 \\ 0 & 0 & 0 & 0 & \mu_{ax}^{(2)} & 0 \\ 0 & 0 & 0 & 0 & 0 & \mu_{ax}^{(2)} \end{bmatrix}. \quad (42)$$

The dilute concentration tensors for the inhomogeneity, in Voigt notation, take the form

$$\mathbb{T}^{(1)} = \begin{bmatrix} T_{11}^{(1)} & T_{11}^{(1)} - T_{44}^{(1)} & T_{13}^{(1)} & 0 & 0 & 0 \\ T_{11}^{(1)} - T_{44}^{(1)} & T_{11}^{(1)} & T_{13}^{(1)} & 0 & 0 & 0 \\ 0 & 0 & 1 & 0 & 0 & 0 \\ 0 & 0 & 0 & T_{44}^{(1)} & 0 & 0 \\ 0 & 0 & 0 & 0 & T_{55}^{(1)} & 0 \\ 0 & 0 & 0 & 0 & 0 & T_{55}^{(1)} \end{bmatrix}, \quad \mathbb{H}^{(1)} = \begin{bmatrix} H_{11}^{(1)} & H_{11}^{(1)} - 2H_{44}^{(1)} & H_{13}^{(1)} & 0 & 0 & 0 \\ H_{11}^{(1)} - 2H_{44}^{(1)} & H_{11}^{(1)} & H_{13}^{(1)} & 0 & 0 & 0 \\ H_{31}^{(1)} & H_{31}^{(1)} & H_{33}^{(1)} & 0 & 0 & 0 \\ 0 & 0 & 0 & H_{44}^{(1)} & 0 & 0 \\ 0 & 0 & 0 & 0 & H_{55}^{(1)} & 0 \\ 0 & 0 & 0 & 0 & 0 & H_{55}^{(1)} \end{bmatrix}. \quad (43)$$

For the equivalent inhomogeneity, the interactions tensors read

$$\mathbb{T}^{(eq)} = \begin{bmatrix} T_{11}^{(eq)} & T_{11}^{(eq)} - T_{44}^{(eq)} & T_{13}^{(eq)} & 0 & 0 & 0 \\ T_{11}^{(eq)} - T_{44}^{(eq)} & T_{11}^{(eq)} & T_{13}^{(eq)} & 0 & 0 & 0 \\ 0 & 0 & 1 & 0 & 0 & 0 \\ 0 & 0 & 0 & T_{44}^{(eq)} & 0 & 0 \\ 0 & 0 & 0 & 0 & T_{55}^{(eq)} & 0 \\ 0 & 0 & 0 & 0 & 0 & T_{55}^{(eq)} \end{bmatrix}, \quad \mathbb{H}^{(eq)} = \begin{bmatrix} H_{11}^{(eq)} & H_{11}^{(eq)} - 2H_{44}^{(eq)} & H_{13}^{(eq)} & 0 & 0 & 0 \\ H_{11}^{(eq)} - 2H_{44}^{(eq)} & H_{11}^{(eq)} & H_{13}^{(eq)} & 0 & 0 & 0 \\ H_{31}^{(eq)} & H_{31}^{(eq)} & H_{33}^{(eq)} & 0 & 0 & 0 \\ 0 & 0 & 0 & H_{44}^{(eq)} & 0 & 0 \\ 0 & 0 & 0 & 0 & H_{55}^{(eq)} & 0 \\ 0 & 0 & 0 & 0 & 0 & H_{55}^{(eq)} \end{bmatrix}. \quad (44)$$

Equipped with these preliminaries, we can now proceed with the boundary value problems to determine the components of the interaction tensors.

3.1.1. Axial shear loading

Consider an RVE subject to a far field displacement/strain as

$$\mathbf{u}^{(0)} = \begin{bmatrix} 0 \\ 0 \\ \beta r \cos \theta \end{bmatrix} \implies \boldsymbol{\varepsilon}^{(0)} = \begin{bmatrix} 0 & 0 & \frac{\beta}{2} \cos \theta \\ 0 & 0 & -\frac{\beta}{2} \sin \theta \\ \frac{\beta}{2} \cos \theta & -\frac{\beta}{2} \sin \theta & 0 \end{bmatrix}, \quad (45)$$

where the superscript 0 denotes the prescribed condition. Demonstrated by Hashin and Rosen [213], the corresponding displacement fields within each constituent read

$$\begin{aligned} u_z^{(1)} &= \beta r \cos \theta \left[X_1 + X_2 \frac{1}{[r/r_1]^2} \right] \quad \text{and} \quad u_r^{(1)} = u_\theta^{(1)} = 0, \\ u_z^{(2)} &= \beta r \cos \theta \left[X_3 + X_4 \frac{1}{[r/r_1]^2} \right] \quad \text{and} \quad u_r^{(2)} = u_\theta^{(2)} = 0, \end{aligned} \quad (46)$$

resulting in the four unknowns X_1 – X_4 that can be determined via imposing the boundary and interface conditions which read

- finite displacement at $r = 0$:

$$u_z^{(1)}(r = 0) \rightarrow \infty \implies X_2 = 0, \quad (47)$$

- orthogonal equilibrium at $r = r_1$:

$$\bar{t}_z = \bar{k}_z \llbracket u_z \rrbracket \implies [1 - \bar{\alpha}] \sigma_{rz}^{(2)}(r_1) + \bar{\alpha} \sigma_{rz}^{(1)}(r_1) = \bar{k}_z [u_z^{(2)}(r_1) - u_z^{(1)}(r_1)], \quad (48)$$

- tangential equilibrium at $r = r_1$:

$$\llbracket \text{div } \bar{\boldsymbol{\sigma}} \rrbracket_z + \llbracket t_z \rrbracket = 0 \implies \frac{1}{r_1} \frac{\partial \bar{\sigma}_{\theta z}}{\partial \theta} + \sigma_{rz}^{(2)}(r_1) - \sigma_{rz}^{(1)}(r_1) = 0, \quad (49)$$

- prescribed displacement at $r \rightarrow \infty$:

$$u_z^{(2)}(r \rightarrow \infty) = \beta r \cos \theta \implies X_3 = 1. \quad (50)$$

The conditions (47)–(50) lead to the system of equations

$$\begin{bmatrix} \mu_{\text{ax}}^{(1)} + \frac{[1 - \bar{\alpha}] \bar{\mu}_{\text{ax}}}{r_1} & \mu_{\text{ax}}^{(2)} + \frac{\bar{\alpha} \bar{\mu}_{\text{ax}}}{r_1} \\ r_1 + \frac{\bar{\alpha} \mu_{\text{ax}}^{(1)}}{\bar{k}_z} & -r_1 - \frac{[1 - \bar{\alpha}] \mu_{\text{ax}}^{(2)}}{\bar{k}_z} \end{bmatrix} \begin{bmatrix} X_1 \\ X_4 \end{bmatrix} = \begin{bmatrix} \mu_{\text{ax}}^{(2)} - \frac{\bar{\alpha} \bar{\mu}_{\text{ax}}}{r_1} \\ r_1 - \frac{[1 - \bar{\alpha}] \mu_{\text{ax}}^{(2)}}{\bar{k}_z} \end{bmatrix}, \quad (51)$$

from which the unknowns X_1 and X_4 can be determined. Using Eqs. (28) and (29), we can write

$$\boldsymbol{\varepsilon}^{(1)} = X_1 \boldsymbol{\varepsilon}^{(0)}, \quad \boldsymbol{\varepsilon}^{(\text{eq})} = [1 + X_4] \boldsymbol{\varepsilon}^{(0)}, \quad \boldsymbol{\sigma}^{(\text{eq})} = \mu_{\text{ax}}^{(2)} [1 - X_4] \boldsymbol{\varepsilon}^{(0)}, \quad (52)$$

which yields

$$T_{55}^{(1)} = X_1, \quad T_{55}^{(\text{eq})} = [1 + X_4], \quad H_{55}^{(\text{eq})} = \mu_{\text{ax}}^{(2)} [1 - X_4], \quad (53)$$

where X_1 and X_4 are the solution of the system (51).

3.1.2. Transverse shear loading

For this case, the far field displacement/strain applied to the RVE read

$$\mathbf{u}^{(0)} = \begin{bmatrix} \beta r \sin 2\theta \\ \beta r \cos 2\theta \\ 0 \end{bmatrix} \Rightarrow \boldsymbol{\varepsilon}^{(0)} = \begin{bmatrix} \beta \sin 2\theta & \beta \cos 2\theta & 0 \\ \beta \cos 2\theta & -\beta \sin 2\theta & 0 \\ 0 & 0 & 0 \end{bmatrix}. \quad (54)$$

The displacement fields within each constituent due to the prescribed boundary condition read

$$\begin{aligned} u_r^{(1)} &= \beta r \sin(2\theta) \left[\frac{\kappa^{(1)} - \mu^{(1)}}{[2\kappa^{(1)} + \mu^{(1)}]} [r/r_1]^2 X_1 + X_2 - \frac{X_3}{[r/r_1]^4} + \frac{\kappa^{(1)} + \mu^{(1)}}{\mu^{(1)}} \frac{X_4}{[r/r_1]^2} \right], \\ u_\theta^{(1)} &= \beta r \cos(2\theta) \left[[r/r_1]^2 X_1 + X_2 + \frac{X_3}{[r/r_1]^4} + \frac{X_4}{[r/r_1]^2} \right], \\ u_z^{(1)} &= 0, \\ u_r^{(2)} &= \beta r \sin(2\theta) \left[\frac{\kappa^{(2)} - \mu^{(2)}}{[2\kappa^{(2)} + \mu^{(2)}]} [r/r_1]^2 X_5 + X_6 - \frac{X_7}{[r/r_1]^4} + \frac{\kappa^{(2)} + \mu^{(2)}}{\mu^{(2)}} \frac{X_8}{[r/r_1]^2} \right], \\ u_\theta^{(2)} &= \beta r \cos(2\theta) \left[[r/r_1]^2 X_5 + X_6 + \frac{X_7}{[r/r_1]^4} + \frac{X_8}{[r/r_1]^2} \right], \\ u_z^{(2)} &= 0, \end{aligned} \quad (55)$$

with the eight unknowns X_1 – X_8 which can be determined via applying the boundary and interface conditions

- finite displacement at $r = 0$:

$$u_r^{(1)}(r = 0) \rightarrow \infty \quad \text{and} \quad u_\theta^{(1)}(r = 0) \rightarrow \infty \Rightarrow X_3 = 0 \quad \text{and} \quad X_4 = 0, \quad (56)$$

- orthogonal equilibrium in r direction at $r = r_1$:

$$\bar{t}_r = \bar{k}_r \llbracket u_r \rrbracket \Rightarrow [1 - \bar{\alpha}] \sigma_{rr}^{(2)}(r_1) + \bar{\alpha} \sigma_{rr}^{(1)}(r_1) = \bar{k}_r [u_r^{(2)}(r_1) - u_r^{(1)}(r_1)], \quad (57)$$

- orthogonal equilibrium in θ direction at $r = r_1$:

$$\bar{t}_\theta = \bar{k}_\theta \llbracket u_\theta \rrbracket \Rightarrow [1 - \bar{\alpha}] \sigma_{r\theta}^{(2)}(r_1) + \bar{\alpha} \sigma_{r\theta}^{(1)}(r_1) = \bar{k}_\theta [u_\theta^{(2)}(r_1) - u_\theta^{(1)}(r_1)], \quad (58)$$

- tangential equilibrium in r direction at $r = r_1$:

$$\left[\overline{\text{div}} \bar{\sigma} \right]_r + \llbracket t_r \rrbracket = 0 \Rightarrow -\frac{\bar{\sigma}_{\theta\theta}}{r_1} + \sigma_{rr}^{(2)}(r_1) - \sigma_{rr}^{(1)}(r_1) = 0, \quad (59)$$

- tangential equilibrium in θ direction at $r = r_1$:

$$\left[\overline{\text{div}} \bar{\sigma} \right]_\theta + \llbracket t_\theta \rrbracket = 0 \Rightarrow \frac{1}{r_1} \frac{\partial \bar{\sigma}_{\theta\theta}}{\partial \theta} + \sigma_{r\theta}^{(2)}(r_1) - \sigma_{r\theta}^{(1)}(r_1) = 0, \quad (60)$$

- prescribed displacements at $r \rightarrow \infty$:

$$u_r^{(2)}(r \rightarrow \infty) = \beta r_2 \sin(2\theta) \quad \text{and} \quad u_\theta^{(2)}(r \rightarrow \infty) = \beta r_2 \cos(2\theta) \Rightarrow X_5 = 1 \quad \text{and} \quad X_6 = 1. \quad (61)$$

The conditions (56)–(61) lead to the system of equations

$$\begin{bmatrix} \frac{\xi_1}{[2\kappa^{(1)} + \mu_{tr}^{(1)}]r_1} & -2\mu_{tr}^{(1)} + \frac{2[1 - \bar{\alpha}]\bar{\mu}_{tr}}{r_1} & 6\mu_{tr}^{(2)} + \frac{6\bar{\mu}_{tr}\bar{\alpha}}{r_1} & -4\kappa^{(2)} - \frac{2\bar{\alpha}\bar{\mu}_{tr}\lambda^{(2)}}{\mu_{tr}^{(2)}r_1} \\ \frac{\xi_2}{[2\kappa^{(1)} + \mu_{tr}^{(1)}]r_1} & -2\mu_{tr}^{(1)} - \frac{4\bar{\mu}_{tr}[1 - \bar{\alpha}]}{r_1} & -6\mu_{tr}^{(2)} - \frac{12\bar{\alpha}\bar{\mu}_{tr}}{r_1} & 2\kappa^{(2)} + \frac{4\bar{\alpha}\bar{\mu}_{tr}\lambda^{(2)}}{\mu_{tr}^{(2)}r_1} \\ \frac{\lambda^{(1)}r_1}{2\kappa^{(1)} + \mu_{tr}^{(1)}} & r_1 + \frac{2\bar{\alpha}\mu_{tr}^{(1)}}{\bar{k}_r} & r_1 + \frac{6[1 - \bar{\alpha}]\mu_{tr}^{(2)}}{\bar{k}_r} & -r_1 - \frac{r_1\kappa^{(2)}}{\mu_{tr}^{(2)}} - \frac{4[1 - \bar{\alpha}]\kappa^{(2)}}{\bar{k}_r r_1} \\ r_1 + \frac{6\bar{\alpha}\kappa^{(1)}\mu_{tr}^{(1)}}{[2\kappa^{(1)} + \mu_{tr}^{(1)}]\bar{k}_\theta} & r_1 + \frac{2\bar{\alpha}\mu_{tr}^{(1)}}{\bar{k}_\theta} & -r_1 - \frac{6[1 - \bar{\alpha}]\mu_{tr}^{(2)}}{\bar{k}_\theta} & -r_1 + \frac{2[1 - \bar{\alpha}]\kappa^{(2)}}{\bar{k}_\theta} \end{bmatrix} \begin{bmatrix} X_1 \\ X_2 \\ X_7 \\ X_8 \end{bmatrix} = \begin{bmatrix} -2\mu_{tr}^{(2)} - \frac{2\bar{\alpha}\bar{\mu}_{tr}}{r_1} \\ -2\mu_{tr}^{(2)} + \frac{4\bar{\alpha}\bar{\mu}_{tr}}{r_1} \\ r_1 - \frac{2[1 - \bar{\alpha}]\mu_{tr}^{(2)}}{\bar{k}_r r_1} \\ r_1 - \frac{2[1 - \bar{\alpha}]\mu_{tr}^{(2)}}{\bar{k}_\theta r_1} \end{bmatrix}, \quad (62)$$

with

$$\xi_1 = 6[1 - \bar{\alpha}]\bar{\mu}_{tr}[\kappa^{(1)} + \mu_{tr}^{(1)}], \quad \xi_2 = -6[2\bar{\mu}_{tr}[1 - \bar{\alpha}][\kappa^{(1)} + \mu_{tr}^{(1)}] + \kappa^{(1)}\mu_{tr}^{(1)}r_1]. \quad (63)$$

The unknowns X_1 , X_2 , X_7 and X_8 can be determined from Eq. (62). Using Eqs. (28) and (29) we can write

$$\begin{aligned} \boldsymbol{\varepsilon}^{(1)} &= \frac{1}{2} \left[\frac{u_r^{(1)}(r_1)}{\beta r_1 \sin(2\theta)} + \frac{u_\theta^{(1)}(r_1)}{\beta r_1 \cos(2\theta)} \right] \boldsymbol{\varepsilon}^{(0)}, \\ \boldsymbol{\varepsilon}^{(eq)} &= \frac{1}{2} \left[\frac{u_r^{(2)}(r_1)}{\beta r_1 \sin(2\theta)} + \frac{u_\theta^{(2)}(r_1)}{\beta r_1 \cos(2\theta)} \right] \boldsymbol{\varepsilon}^{(0)}, \\ \boldsymbol{\sigma}^{(eq)} &= \frac{1}{2} \left[\frac{\sigma_{rr}^{(2)}(r_1)}{\beta \sin(2\theta)} + \frac{\sigma_{r\theta}^{(2)}(r_1)}{\beta \cos(2\theta)} \right] \boldsymbol{\varepsilon}^{(0)}, \end{aligned} \quad (64)$$

leading to

$$\begin{aligned}
 T_{44}^{(1)} &= \frac{3\kappa^{(1)}}{4\kappa^{(1)} + 2\mu_{tr}^{(1)}} X_1 + X_2, \\
 T_{44}^{(eq)} &= 1 + \frac{\kappa^{(2)} + 2\mu_{tr}^{(2)}}{2\mu_{tr}^{(2)}} X_8, \\
 H_{44}^{(eq)} &= \mu_{tr}^{(2)} - \frac{\kappa^{(2)}}{2} X_8,
 \end{aligned} \tag{65}$$

where X_1 , X_2 and X_8 are the solution of the system (62).

3.1.3. Overall axisymmetric loading

For this case, consider the far field displacement/strain applied to the RVE are

$$\mathbf{u}^{(0)} = \begin{bmatrix} \beta r \\ 0 \\ \beta z \end{bmatrix} \implies \boldsymbol{\varepsilon}^{(0)} = \begin{bmatrix} \beta & 0 & 0 \\ 0 & \beta & 0 \\ 0 & 0 & \beta \end{bmatrix}. \tag{66}$$

The displacement fields within each constituent due to the prescribed boundary condition read

$$\begin{aligned}
 u_r^{(1)} &= \beta r \left[X_1 + X_2 \frac{1}{[r/r_1]^2} \right] \quad \text{and} \quad u_\theta^{(1)} = 0 \quad \text{and} \quad u_z^{(1)} = \beta z, \\
 u_r^{(2)} &= \beta r \left[X_3 + X_4 \frac{1}{[r/r_1]^2} \right] \quad \text{and} \quad u_\theta^{(2)} = 0 \quad \text{and} \quad u_z^{(2)} = \beta z,
 \end{aligned} \tag{67}$$

with the four unknowns X_1 – X_4 which can be determined via applying the boundary and interface conditions

- finite displacement at $r = 0$:

$$u_r^{(1)}(r = 0) \rightarrow \infty \implies X_2 = 0, \tag{68}$$

- orthogonal equilibrium at $r = r_1$:

$$\bar{t}_r = \bar{k}_r \llbracket u_r \rrbracket \implies [1 - \bar{\alpha}] \sigma_{rr}^{(2)}(r_1) + \bar{\alpha} \sigma_{rr}^{(1)}(r_1) = \bar{k}_r [u_r^{(2)}(r_1) - u_r^{(1)}(r_1)], \tag{69}$$

- tangential equilibrium at $r = r_1$:

$$\left[\overline{\text{div}} \bar{\boldsymbol{\sigma}} \right]_r + \llbracket t_r \rrbracket = 0 \implies -\frac{\bar{\sigma}_{\theta\theta}}{r_1} + \sigma_{rr}^{(2)}(r_1) - \sigma_{rr}^{(1)}(r_1) = 0, \tag{70}$$

- prescribed displacement at $r \rightarrow \infty$:

$$u_r^{(2)}(r \rightarrow \infty) = \beta r \implies X_3 = 1. \tag{71}$$

The conditions (68)–(71) lead to the system of equations

$$\begin{bmatrix} 2\kappa^{(1)} + \frac{2[1-\bar{\alpha}]\bar{\mu}_{tr}}{r_1} & 2\mu_{tr}^{(2)} + \frac{2\bar{\alpha}\bar{\mu}_{tr}}{r_1} \\ r_1 + \frac{2\bar{\alpha}\kappa^{(1)}}{\bar{k}_r} & -r_1 - \frac{2[1-\bar{\alpha}]\mu_{tr}^{(2)}}{\bar{k}_r} \end{bmatrix} \begin{bmatrix} X_1 \\ X_4 \end{bmatrix} = \begin{bmatrix} 2\kappa^{(2)} - \frac{2\bar{\alpha}\bar{\mu}_{tr}}{r_1} \\ r_1 - \frac{2[1-\bar{\alpha}]\kappa^{(2)}}{\bar{k}_r} \end{bmatrix}, \quad (72)$$

from which the unknowns X_1 and X_4 can be determined. Using Eqs. (28) and (29) we can write

$$\begin{aligned} \boldsymbol{\varepsilon}^{(1)} &= \begin{bmatrix} \beta X_1 & 0 & 0 \\ 0 & \beta X_1 & 0 \\ 0 & 0 & \beta \end{bmatrix}, \\ \boldsymbol{\varepsilon}^{(eq)} &= \begin{bmatrix} \beta[1+X_4] & 0 & 0 \\ 0 & \beta[1+X_4] & 0 \\ 0 & 0 & \beta \end{bmatrix}, \\ \boldsymbol{\sigma}^{(eq)} &= \begin{bmatrix} \beta[2\kappa^{(2)} - 2\mu_{tr}^{(2)}X_4] & 0 & 0 \\ 0 & \beta[2\kappa^{(2)} - 2\mu_{tr}^{(2)}X_4] & 0 \\ 0 & 0 & \beta 2\lambda^{(1)}X_1 \end{bmatrix} + \begin{bmatrix} \beta\lambda^{(2)} & 0 & 0 \\ 0 & \beta\lambda^{(2)} & 0 \\ 0 & 0 & \beta \left[\kappa^{(1)} + \mu_{tr}^{(1)} + \frac{4\bar{\mu}_{tr}}{r_1} \right] \end{bmatrix}, \end{aligned} \quad (73)$$

which leads to

$$\begin{aligned} T_{13}^{(1)} &= X_1 + T_{44}^{(1)} - 2T_{11}^{(1)}, \\ T_{13}^{(eq)} &= 1 + X_4 + T_{44}^{(eq)} - 2T_{11}^{(eq)}, \\ H_{13}^{(eq)} &= 2\kappa^{(2)} - 2\mu_{tr}^{(2)}X_4 + \lambda^{(2)} + 2H_{44}^{(eq)} - 2H_{11}^{(eq)}, \\ H_{33}^{(eq)} &= 2\lambda^{(1)}X_1 + \kappa^{(1)} + \mu_{tr}^{(1)} + \frac{4\bar{\mu}_{tr}}{r_1} - 2H_{31}^{(eq)}. \end{aligned} \quad (74)$$

where X_1 and X_4 are the solution of the system (72).

3.1.4. In-plane axisymmetric loading

For this case, consider the far field displacement/strain applied to the RVE are

$$\mathbf{u}^{(0)} = \begin{bmatrix} \beta r \\ 0 \\ 0 \end{bmatrix} \implies \boldsymbol{\varepsilon}^{(0)} = \begin{bmatrix} \beta & 0 & 0 \\ 0 & \beta & 0 \\ 0 & 0 & 0 \end{bmatrix}. \quad (75)$$

The displacement fields within each constituent due to the prescribed boundary condition read

$$\begin{aligned} u_r^{(1)} &= \beta r \left[X_1 + X_2 \frac{1}{[r/r_1]^2} \right] \quad \text{and} \quad u_\theta^{(1)} = u_z^{(1)} = 0, \\ u_r^{(2)} &= \beta r \left[X_3 + X_4 \frac{1}{[r/r_1]^2} \right] \quad \text{and} \quad u_\theta^{(2)} = u_z^{(2)} = 0, \end{aligned} \quad (76)$$

with the four unknowns X_1 – X_4 which can be determined via applying the boundary and interface conditions

- finite displacement at $r = 0$:

$$u_r^{(1)}(r = 0) \rightarrow \infty \Rightarrow X_2 = 0, \quad (77)$$

- orthogonal equilibrium at $r = r_1$:

$$\bar{t}_r = \bar{k}_r \llbracket u_r \rrbracket \Rightarrow [1 - \bar{\alpha}] \sigma_{rr}^{(2)}(r_1) + \bar{\alpha} \sigma_{rr}^{(1)}(r_1) = \bar{k}_r [u_r^{(2)}(r_1) - u_r^{(1)}(r_1)], \quad (78)$$

- tangential equilibrium at $r = r_1$:

$$\left[\overline{\text{div}} \bar{\sigma} \right]_r + \llbracket t_r \rrbracket = 0 \Rightarrow -\frac{\bar{\sigma}_{\theta\theta}}{r_1} + \sigma_{rr}^{(2)}(r_1) - \sigma_{rr}^{(1)}(r_1) = 0, \quad (79)$$

- prescribed displacement at $r \rightarrow \infty$:

$$u_r^{(2)}(r \rightarrow \infty) = \beta r \Rightarrow X_3 = 1. \quad (80)$$

The conditions (77)–(80) lead to the system of equations

$$\begin{bmatrix} 2\kappa^{(1)} + \frac{2[1 - \bar{\alpha}]\bar{\mu}_t}{r_1} & 2\mu_t^{(2)} + \frac{2\bar{\alpha}\bar{\mu}_t}{r_1} \\ r_1 + \frac{2\bar{\alpha}\kappa^{(1)}}{\bar{k}_r} & -r_1 - \frac{2[1 - \bar{\alpha}]\mu^{(2)}}{\bar{k}_r} \end{bmatrix} \begin{bmatrix} X_1 \\ X_4 \end{bmatrix} = \begin{bmatrix} 2\kappa^{(2)} - \frac{2\bar{\alpha}\bar{\mu}_t}{r_1} \\ r_1 - \frac{2[1 - \bar{\alpha}]\kappa^{(2)}}{\bar{k}_r} \end{bmatrix}, \quad (81)$$

from which the unknowns X_1 and X_4 can be determined. Using Eqs. (28) and (29) we can write

$$\begin{aligned}
 \boldsymbol{\varepsilon}^{(1)} &= \begin{bmatrix} \beta X_1 & 0 & 0 \\ 0 & \beta X_1 & 0 \\ 0 & 0 & 0 \end{bmatrix}, \\
 \boldsymbol{\varepsilon}^{(\text{eq})} &= \begin{bmatrix} \beta[1 + X_4] & 0 & 0 \\ 0 & \beta[1 + X_4] & 0 \\ 0 & 0 & 0 \end{bmatrix}, \\
 \boldsymbol{\sigma}^{(\text{eq})} &= \begin{bmatrix} \beta[2\kappa^{(2)} - 2\mu_{\text{tr}}^{(2)}X_4] & 0 & 0 \\ 0 & \beta[2\kappa^{(2)} - 2\mu_{\text{tr}}^{(2)}X_4] & 0 \\ 0 & 0 & 2\beta\lambda^{(1)}X_1 \end{bmatrix},
 \end{aligned} \tag{82}$$

which leads to

$$\begin{aligned}
 T_{11}^{(1)} &= \frac{1}{2} [X_1 + T_{44}^{(1)}], \\
 T_{11}^{(\text{eq})} &= \frac{1}{2} [1 + X_4 + T_{44}^{(\text{eq})}], \\
 H_{11}^{(\text{eq})} &= \kappa^{(2)} - \mu_{\text{tr}}^{(2)}X_4 + H_{44}^{(\text{eq})}, \\
 H_{31}^{(\text{eq})} &= \lambda^{(1)}X_1,
 \end{aligned} \tag{83}$$

where X_1 and X_4 are the solution of the system (81).

3.2. Particle-reinforced composites

This section aims to elaborate on boundary value problems which yield the component of the dilute concentration tensors for particle-reinforced composites. The structure of this section is deliberately organized similar to the previous section in order highlight the similarities and differences between the two problems. To determine the components of the dilute concentration tensors for particle-reinforced composites, the extended Eshelby's problem is solved analytically for two boundary value problems similar to those described by Hashin [214] in the composite sphere assemblage approach. Before proceeding with the elaboration of the boundary value problems, a brief introduction to preliminaries of particle-reinforced composites seems desirable. According to Fig. 4, a spherical coordinate system proves to be convenient to analyze particle-reinforced composites.

Table 3: Summary of relevant relations in the bulk and on the interface for particle-reinforced composites.

	bulk	interface
constitutive relations	$\begin{bmatrix} \sigma_{rr} \\ \sigma_{\theta\theta} \\ \sigma_{\phi\phi} \\ \sigma_{r\theta} \\ \sigma_{r\phi} \\ \sigma_{\theta\phi} \end{bmatrix} = \begin{bmatrix} \lambda + 2\mu & \lambda & \lambda & 0 & 0 & 0 \\ \lambda & \lambda + 2\mu & \lambda & 0 & 0 & 0 \\ \lambda & \lambda & \lambda + 2\mu & 0 & 0 & 0 \\ 0 & 0 & 0 & \mu & 0 & 0 \\ 0 & 0 & 0 & 0 & \mu & 0 \\ 0 & 0 & 0 & 0 & 0 & \mu \end{bmatrix} \begin{bmatrix} \varepsilon_{rr} \\ \varepsilon_{\theta\theta} \\ \varepsilon_{\phi\phi} \\ 2\varepsilon_{r\theta} \\ 2\varepsilon_{r\phi} \\ 2\varepsilon_{\theta\phi} \end{bmatrix}$	<p>tangential: $\begin{bmatrix} \bar{\sigma}_{\theta\theta} \\ \bar{\sigma}_{\phi\phi} \\ \bar{\sigma}_{\theta\phi} \end{bmatrix} = \begin{bmatrix} \bar{\lambda} + 2\bar{\mu} & \bar{\lambda} & 0 \\ \bar{\lambda} & \bar{\lambda} + 2\bar{\mu} & 0 \\ 0 & 0 & \bar{\mu} \end{bmatrix} \begin{bmatrix} \bar{\varepsilon}_{\theta\theta} \\ \bar{\varepsilon}_{\phi\phi} \\ 2\bar{\varepsilon}_{\theta\phi} \end{bmatrix}$</p> <p>normal: $\begin{bmatrix} \bar{t}_r \\ \bar{t}_\theta \\ \bar{t}_\phi \end{bmatrix} = \begin{bmatrix} \bar{k}_r [u_r] \\ \bar{k}_\theta [u_\theta] \\ \bar{k}_\phi [u_\phi] \end{bmatrix}$</p>
strain relations	$\varepsilon_{rr} = \frac{\partial u_r}{\partial r}$ $\varepsilon_{\theta\theta} = \frac{1}{r} \frac{\partial u_\theta}{\partial \theta} + \frac{u_r}{r}$ $\varepsilon_{\phi\phi} = \frac{1}{r \sin \theta} \frac{\partial u_\phi}{\partial \phi} + \frac{u_r}{r} + \frac{u_\theta \cos \theta}{r \sin \theta}$ $2\varepsilon_{r\theta} = \frac{\partial u_\theta}{\partial r} + \frac{1}{r} \frac{\partial u_r}{\partial \theta} - \frac{u_\theta}{r}$ $2\varepsilon_{r\phi} = \frac{\partial u_\phi}{\partial r} + \frac{1}{r \sin \theta} \frac{\partial u_r}{\partial \phi} - \frac{u_\phi}{r}$ $2\varepsilon_{\theta\phi} = \frac{1}{r} \frac{\partial u_\phi}{\partial \theta} + \frac{1}{r \sin \theta} \frac{\partial u_\theta}{\partial \phi} - \frac{u_\phi \cos \theta}{r \sin \theta}$	$\bar{\varepsilon}_{rr} = 0$ $\bar{\varepsilon}_{\theta\theta} = \frac{1}{r_1} \frac{\partial \bar{u}_\theta}{\partial \theta} + \frac{\bar{u}_r}{r_1}$ $\bar{\varepsilon}_{\phi\phi} = \frac{1}{r_1 \sin \theta} \frac{\partial \bar{u}_\phi}{\partial \phi} + \frac{\bar{u}_r}{r_1} + \frac{\bar{u}_\theta \cos \theta}{r_1 \sin \theta}$ $2\bar{\varepsilon}_{r\theta} = 0$ $2\bar{\varepsilon}_{r\phi} = 0$ $2\bar{\varepsilon}_{\theta\phi} = \frac{1}{r_1} \frac{\partial \bar{u}_\phi}{\partial \theta} + \frac{1}{r_1 \sin \theta} \frac{\partial \bar{u}_\theta}{\partial \phi} - \frac{\bar{u}_\phi \cos \theta}{r_1 \sin \theta}$
balance equations	$\frac{\partial \sigma_{rr}}{\partial r} + \frac{1}{r} \frac{\partial \sigma_{r\theta}}{\partial \theta} + \frac{\sigma_{r\theta} \cos \theta}{r \sin \theta} + \frac{2\sigma_{rr} - \sigma_{\theta\theta} - \sigma_{\phi\phi}}{r} + \frac{1}{r \sin \theta} \frac{\partial \sigma_{r\phi}}{\partial \phi} = 0$ $\frac{\partial \sigma_{r\theta}}{\partial r} + \frac{1}{r} \frac{\partial \sigma_{\theta\theta}}{\partial \theta} + \frac{3\sigma_{r\theta}}{r} + \frac{[\sigma_{\theta\theta} - \sigma_{\phi\phi}] \cos \theta}{r \sin \theta} + \frac{1}{r \sin \theta} \frac{\partial \sigma_{\theta\phi}}{\partial \phi} = 0$ $\frac{\partial \sigma_{r\phi}}{\partial r} + \frac{1}{r} \frac{\partial \sigma_{\theta\phi}}{\partial \theta} + \frac{3\sigma_{r\phi}}{r} + \frac{2\sigma_{\theta\phi} \cos \theta}{r \sin \theta} + \frac{1}{r \sin \theta} \frac{\partial \sigma_{\phi\phi}}{\partial \phi} = 0$	$\frac{\bar{\sigma}_{\theta\theta} + \bar{\sigma}_{\phi\phi}}{r_1} - [\bar{\sigma}_{rr}] = 0$ $\frac{1}{r_1} \frac{\partial \bar{\sigma}_{\theta\theta}}{\partial \theta} + \frac{1}{r_1 \sin \theta} \frac{\partial \bar{\sigma}_{\theta\phi}}{\partial \phi} + \frac{[\bar{\sigma}_{\theta\theta} - \bar{\sigma}_{\phi\phi}] \cos \theta}{r_1 \sin \theta} + [\bar{\sigma}_{r\theta}] = 0$ $\frac{1}{r_1} \frac{\partial \bar{\sigma}_{\theta\phi}}{\partial \theta} + \frac{1}{r_1 \sin \theta} \frac{\partial \bar{\sigma}_{\phi\phi}}{\partial \phi} + \frac{2\bar{\sigma}_{\theta\phi} \cos \theta}{r_1 \sin \theta} + [\bar{\sigma}_{r\phi}] = 0$

The constitutive material behavior for the bulk, in Voigt notation, reads

$$\begin{bmatrix} \sigma_{rr} \\ \sigma_{\theta\theta} \\ \sigma_{\phi\phi} \\ \sigma_{r\theta} \\ \sigma_{r\phi} \\ \sigma_{\theta\phi} \end{bmatrix} = \begin{bmatrix} \lambda + 2\mu & \lambda & \lambda & 0 & 0 & 0 \\ \lambda & \lambda + 2\mu & \lambda & 0 & 0 & 0 \\ \lambda & \lambda & \lambda + 2\mu & 0 & 0 & 0 \\ 0 & 0 & 0 & \mu & 0 & 0 \\ 0 & 0 & 0 & 0 & \mu & 0 \\ 0 & 0 & 0 & 0 & 0 & \mu \end{bmatrix} \begin{bmatrix} \varepsilon_{rr} \\ \varepsilon_{\theta\theta} \\ \varepsilon_{\phi\phi} \\ 2\varepsilon_{r\theta} \\ 2\varepsilon_{r\phi} \\ 2\varepsilon_{\theta\phi} \end{bmatrix}. \quad (84)$$

For this case, the bulk modulus κ relates to the Lamé parameters via $\kappa = \lambda + 2\mu/3$. The strain field in the bulk reads

$$\varepsilon_{rr} = \frac{\partial u_r}{\partial r}, \quad \varepsilon_{\theta\theta} = \frac{1}{r} \frac{\partial u_\theta}{\partial \theta} + \frac{u_r}{r}, \quad \varepsilon_{\phi\phi} = \frac{1}{r \sin \theta} \frac{\partial u_\phi}{\partial \phi} + \frac{u_r}{r} + \frac{u_\theta \cos \theta}{r \sin \theta},$$

$$2\varepsilon_{r\theta} = \frac{\partial u_\theta}{\partial r} + \frac{1}{r} \frac{\partial u_r}{\partial \theta} - \frac{u_\theta}{r}, \quad 2\varepsilon_{\theta\phi} = \frac{1}{r} \frac{\partial u_\phi}{\partial \theta} + \frac{1}{r \sin \theta} \frac{\partial u_\theta}{\partial \phi} - \frac{u_\phi \cos \theta}{r \sin \theta}, \quad 2\varepsilon_{r\phi} = \frac{\partial u_\phi}{\partial r} + \frac{1}{r} \frac{\partial u_r}{\partial \phi} - \frac{u_\phi}{r}, \quad (85)$$

and the balance equations for the bulk read

$$\begin{aligned}
 \frac{\partial \sigma_{rr}}{\partial r} + \frac{1}{r} \frac{\partial \sigma_{r\theta}}{\partial \theta} + \frac{\sigma_{r\theta} \cos \theta}{r \sin \theta} + \frac{2\sigma_{rr} - \sigma_{\theta\theta} - \sigma_{\phi\phi}}{r} + \frac{1}{r \sin \theta} \frac{\partial \sigma_{r\phi}}{\partial \phi} &= 0, \\
 \frac{\partial \sigma_{r\theta}}{\partial r} + \frac{1}{r} \frac{\partial \sigma_{\theta\theta}}{\partial \theta} + \frac{3\sigma_{r\theta}}{r} + \frac{[\sigma_{\theta\theta} - \sigma_{\phi\phi}] \cos \theta}{r \sin \theta} + \frac{1}{r \sin \theta} \frac{\partial \sigma_{\theta\phi}}{\partial \phi} &= 0, \\
 \frac{\partial \sigma_{r\phi}}{\partial r} + \frac{1}{r} \frac{\partial \sigma_{\theta\phi}}{\partial \theta} + \frac{3\sigma_{r\phi}}{r} + \frac{2\sigma_{\theta\phi} \cos \theta}{r \sin \theta} + \frac{1}{r \sin \theta} \frac{\partial \sigma_{\phi\phi}}{\partial \phi} &= 0.
 \end{aligned} \tag{86}$$

As mentioned before, for the interface, the constitutive behavior is decomposed into tangential and orthogonal behavior reading

$$\text{tangential: } \begin{bmatrix} \bar{\sigma}_{\theta\theta} \\ \bar{\sigma}_{\phi\phi} \\ \bar{\sigma}_{\theta\phi} \end{bmatrix} = \begin{bmatrix} \bar{\lambda} + 2\bar{\mu} & \bar{\lambda} & 0 \\ \bar{\lambda} & \bar{\lambda} + 2\bar{\mu} & 0 \\ 0 & 0 & \bar{\mu} \end{bmatrix} \begin{bmatrix} \bar{\varepsilon}_{\theta\theta} \\ \bar{\varepsilon}_{\phi\phi} \\ 2\bar{\varepsilon}_{\theta\phi} \end{bmatrix}, \quad \text{orthogonal: } \begin{bmatrix} \bar{t}_r \\ \bar{t}_\theta \\ \bar{t}_\phi \end{bmatrix} = \begin{bmatrix} \bar{k}_r \llbracket u_r \rrbracket \\ \bar{k}_\theta \llbracket u_\theta \rrbracket \\ \bar{k}_\phi \llbracket u_\phi \rrbracket \end{bmatrix}. \tag{87}$$

Note, we assumed that the interface orthogonal stiffness in all the three directions is the same. The strain field on the interface reads

$$\bar{\varepsilon}_{\theta\theta} = \frac{1}{r_1} \frac{\partial \bar{u}_\theta}{\partial \theta} + \frac{\bar{u}_r}{r_1}, \quad \bar{\varepsilon}_{\phi\phi} = \frac{1}{r_1 \sin \theta} \frac{\partial \bar{u}_\phi}{\partial \phi} + \frac{\bar{u}_r}{r_1} + \frac{\bar{u}_\theta \cos \theta}{r_1 \sin \theta}, \quad 2\bar{\varepsilon}_{\theta\phi} = \frac{1}{r_1} \frac{\partial \bar{u}_\phi}{\partial \theta} + \frac{1}{r_1 \sin \theta} \frac{\partial \bar{u}_\theta}{\partial \phi} - \frac{\bar{u}_\phi \cos \theta}{r_1 \sin \theta}, \tag{88}$$

and the interface balance equations read

$$\begin{aligned}
 \frac{\bar{\sigma}_{\theta\theta} + \bar{\sigma}_{\phi\phi}}{r_1} - \llbracket \sigma_{rr} \rrbracket &= 0, \\
 \frac{1}{r_1} \frac{\partial \bar{\sigma}_{\theta\theta}}{\partial \theta} + \frac{1}{r_1 \sin \theta} \frac{\partial \bar{\sigma}_{\theta\phi}}{\partial \phi} + \frac{[\bar{\sigma}_{\theta\theta} - \bar{\sigma}_{\phi\phi}] \cos \theta}{r_1 \sin \theta} + \llbracket \sigma_{r\theta} \rrbracket &= 0, \\
 \frac{1}{r_1} \frac{\partial \bar{\sigma}_{\theta\phi}}{\partial \theta} + \frac{1}{r_1 \sin \theta} \frac{\partial \bar{\sigma}_{\phi\phi}}{\partial \phi} + \frac{2\bar{\sigma}_{\theta\phi} \cos \theta}{r_1 \sin \theta} + \llbracket \sigma_{r\phi} \rrbracket &= 0.
 \end{aligned} \tag{89}$$

Table 3 summarizes the relevant constitutive relations, strain relations and balance equations for the bulk and the interface for fiber-reinforced composites.

According to Eq. (84), the elasticity tensors for the particle and the matrix, in Voigt notation, can be written as

$$\mathbb{C}^{(1)} = \begin{bmatrix} \lambda^{(1)} + 2\mu^{(1)} & \lambda^{(1)} & \lambda^{(1)} & 0 & 0 & 0 \\ \lambda^{(1)} & \lambda^{(1)} + 2\mu^{(1)} & \lambda^{(1)} & 0 & 0 & 0 \\ \lambda^{(1)} & \lambda^{(1)} & \lambda^{(1)} + 2\mu^{(1)} & 0 & 0 & 0 \\ 0 & 0 & 0 & \mu^{(1)} & 0 & 0 \\ 0 & 0 & 0 & 0 & \mu^{(1)} & 0 \\ 0 & 0 & 0 & 0 & 0 & \mu^{(1)} \end{bmatrix}, \quad \mathbb{C}^{(2)} = \begin{bmatrix} \lambda^{(2)} + 2\mu^{(2)} & \lambda^{(2)} & \lambda^{(2)} & 0 & 0 & 0 \\ \lambda^{(2)} & \lambda^{(2)} + 2\mu^{(2)} & \lambda^{(2)} & 0 & 0 & 0 \\ \lambda^{(2)} & \lambda^{(2)} & \lambda^{(2)} + 2\mu^{(2)} & 0 & 0 & 0 \\ 0 & 0 & 0 & \mu^{(2)} & 0 & 0 \\ 0 & 0 & 0 & 0 & \mu^{(2)} & 0 \\ 0 & 0 & 0 & 0 & 0 & \mu^{(2)} \end{bmatrix}. \tag{90}$$

The interactions tensors for the inhomogeneity, in Voigt notation, take the form

$$\mathbb{T}^{(1)} = \begin{bmatrix} T_{11}^{(1)} & T_{11}^{(1)} - T_{44}^{(1)} & T_{11}^{(1)} - T_{44}^{(1)} & 0 & 0 & 0 \\ T_{11}^{(1)} - T_{44}^{(1)} & T_{11}^{(1)} & T_{11}^{(1)} - T_{44}^{(1)} & 0 & 0 & 0 \\ T_{11}^{(1)} - T_{44}^{(1)} & T_{11}^{(1)} - T_{44}^{(1)} & T_{11}^{(1)} & 0 & 0 & 0 \\ 0 & 0 & 0 & T_{44}^{(1)} & 0 & 0 \\ 0 & 0 & 0 & 0 & T_{44}^{(1)} & 0 \\ 0 & 0 & 0 & 0 & 0 & T_{44}^{(1)} \end{bmatrix}, \quad \mathbb{H}^{(1)} = \begin{bmatrix} H_{11}^{(1)} & H_{11}^{(1)} - 2H_{44}^{(1)} & H_{11}^{(1)} - 2H_{44}^{(1)} & 0 & 0 & 0 \\ H_{11}^{(1)} - 2H_{44}^{(1)} & H_{11}^{(1)} & H_{11}^{(1)} - 2H_{44}^{(1)} & 0 & 0 & 0 \\ H_{11}^{(1)} - 2H_{44}^{(1)} & H_{11}^{(1)} - 2H_{44}^{(1)} & H_{11}^{(1)} & 0 & 0 & 0 \\ 0 & 0 & 0 & H_{44}^{(1)} & 0 & 0 \\ 0 & 0 & 0 & 0 & H_{44}^{(1)} & 0 \\ 0 & 0 & 0 & 0 & 0 & H_{44}^{(1)} \end{bmatrix}. \quad (91)$$

The interaction tensors for the inhomogeneity/interface system read

$$\mathbb{T}^{(eq)} = \begin{bmatrix} T_{11}^{(eq)} & T_{11}^{(eq)} - T_{44}^{(eq)} & T_{11}^{(eq)} - T_{44}^{(eq)} & 0 & 0 & 0 \\ T_{11}^{(eq)} - T_{44}^{(eq)} & T_{11}^{(eq)} & T_{11}^{(eq)} - T_{44}^{(eq)} & 0 & 0 & 0 \\ T_{11}^{(eq)} - T_{44}^{(eq)} & T_{11}^{(eq)} - T_{44}^{(eq)} & T_{11}^{(eq)} & 0 & 0 & 0 \\ 0 & 0 & 0 & T_{44}^{(eq)} & 0 & 0 \\ 0 & 0 & 0 & 0 & T_{44}^{(eq)} & 0 \\ 0 & 0 & 0 & 0 & 0 & T_{44}^{(eq)} \end{bmatrix}, \quad \mathbb{H}^{(eq)} = \begin{bmatrix} H_{11}^{(eq)} & H_{11}^{(eq)} - 2H_{44}^{(eq)} & H_{11}^{(eq)} - 2H_{44}^{(eq)} & 0 & 0 & 0 \\ H_{11}^{(eq)} - 2H_{44}^{(eq)} & H_{11}^{(eq)} & H_{11}^{(eq)} - 2H_{44}^{(eq)} & 0 & 0 & 0 \\ H_{11}^{(eq)} - 2H_{44}^{(eq)} & H_{11}^{(eq)} - 2H_{44}^{(eq)} & H_{11}^{(eq)} & 0 & 0 & 0 \\ 0 & 0 & 0 & H_{44}^{(eq)} & 0 & 0 \\ 0 & 0 & 0 & 0 & H_{44}^{(eq)} & 0 \\ 0 & 0 & 0 & 0 & 0 & H_{44}^{(eq)} \end{bmatrix}. \quad (92)$$

Equipped with these preliminaries, we can now proceed with the boundary value problems to determine the components of the interaction tensors.

3.2.1. Volumetric expansion loading

Consider the RVE subject to a far field displacement and strain according to

$$\mathbf{u}^{(0)} = \begin{bmatrix} \beta r \\ 0 \\ 0 \end{bmatrix} \Rightarrow \boldsymbol{\varepsilon}^{(0)} = \begin{bmatrix} \beta & 0 & 0 \\ 0 & \beta & 0 \\ 0 & 0 & \beta \end{bmatrix}. \quad (93)$$

Demonstrated by Hashin [214], the emerging displacement fields in the particle and the matrix read

$$\begin{aligned} u_r^{(1)} &= \beta r \left[X_1 + \frac{1}{[r/r_1]^3} X_2 \right] & \text{and} & \quad u_\theta^{(1)} = u_\phi^{(1)} = 0, \\ u_r^{(2)} &= \beta r \left[X_3 + \frac{1}{[r/r_1]^3} X_4 \right] & \text{and} & \quad u_\theta^{(2)} = u_\phi^{(2)} = 0, \end{aligned} \quad (94)$$

with the four unknowns X_1 – X_4 that can be determined via imposing the boundary and interface conditions

- finite displacement at $r = 0$:

$$u_r^{(1)}(r = 0) \not\rightarrow \infty \Rightarrow X_2 = 0, \quad (95)$$

- orthogonal equilibrium at $r = r_1$:

$$\bar{t}_r = \bar{k} \llbracket u_r \rrbracket \Rightarrow [1 - \bar{\alpha}] \sigma_{rr}^{(2)}(r_1) + \bar{\alpha} \sigma_{rr}^{(1)}(r_1) = \bar{k}_r [u_r^{(2)}(r_1) - u_r^{(1)}(r_1)], \quad (96)$$

- tangential equilibrium at $r = r_1$:

$$\left[\overline{\text{div}} \bar{\sigma} \right]_r + \llbracket t_r \rrbracket = 0 \Rightarrow -\frac{\bar{\sigma}_{\theta\theta} + \bar{\sigma}_{\phi\phi}}{r_1} + \sigma_{rr}^{(2)}(r_1) - \sigma_{rr}^{(1)}(r_1) = 0, \quad (97)$$

- prescribed displacement at $r \rightarrow \infty$:

$$u_r^{(2)}(r \rightarrow \infty) = \beta r \Rightarrow X_3 = 1. \quad (98)$$

The conditions (95)–(98) lead to the system of equations

$$\begin{bmatrix} r_1 + \frac{3\bar{\alpha}k^{(1)}}{\bar{k}_r} & -r_1 - \frac{4[1 - \bar{\alpha}]\mu^{(2)}}{\bar{k}_r} \\ 3\kappa^{(1)} + \frac{4[1 - \bar{\alpha}][\bar{\lambda} + \bar{\mu}]}{r_1} & 4\mu^{(2)} + \frac{4\bar{\alpha}[\bar{\lambda} + \bar{\mu}]}{r_1} \end{bmatrix} \begin{bmatrix} X_1 \\ X_4 \end{bmatrix} = \begin{bmatrix} r_1 - \frac{3[1 - \bar{\alpha}]k^{(2)}}{\bar{k}_r} \\ 3\kappa^{(2)} - \frac{4\bar{\alpha}[\bar{\lambda} + \bar{\mu}]}{r_1} \end{bmatrix}, \quad (99)$$

from which the unknowns X_1 and X_4 can be determined. Using Eqs. (28) and (29) we can write

$$\boldsymbol{\varepsilon}^{(1)} = X_1 \boldsymbol{\varepsilon}^{(0)}, \quad \boldsymbol{\varepsilon}^{(\text{eq})} = [1 + X_4] \boldsymbol{\varepsilon}^{(0)}, \quad \boldsymbol{\sigma}^{(\text{eq})} = [3\kappa^{(2)} - 4\mu^{(2)}X_4] \boldsymbol{\varepsilon}^{(0)}, \quad (100)$$

which yields

$$3T_{11}^{(1)} - 2T_{44}^{(1)} = X_1, \quad 3T_{11}^{(\text{eq})} - 2T_{44}^{(\text{eq})} = [1 + X_4], \quad 3H_{11}^{(\text{eq})} - 4H_{44}^{(\text{eq})} = [3\kappa^{(2)} - 4\mu^{(2)}X_4]. \quad (101)$$

where X_1 and X_4 are the solution of the system (99).

3.2.2. Deviatoric loading

Assume the RVE is subject to a deviatoric far field displacement

$$\mathbf{u}^{(0)} = \begin{bmatrix} \beta r \sin^2 \theta \cos 2\phi \\ \beta r \sin \theta \cos \theta \cos 2\phi \\ -\beta r \sin \theta \sin 2\phi \end{bmatrix} \Rightarrow \boldsymbol{\varepsilon}^{(0)} = \begin{bmatrix} \beta \cos 2\phi \sin^2 \theta & 2\beta \cos 2\phi \cos \theta \sin \theta & -2\beta \sin 2\phi \sin \theta \\ 2\beta \cos 2\phi \cos \theta \sin \theta & \beta \cos 2\phi \cos^2 \theta & -2\beta \sin 2\phi \cos \theta \\ -2\beta \sin 2\phi \sin \theta & -2\beta \sin 2\phi \cos \theta & -\beta \cos 2\phi \end{bmatrix}.$$

(102)

For this boundary condition, the displacement fields in the matrix and particle read

$$\begin{aligned}
 u_r^{(1)} &= \beta r \sin^2(\theta) \cos(2\phi) \left[X_1 + \left[2 - 3 \frac{\kappa^{(1)}}{\mu^{(1)}} \right] [r/r_1]^2 X_2 + \frac{3X_3}{[r/r_1]^5} + \left[3 + 3 \frac{\kappa^{(1)}}{\mu^{(1)}} \right] \frac{X_4}{[r/r_1]^3} \right], \\
 u_\theta^{(1)} &= \beta r \sin(\theta) \cos(\theta) \cos(2\phi) \left[X_1 - \left[\frac{11}{3} + 5 \frac{\kappa^{(1)}}{\mu^{(1)}} \right] [r/r_1]^2 X_2 - \frac{2X_3}{[r/r_1]^5} + \frac{2X_4}{[r/r_1]^3} \right], \\
 u_\phi^{(1)} &= -\beta r \sin(\theta) \sin(2\phi) \left[X_1 - \left[\frac{11}{3} + 5 \frac{\kappa^{(1)}}{\mu^{(1)}} \right] [r/r_1]^2 X_2 - \frac{2X_3}{[r/r_1]^5} + \frac{2X_4}{[r/r_1]^3} \right], \\
 u_r^{(2)} &= \beta r \sin^2(\theta) \cos(2\phi) \left[X_5 + \left[2 - 3 \frac{\kappa^{(2)}}{\mu^{(2)}} \right] [r/r_1]^2 X_6 + \frac{3X_7}{[r/r_1]^5} + \left[3 + 3 \frac{\kappa^{(2)}}{\mu^{(2)}} \right] \frac{X_8}{[r/r_1]^3} \right], \\
 u_\theta^{(2)} &= \beta r \sin(\theta) \cos(\theta) \cos(2\phi) \left[X_5 - \left[\frac{11}{3} + 5 \frac{\kappa^{(2)}}{\mu^{(2)}} \right] [r/r_1]^2 X_6 - \frac{2X_7}{[r/r_1]^5} + \frac{2X_8}{[r/r_1]^3} \right], \\
 u_\phi^{(2)} &= -\beta r \sin(\theta) \sin(2\phi) \left[X_5 - \left[\frac{11}{3} + 5 \frac{\kappa^{(2)}}{\mu^{(2)}} \right] [r/r_1]^2 X_6 - \frac{2X_7}{[r/r_1]^5} + \frac{2X_8}{[r/r_1]^3} \right],
 \end{aligned} \tag{103}$$

with the eight unknowns X_1 – X_8 that can be determined via imposing the boundary and interface conditions. The boundary and interface conditions necessitate

- finite displacement at $r = 0$:

$$u_r^{(1)}(r = 0) \rightarrow \infty \quad \text{and} \quad u_\theta^{(1)}(r = 0) \rightarrow \infty \Rightarrow X_3 = 0 \quad \text{and} \quad X_4 = 0, \tag{104}$$

- orthogonal equilibrium in r direction at $r = r_1$:

$$\bar{t}_r = \bar{k} \llbracket u_r \rrbracket \Rightarrow [1 - \bar{\alpha}] \sigma_{rr}^{(2)}(r_1) + \bar{\alpha} \sigma_{rr}^{(1)}(r_1) = \bar{k}_r [u_r^{(2)}(r_1) - u_r^{(1)}(r_1)], \tag{105}$$

- orthogonal equilibrium in θ direction at $r = r_1$:

$$\bar{t}_\theta = \bar{k} \llbracket u_\theta \rrbracket \Rightarrow [1 - \bar{\alpha}] \sigma_{r\theta}^{(2)}(r_1) + \bar{\alpha} \sigma_{r\theta}^{(1)}(r_1) = \bar{k}_\theta [u_\theta^{(2)}(r_1) - u_\theta^{(1)}(r_1)], \tag{106}$$

- tangential equilibrium in r direction at $r = r_1$:

$$\left[\overline{\text{div}} \bar{\sigma} \right]_r + \llbracket t_r \rrbracket = 0 \rightarrow -\frac{\bar{\sigma}_{\theta\theta} + \bar{\sigma}_{\phi\phi}}{r_1} + \sigma_{rr}^{(2)}(r_1) - \sigma_{rr}^{(1)}(r_1) = 0 \tag{107}$$

- tangential equilibrium in θ direction at $r = r_1$:

$$\left[\overline{\text{div}} \bar{\sigma} \right]_\theta + \llbracket t_\theta \rrbracket = 0 \rightarrow \frac{1}{r_1} \frac{\partial \bar{\sigma}_{\theta\theta}}{\partial \theta} + \frac{1}{r_1 \sin \theta} \frac{\partial \bar{\sigma}_{\theta\phi}}{\partial \phi} + \frac{[\bar{\sigma}_{\theta\theta} - \bar{\sigma}_{\phi\phi}] \cos \theta}{r_1 \sin \theta} + \sigma_{r\theta}^{(2)}(r_1) - \sigma_{r\theta}^{(1)}(r_1) = 0 \tag{108}$$

- prescribed displacements at $r \rightarrow \infty$:

$$u_r^{(2)}(r \rightarrow \infty) = \beta r \sin^2 \theta \cos 2\phi \quad \text{and} \quad u_\theta^{(2)}(r \rightarrow \infty) = \beta r \sin \theta \cos \theta \cos 2\phi \Rightarrow X_5 = 1 \quad \text{and} \quad X_6 = 1, \tag{109}$$

resulting in the system of equations

$$\begin{bmatrix} 1 + \frac{2\bar{\alpha}\mu^{(1)}}{\bar{k}_r r_1} & 2 - 3\frac{\kappa^{(1)}}{\mu^{(1)}} + \bar{\alpha}\zeta_1 & -3 - \frac{24[1 - \bar{\alpha}]\mu^{(2)}}{\bar{k}_r r_1} & -3 - 3\frac{\kappa^{(2)}}{\mu^{(2)}} - [1 - \bar{\alpha}]\zeta_2 \\ 1 + \frac{2\bar{\alpha}\mu^{(1)}}{\bar{k}_\theta r_1} & -\frac{11}{3} - 5\frac{\kappa^{(1)}}{\mu^{(1)}} - 2\bar{\alpha}\zeta_3 & 2 + \frac{16[1 - \bar{\alpha}]\mu^{(2)}}{\bar{k}_\theta r_1} & -2 + \frac{6[1 - \bar{\alpha}]\kappa^{(2)}}{\bar{k}_\theta r_1} \\ -2\mu^{(1)} + \frac{2[1 - \bar{\alpha}]\zeta_0}{r_1} & 2\mu^{(1)} - 3\kappa^{(1)} - 2[1 - \bar{\alpha}]\zeta_4 & -24\mu^{(2)} - \frac{24\bar{\alpha}\zeta_0}{r_1} & -\bar{k}_r \zeta_2 - \frac{12\bar{\alpha}\kappa^{(2)}\zeta_0}{\mu^{(2)}r_1} \\ -2\mu^{(1)} - 2[1 - \bar{\alpha}]\zeta_5 & 16\kappa^{(1)} + \frac{10}{3}\mu^{(1)} + 2[1 - \bar{\alpha}]\zeta_6 & 16\mu^{(2)} + 8\bar{\alpha}\zeta_7 & 6\kappa^{(2)} + 2\bar{\alpha}\zeta_8 \end{bmatrix} \begin{bmatrix} X_1 \\ X_2 \\ X_7 \\ X_8 \end{bmatrix} = \begin{bmatrix} 1 - \frac{2[1 - \bar{\alpha}]\mu^{(2)}}{\bar{k}_r r_1} \\ 1 - \frac{2\bar{\alpha}\mu^{(2)}}{\bar{k}_\theta r_1} \\ -2\mu^{(2)} - \frac{2\bar{\alpha}\zeta_0}{r_1} \\ -2\mu^{(2)} + 2\bar{\alpha}\zeta_5 \end{bmatrix}, \quad (110)$$

with

$$\begin{aligned} \zeta_0 &= \bar{\lambda} + \bar{\mu}, \quad \zeta_1 = \frac{3\kappa^{(1)} - 2\mu^{(1)}}{\bar{k}_r r_1}, \quad \zeta_2 = \frac{18\kappa^{(2)} + 8\mu^{(2)}}{\bar{k}_r r_1}, \quad \zeta_3 = \frac{8\kappa^{(1)} + 5\mu^{(1)}}{3\bar{k}_\theta r_1}, \quad \zeta_4 = \frac{[9\kappa^{(1)} + 15\mu^{(1)}][\bar{\lambda} + \bar{\mu}]}{\mu^{(1)}r_1}, \\ \zeta_5 &= \frac{[\bar{\lambda} + 3\bar{\mu}]}{r_1}, \quad \zeta_6 = \frac{\kappa^{(1)}[27\bar{\lambda} + 57\bar{\mu}]}{\mu^{(1)}r_1} + \frac{\mu^{(1)}[45\bar{\lambda} + 67\bar{\mu}]}{3r_1}, \quad \zeta_7 = \frac{[3\bar{\lambda} + 4\bar{\mu}]}{r_1}, \quad \zeta_8 = \frac{6\kappa^{(2)}[\bar{\lambda} + \bar{\mu}] - 4\mu^{(2)}\bar{\mu}}{\mu^{(2)}r_1}. \end{aligned} \quad (111)$$

Using Eqs. (28) and (29) we can write

$$\begin{aligned} \boldsymbol{\varepsilon}^{(1)} &= \frac{1}{5} \left[5X_1 - 7 \left[1 + 3\frac{\kappa^{(1)}}{\mu^{(1)}} \right] X_2 \right] \boldsymbol{\varepsilon}^{(0)}, \\ \boldsymbol{\varepsilon}^{(eq)} &= \frac{1}{5} \left[5 + 6 \left[2 + \frac{\kappa^{(2)}}{\mu^{(2)}} \right] X_8 \right] \boldsymbol{\varepsilon}^{(0)}, \\ \boldsymbol{\sigma}^{(eq)} &= \frac{1}{5} \left[10\mu^{(2)} - 2 \left[9\kappa^{(2)} + 8\mu^{(2)} \right] X_8 \right] \boldsymbol{\varepsilon}^{(0)}. \end{aligned} \quad (112)$$

Consequently, the shear interaction terms read

$$2T_{44}^{(1)} = \frac{1}{5} \left[5X_1 - 7 \left[1 + 3\frac{\kappa^{(1)}}{\mu^{(1)}} \right] X_2 \right], \quad 2T_{44}^{(eq)} = \frac{1}{5} \left[5 + 6 \left[2 + \frac{\kappa^{(2)}}{\mu^{(2)}} \right] X_8 \right], \quad 2H_{44}^{(eq)} = \frac{1}{5} \left[10\mu^{(2)} - 2 \left[9\kappa^{(2)} + 8\mu^{(2)} \right] X_8 \right], \quad (113)$$

where X_1 , X_2 and X_8 are obtained from the system of equations (110).

4. Finite element implementation

The objective of this section is to develop a finite element framework suitable to account for the extended general

interface model. In this context, it proves convenient to use a curvilinear-coordinate-based finite element method [185] since it mimics the underlying geometrical and mathematical concepts for two dimensional manifolds embedded into a three dimensional space. For detailed expositions of the finite element formulation and implementation, see [215, 216] among others.

The first step towards the finite element implementation of our theory is to derive the weak form of the governing equations. To do so, the strong form of the linear momentum balance for the bulk and interface is contracted from left by a vector-valued test function $\delta\boldsymbol{\varphi} \in \mathcal{H}^1(\mathcal{B})$ and $\delta\bar{\boldsymbol{\varphi}} \in \mathcal{H}^1(\mathcal{I})$, respectively, where \mathcal{H}^1 denotes the Sobolev space of order one. Then the resulting equation is integrated over the corresponding domain. The test functions are specified to be zero on the Dirichlet part of the boundary. Integrating equations in (6) over their respective domains, the integral form of the linear momentum balance reads

$$\int_{\mathcal{B}} \text{Div} \boldsymbol{\sigma} \, dV + \int_{\mathcal{I}} \overline{\text{Div}} \bar{\boldsymbol{\sigma}} \, dA + \int_{\mathcal{I}} \llbracket \boldsymbol{\sigma} \rrbracket \cdot \bar{\mathbf{n}} \, dA = \mathbf{0}. \quad (114)$$

Upon contracting with the test functions and using the divergence theorem, after some mathematical steps, the weak form of the linear momentum balance reads

$$\begin{aligned} & \int_{\mathcal{B}} \delta\boldsymbol{\varphi} \cdot \text{Div} \boldsymbol{\sigma} \, dV + \int_{\mathcal{I}} \delta\bar{\boldsymbol{\varphi}} \cdot \overline{\text{Div}} \bar{\boldsymbol{\sigma}} \, dA + \int_{\mathcal{I}} \delta\bar{\boldsymbol{\varphi}} \cdot \llbracket \boldsymbol{\sigma} \rrbracket \cdot \bar{\mathbf{n}} \, dA \\ &= \int_{\mathcal{B}} \text{Div} [\delta\boldsymbol{\varphi} \cdot \boldsymbol{\sigma}] \, dV - \int_{\mathcal{B}} \boldsymbol{\sigma} : \text{Grad} \delta\boldsymbol{\varphi} \, dV + \int_{\mathcal{I}} \overline{\text{Div}} [\delta\bar{\boldsymbol{\varphi}} \cdot \bar{\boldsymbol{\sigma}}] \, dA - \int_{\mathcal{I}} \bar{\boldsymbol{\sigma}} : \overline{\text{Grad}} \delta\bar{\boldsymbol{\varphi}} \, dA + \int_{\mathcal{I}} \delta\bar{\boldsymbol{\varphi}} \cdot \llbracket \boldsymbol{\sigma} \rrbracket \cdot \bar{\mathbf{n}} \, dA \\ &= \int_{\partial\mathcal{B}} \delta\boldsymbol{\varphi} \cdot \boldsymbol{\sigma} \cdot \mathbf{n} \, dA - \int_{\mathcal{I}} \llbracket \delta\boldsymbol{\varphi} \cdot \boldsymbol{\sigma} \rrbracket \cdot \bar{\mathbf{n}} \, dA - \int_{\mathcal{B}} \boldsymbol{\sigma} : \text{Grad} \delta\boldsymbol{\varphi} \, dV + \int_{\partial\mathcal{I}} \delta\bar{\boldsymbol{\varphi}} \cdot \bar{\boldsymbol{\sigma}} \cdot \bar{\mathbf{n}} \, dL - \int_{\mathcal{I}} \bar{\boldsymbol{\sigma}} : \overline{\text{Grad}} \delta\bar{\boldsymbol{\varphi}} \, dA \\ &\quad - \int_{\mathcal{I}} \bar{\boldsymbol{\sigma}} : \overline{\text{Grad}} \delta\bar{\boldsymbol{\varphi}} \, dA + \int_{\mathcal{I}} \delta\bar{\boldsymbol{\varphi}} \cdot \llbracket \boldsymbol{\sigma} \rrbracket \cdot \bar{\mathbf{n}} \, dA = 0 \end{aligned} \quad (115)$$

The fifth term also vanishes due to the superficiality of the interface stress. Using identity for the jump of dot product and the relation $\delta\bar{\boldsymbol{\varphi}} = \llbracket \delta\boldsymbol{\varphi} \rrbracket_{\bar{\alpha}}$, Eq. (115) reads

$$\begin{aligned} & \int_{\partial\mathcal{B}} \delta\boldsymbol{\varphi} \cdot \boldsymbol{\sigma} \cdot \mathbf{n} \, dA - \int_{\mathcal{I}} \llbracket \delta\boldsymbol{\varphi} \rrbracket_{\bar{\alpha}} \cdot \llbracket \boldsymbol{\sigma} \rrbracket \cdot \bar{\mathbf{n}} \, dA - \int_{\mathcal{I}} \llbracket \delta\boldsymbol{\varphi} \rrbracket \cdot \bar{\mathbf{t}} \, dA - \int_{\mathcal{B}} \boldsymbol{\sigma} : \text{Grad} \delta\boldsymbol{\varphi} \, dV \\ &+ \int_{\partial\mathcal{I}} \llbracket \delta\boldsymbol{\varphi} \rrbracket_{\bar{\alpha}} \cdot \bar{\boldsymbol{\sigma}} \cdot \bar{\mathbf{n}} \, dL - \int_{\mathcal{I}} \bar{\boldsymbol{\sigma}} : \overline{\text{Grad}} \llbracket \delta\boldsymbol{\varphi} \rrbracket_{\bar{\alpha}} \, dA + \int_{\mathcal{I}} \llbracket \delta\boldsymbol{\varphi} \rrbracket_{\bar{\alpha}} \cdot \llbracket \boldsymbol{\sigma} \rrbracket \cdot \bar{\mathbf{n}} \, dA \\ &= \int_{\partial\mathcal{B}} \delta\boldsymbol{\varphi} \cdot \boldsymbol{\sigma} \cdot \mathbf{n} \, dA - \int_{\mathcal{I}} \llbracket \delta\boldsymbol{\varphi} \rrbracket \cdot \bar{\mathbf{t}} \, dA - \int_{\mathcal{B}} \boldsymbol{\sigma} : \text{Grad} \delta\boldsymbol{\varphi} \, dV + \int_{\partial\mathcal{I}} \llbracket \delta\boldsymbol{\varphi} \rrbracket_{\bar{\alpha}} \cdot \bar{\boldsymbol{\sigma}} \cdot \bar{\mathbf{n}} \, dL - \int_{\mathcal{I}} \bar{\boldsymbol{\sigma}} : \overline{\text{Grad}} \llbracket \delta\boldsymbol{\varphi} \rrbracket_{\bar{\alpha}} \, dA \\ &= \int_{\partial\mathcal{B}} \delta\boldsymbol{\varphi} \cdot \mathbf{t}_0 \, dA - \int_{\mathcal{I}} \llbracket \delta\boldsymbol{\varphi} \rrbracket \cdot \bar{\mathbf{t}} \, dA - \int_{\mathcal{B}} \boldsymbol{\sigma} : \text{Grad} \delta\boldsymbol{\varphi} \, dV + \int_{\partial\mathcal{I}} \llbracket \delta\boldsymbol{\varphi} \rrbracket_{\bar{\alpha}} \cdot \bar{\mathbf{t}}_0 \, dL - \int_{\mathcal{I}} \bar{\boldsymbol{\sigma}} : \overline{\text{Grad}} \llbracket \delta\boldsymbol{\varphi} \rrbracket_{\bar{\alpha}} \, dA = 0, \end{aligned} \quad (116)$$

where \mathbf{t}_0 and $\bar{\mathbf{t}}_0$ are the prescribed traction on the boundary of the body and the interface, respectively. Therefore, the

final version of the weak form of the linear momentum balance reads

$$\int_{\mathcal{B}} \boldsymbol{\sigma} : \text{Grad} \delta \boldsymbol{\varphi} \, dV + \int_I \bar{\boldsymbol{\sigma}} : \overline{\text{Grad}} \{\delta \boldsymbol{\varphi}\}_{\bar{\alpha}} \, dA + \int_I \llbracket \delta \boldsymbol{\varphi} \rrbracket \cdot \bar{\boldsymbol{\tau}} \, dA - \int_{\partial I} \{\delta \boldsymbol{\varphi}\}_{\bar{\alpha}} \cdot \bar{\boldsymbol{\tau}}_0 \, dL - \int_{\partial \mathcal{B}} \delta \boldsymbol{\varphi} \cdot \boldsymbol{t}_0 \, dA = 0. \quad (117)$$

with \boldsymbol{t}_0 and $\bar{\boldsymbol{\tau}}_0$ being the prescribed traction on the boundary of the bulk and the interface, respectively.

The next step is to discretize the domain. The discretization is carried out by means of the finite element and more specifically using the Bubnov–Galerkin scheme. The interface elements are here taken to be consistent with the bulk elements. In other words, for 3D analysis, the bulk elements are discretized by tri-quadratic elements and the interface elements are discretized by bi-quadratic elements and for 2D analysis, the bulk elements are discretized by bi-quadratic elements while the interface elements are discretized by quadratic elements. This strategy facilitates the implementation since the two sides of adjacent bulk elements can be regarded as the two sides of an interface element. Hence, we do not require additional interpolation or hanging nodes to connect the interface to its adjacent bulk. The bulk and interface domains are discretized into a set of bulk and interface elements as

$$\mathcal{B} \approx \mathcal{B}^h = \mathbf{A}_{e=1}^{\#BE} \mathcal{B}_e, \quad I \approx I^h = \mathbf{A}_{e=1}^{\#IE} I_e, \quad (118)$$

with $\#BE$ and $\#IE$ being the number of bulk and interface elements, respectively, and \mathbf{A} the generic assembly operator. Using standard interpolations and the isoparametric concept, the geometry and the displacement of the bulk and interface elements together with the test functions can be approximated as

$$\begin{aligned} \mathbf{X}|_{\mathcal{B}_e} &\approx \mathbf{X}^h(\boldsymbol{\xi}) = \sum_{i=1}^{\#NPBE} N_i(\boldsymbol{\xi}) \mathbf{X}_i, & \bar{\mathbf{X}}|_{I_e} &\approx \bar{\mathbf{X}}^h(\bar{\boldsymbol{\xi}}) = \sum_{i=1}^{\#NPBE} \bar{N}_i(\bar{\boldsymbol{\xi}}) \bar{\mathbf{X}}_i, \\ \mathbf{u}|_{\mathcal{B}_e} &\approx \mathbf{u}^h(\boldsymbol{\xi}) = \sum_{i=1}^{\#NPBE} N_i(\boldsymbol{\xi}) \mathbf{u}_i, & \bar{\mathbf{u}}|_{I_e} &\approx \bar{\mathbf{u}}^h(\bar{\boldsymbol{\xi}}) = \sum_{i=1}^{\#NPBE} \bar{N}_i(\bar{\boldsymbol{\xi}}) \bar{\mathbf{u}}_i, \\ \delta \boldsymbol{\varphi}|_{\mathcal{B}_e} &\approx \delta \boldsymbol{\varphi}^h(\boldsymbol{\xi}) = \sum_{i=1}^{\#NPBE} N_i(\boldsymbol{\xi}) \delta \boldsymbol{\varphi}_i, & \delta \bar{\boldsymbol{\varphi}}|_{I_e} &\approx \delta \bar{\boldsymbol{\varphi}}^h(\bar{\boldsymbol{\xi}}) = \sum_{i=1}^{\#NPBE} \bar{N}_i(\bar{\boldsymbol{\xi}}) \delta \bar{\boldsymbol{\varphi}}_i, \end{aligned} \quad (119)$$

with $\#NPBE$ and $\#NPBE$ being the number of nodes per bulk element and per interface element, respectively. The functions N_i and \bar{N}_i denote the shape functions of the bulk and interface elements at their local nodes i , respectively. The bulk element shape function N_i is defined over $\boldsymbol{\xi} \in [-1, 1]^{\text{PD}}$ whereas the interface element shape function \bar{N}_i is defined on $\bar{\boldsymbol{\xi}} \in [-1, 1]^{\text{PD}-1}$ with PD being the problem dimension. Figure 5 illustrates the discretization of the bulk and interface elements for both two- and three-dimensional settings. As shown in the figure, the number of nodes per interface element $\#NPBE$ is the same as the number of nodes per each facet of the adjacent bulk elements. Since the

interfacial jump and average operators appear in the weak form (117), the following interpolations prove to be useful

$$\begin{aligned} \llbracket \delta \boldsymbol{\varphi}^h \rrbracket &= \sum_{i=1}^{\# \text{NPIE}} \bar{N}_i \llbracket \delta \boldsymbol{\varphi}_i \rrbracket = \sum_{i=1}^{\# \text{NPIE}} \bar{N}_i \delta \boldsymbol{\varphi}_i^+ - \sum_{i=1}^{\# \text{NPIE}} \bar{N}_i \delta \boldsymbol{\varphi}_i^-, & \{\delta \boldsymbol{\varphi}^h\}_{\bar{\alpha}} &= \sum_{i=1}^{\# \text{NPIE}} \bar{N}_i \{\delta \boldsymbol{\varphi}_i\}_{\bar{\alpha}} = \bar{\alpha} \sum_{i=1}^{\# \text{NPIE}} \bar{N}_i \delta \boldsymbol{\varphi}_i^+ + [1 - \bar{\alpha}] \sum_{i=1}^{\# \text{NPIE}} \bar{N}_i \delta \boldsymbol{\varphi}_i^-, \\ \llbracket \mathbf{u}^h \rrbracket &= \sum_{i=1}^{\# \text{NPIE}} \bar{N}_i \llbracket \mathbf{u}_i \rrbracket = \sum_{i=1}^{\# \text{NPIE}} \bar{N}_i \mathbf{u}_i^+ - \sum_{i=1}^{\# \text{NPIE}} \bar{N}_i \mathbf{u}_i^-, & \{\mathbf{u}^h\}_{\bar{\alpha}} &= \sum_{i=1}^{\# \text{NPIE}} \bar{N}_i \{\mathbf{u}_i\}_{\bar{\alpha}} = \bar{\alpha} \sum_{i=1}^{\# \text{NPIE}} \bar{N}_i \mathbf{u}_i^+ + [1 - \bar{\alpha}] \sum_{i=1}^{\# \text{NPIE}} \bar{N}_i \mathbf{u}_i^-, \end{aligned} \quad (120)$$

where

$$\delta \boldsymbol{\varphi}^+ = \delta \boldsymbol{\varphi}|_{I^+}, \quad \delta \boldsymbol{\varphi}^- = \delta \boldsymbol{\varphi}|_{I^-}, \quad \mathbf{u}^+ = \mathbf{u}|_{I^+}, \quad \mathbf{u}^- = \mathbf{u}|_{I^-}. \quad (121)$$

Applying the approximations (119)–(120) to the weak form (117) renders the fully discrete form

$$\begin{aligned} & \mathbf{A} \int_{\mathcal{B}_e} \boldsymbol{\sigma} : \left[\sum_{i=1}^{\# \text{NPBE}} \delta \boldsymbol{\varphi}_i \otimes \text{Grad } N_i \right] dV \\ & + \mathbf{A} \int_{I_e} \bar{\boldsymbol{\sigma}} : \left[\bar{\alpha} \sum_{i=1}^{\# \text{NPIE}} [\delta \boldsymbol{\varphi}_i^+ \otimes \overline{\text{Grad } \bar{N}_i}] + [1 - \bar{\alpha}] \sum_{i=1}^{\# \text{NPIE}} [\delta \boldsymbol{\varphi}_i^- \otimes \overline{\text{Grad } \bar{N}_i}] \right] dA \\ & + \mathbf{A} \int_{I_e} \bar{\mathbf{t}} \cdot \left[\sum_{i=1}^{\# \text{NPIE}} \bar{N}_i \delta \boldsymbol{\varphi}_i^+ - \sum_{i=1}^{\# \text{NPIE}} \bar{N}_i \delta \boldsymbol{\varphi}_i^- \right] dA + R_{\partial \mathcal{B}} = 0, \end{aligned} \quad (122)$$

where $R_{\partial \mathcal{B}}$ is the discretized boundary residual. Let I denote a global node that could be in the bulk or on the interface. Since the test function $\delta \boldsymbol{\varphi}$ is arbitrary, we assume that $\delta \boldsymbol{\varphi}$ vanishes identically at all nodes except for the global node I . Note, the assembly operator gathers the contributions from all elements at their local node i associated with the global node I . Neglecting the boundary residual $R_{\partial \mathcal{B}}$, this procedure results in the global nodal residual vector \mathbf{R}_I associated with the global node I as

$$\begin{aligned} \mathbf{R}_I &= \mathbf{A} \int_{\mathcal{B}_e} \boldsymbol{\sigma} \cdot \text{Grad } N_i dV \\ & + \mathbf{A} \int_{I_e^+} \bar{\alpha} [\bar{\boldsymbol{\sigma}} \cdot \overline{\text{Grad } \bar{N}_i}] dA + \mathbf{A} \int_{I_e^-} [1 - \bar{\alpha}] [\bar{\boldsymbol{\sigma}} \cdot \overline{\text{Grad } \bar{N}_i}] dA \\ & + \mathbf{A} \int_{I_e^+} \bar{N}_i \bar{\mathbf{t}} dA - \mathbf{A} \int_{I_e^-} \bar{N}_i \bar{\mathbf{t}} dA = 0. \end{aligned} \quad (123)$$

Accordingly, one can split the residual into contributions of the bulk, plus side of the interface and minus side of the

interface as

$$\begin{aligned}
 \mathbf{R}_I &= \mathcal{R}_I + \overline{\mathcal{R}}_I^+ + \overline{\mathcal{R}}_I^-, \\
 \mathcal{R}_I &= \int_{\mathcal{B}} \boldsymbol{\sigma} \cdot \text{Grad } N_i \, dV, \\
 \overline{\mathcal{R}}_I^+ &= \int_I \overline{\alpha} \left[\overline{\boldsymbol{\sigma}} \cdot \overline{\text{Grad}} \overline{N}_i \right] + \overline{N}_i \overline{\mathbf{t}} \, dA, \\
 \overline{\mathcal{R}}_I^- &= \int_I [1 - \overline{\alpha}] \left[\overline{\boldsymbol{\sigma}} \cdot \overline{\text{Grad}} \overline{N}_i \right] - \overline{N}_i \overline{\mathbf{t}} \, dA,
 \end{aligned} \tag{124}$$

where we have omitted the assembly operator by replacing the local node i at the element level with the global node I and therefore the integrals are not only over the individual elements but over the entire domain. From the structure of the residual (124), it is obvious that the bulk elements possess the residual \mathcal{R}_I and the interface elements possess the residuals $\overline{\mathcal{R}}_I^+$ and $\overline{\mathcal{R}}_I^-$. Accordingly the nodal stiffness \mathbf{K}_{IJ} is defined by the derivative of the residual \mathbf{R}_I with respect to the displacement \mathbf{u}_J as

$$\mathbf{K}_{IJ} = \frac{\partial \mathbf{R}_I}{\partial \mathbf{u}_J}. \tag{125}$$

While the structures of the residual vector and stiffness matrix for bulk elements are simple and standard, they are less familiar for the interface since they include combinations of the plus and minus sides of the interface and can be schematically represented as

$$\overline{\mathcal{R}}_I = \begin{bmatrix} \overline{\mathcal{R}}_I^- \\ \overline{\mathcal{R}}_I^+ \end{bmatrix}, \quad \overline{\mathcal{K}}_{ij} = \begin{bmatrix} \frac{\partial \overline{\mathcal{R}}_I^-}{\partial \mathbf{u}_j^-} & \frac{\partial \overline{\mathcal{R}}_I^-}{\partial \mathbf{u}_j^+} \\ \frac{\partial \overline{\mathcal{R}}_I^+}{\partial \mathbf{u}_j^-} & \frac{\partial \overline{\mathcal{R}}_I^+}{\partial \mathbf{u}_j^+} \end{bmatrix} = \begin{bmatrix} \overline{\mathcal{K}}_{IJ}^{--} & \overline{\mathcal{K}}_{IJ}^{+-} \\ \overline{\mathcal{K}}_{IJ}^{-+} & \overline{\mathcal{K}}_{IJ}^{++} \end{bmatrix}. \tag{126}$$

Putting all the unknown coordinates into the global unknown coordinate vector $[\mathbf{u}]$ and assembling the global nodal residual vectors \mathbf{R}^I into the global residual vector $[\mathbf{R}]$ results in the non-linear system of equations $[\mathbf{R}] \stackrel{!}{=} \mathbf{0}$ which can be solved using the Newton–Raphson scheme as

$$[\mathbf{R}]_{n+1} \stackrel{!}{=} \mathbf{0} \quad \Rightarrow \quad [\mathbf{R}]_{n+1} = [\mathbf{R}]_n + [\mathbf{K}]_n \Delta[\boldsymbol{\varphi}]_n \stackrel{!}{=} \mathbf{0} \quad \text{with} \quad [\mathbf{K}]_n := \frac{\partial [\mathbf{R}]_n}{\partial [\mathbf{u}]_n},$$

that yields the incremental updates $[\mathbf{u}]_{n+1} = [\mathbf{u}]_n + \Delta[\mathbf{u}]_n$. Here $[\mathbf{K}]_n$ denotes the tangent stiffness and n is the iteration step. The computational analysis is carried out using our in-house finite element code applied to the RVE discretized by quadratic Lagrange elements as depicted in Fig. 5. For all the examples, the solution procedures are robust and

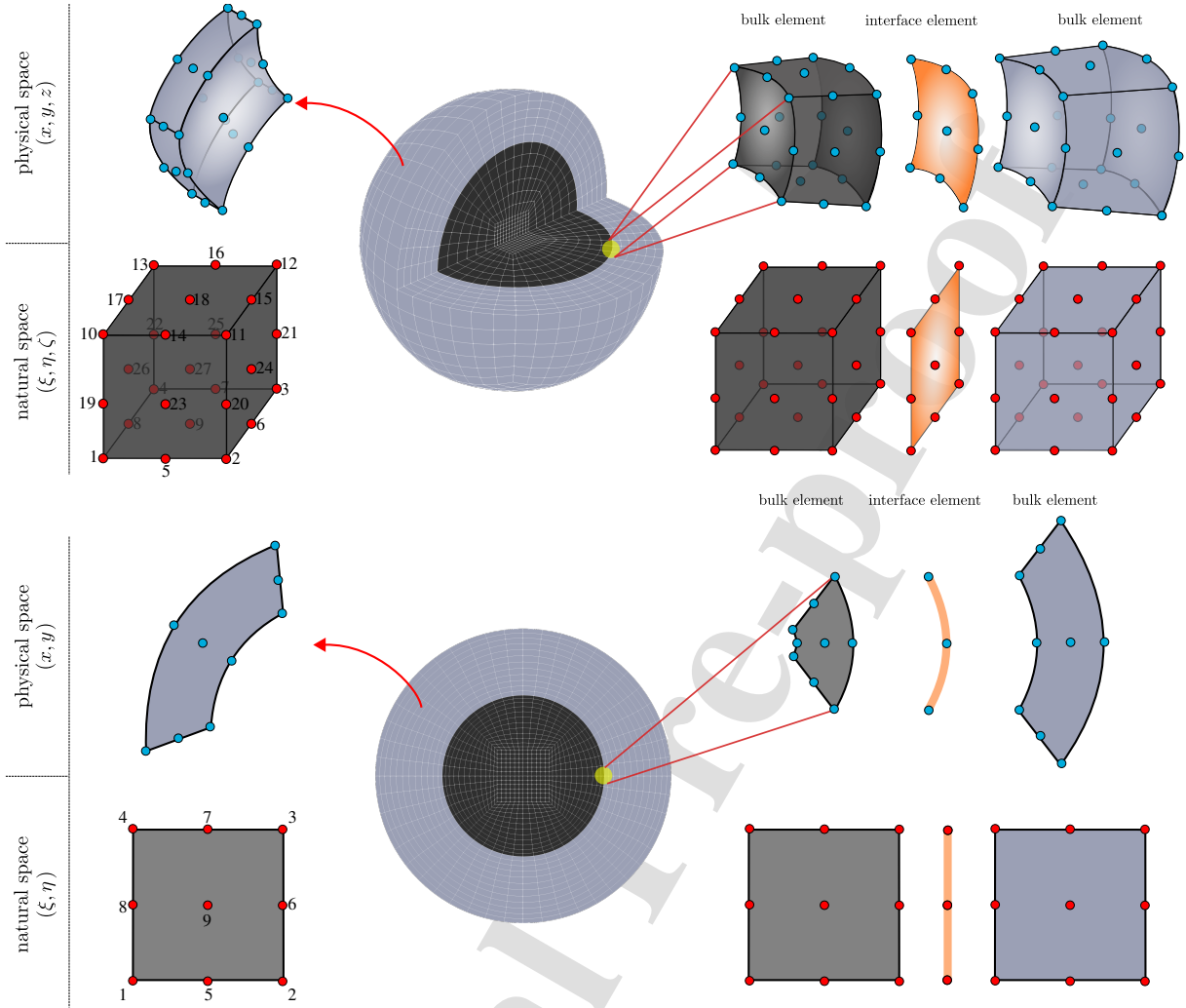


Figure 5: Illustration of domain discretization as well as element types for the bulk and interface domains.

render asymptotically quadratic rate of convergence associated with the Newton–Raphson scheme.

5. Numerical examples

The objective of this section is to illustrate the proposed theory through a set of numerical examples. In doing so, the overall properties as well as average stresses in both fiber-reinforced and particle-reinforced composites are examined for various interface positions $\bar{\alpha}$ as well as stiffness ratios and size. The term size here refers to the physical “size” of the RVE illustrated in Fig 6 for both fiber-reinforced and particle-reinforced composites. Assuming that size is expressed in mm, the bulk material properties λ and μ will be in N/mm^2 while the interface parameters $\bar{\lambda}$ and $\bar{\mu}$ will be in N/mm . The interface orthogonal resistance \bar{k} is then measured in N/mm^3 . The interface position $\bar{\alpha}$ is a measure determining whether the interface is closer to the inhomogeneity or the matrix. In the limits, $\bar{\alpha} = 0$ implies the interface

is totally attached to the inhomogeneity and $\bar{\alpha} = 1$ signifies a totally attached interface to the matrix. The stiffness ratio denoted as incl./matr. is the ratio of the inhomogeneity to the matrix Lamé parameters. The stiffness ratio 0.1, corresponds to a 10 times stiffer matrix than the inhomogeneity and in the limit of $\text{incl./matr.} \rightarrow 0$, the inhomogeneity resembles a void. On the other hand, the stiffness ratio 10 signifies a 10 times stiffer inhomogeneity than the matrix and in the limit of $\text{incl./matr.} \rightarrow \infty$, the inhomogeneity acts as being rigid. For all the examples, the volume fraction of the inhomogeneity is set to $f = 30\%$. Moreover, the matrix Lamé parameters are set to $\lambda^{(2)} = 12 \text{ N/mm}^2$ and $\mu^{(2)} = 8 \text{ N/mm}^2$ and the inhomogeneity Lamé parameters vary in accordance with the prescribed stiffness ratios. For the case with transverse isotropy associated with fiber-reinforced composites, we assume $\lambda = l = m$ and $\mu_{ax} = \mu_{tr}$ for the sake of simplicity. For the interface parameters, the interface in-plane resistance indicating the resistance of the interface against stretches is set to $\bar{\mu} = \bar{\lambda} = 0.1 \text{ N/mm}$ and the orthogonal interface resistance corresponding to the resistance of the interface against opening is set to $\bar{k} = 10 \text{ N/mm}^3$. Also, we assume equal orthogonal resistance for the interface in each direction implying $\bar{k}_r = \bar{k}_\theta = \bar{k}_z = \bar{k}$ in a two-dimensional setting and $\bar{k}_r = \bar{k}_\theta = \bar{k}_\phi = \bar{k}$ in a three-dimensional setting. For a two-dimensional analysis corresponding to fiber-reinforced composites, only one interface material parameter suffices to capture the interface in-plane response thus, we consider $\bar{\lambda} = 0 \text{ N/mm}$ and $\bar{\mu}_{ax} = \bar{\mu}_{tr} = 0.1 \text{ N/mm}$. Computational analysis using the finite element method is carried out in order to compare with the analytical solutions.

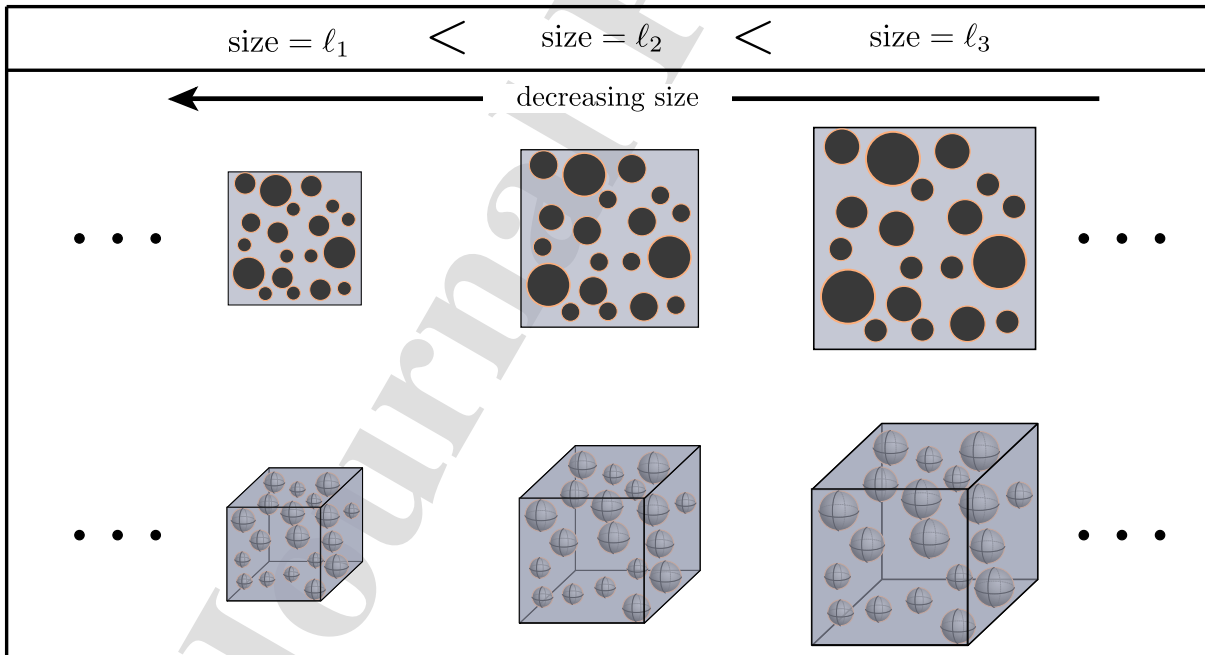


Figure 6: Schematic illustration of RVE size.

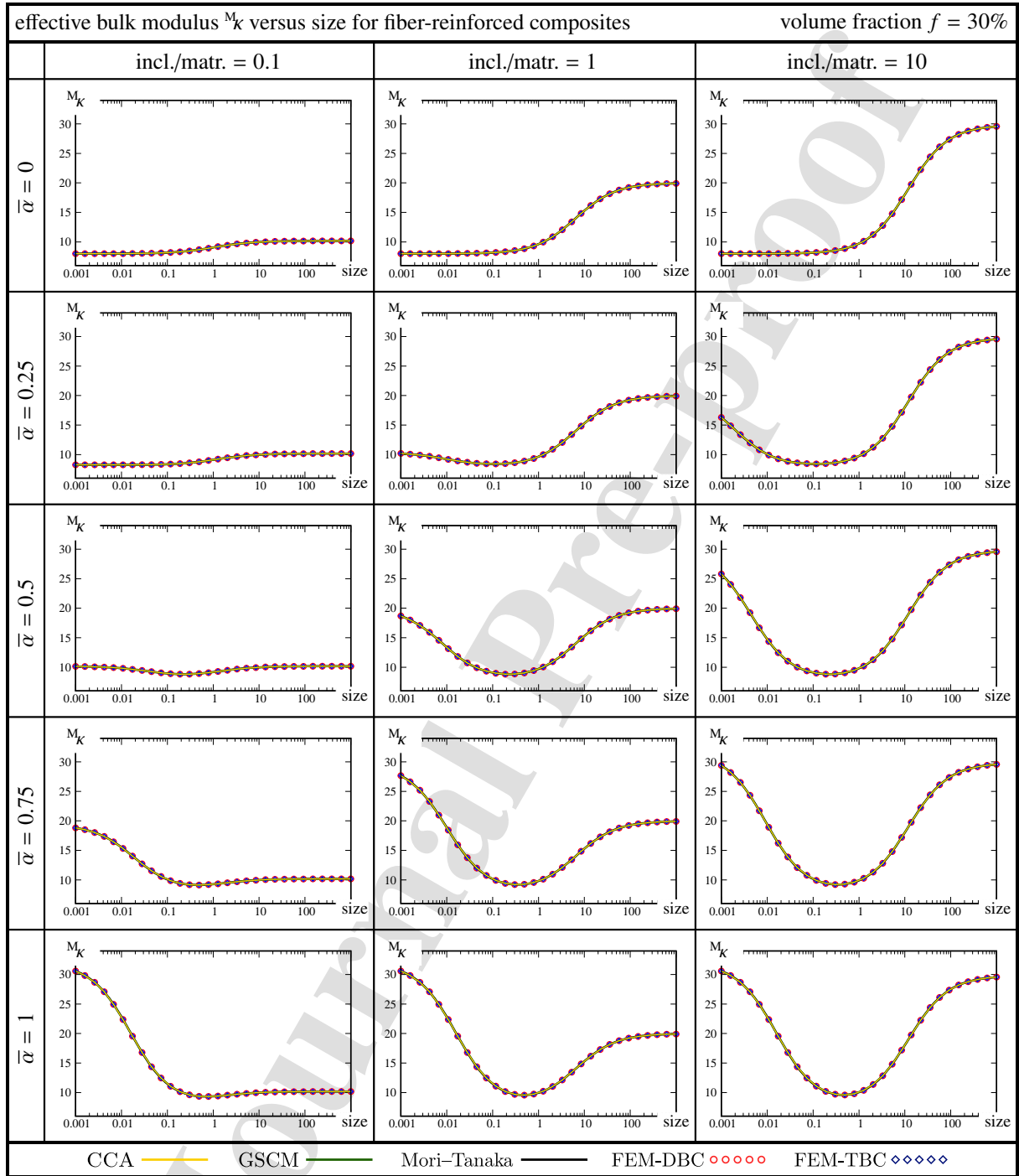


Figure 7: Overall bulk modulus versus size for fiber-reinforced composites. Rows represent the interface positions and columns represent the stiffness ratio. Lines correspond to the analytical solution obtained by the Mori-Tanaka method whereas points correspond to the solutions obtained by FEM.

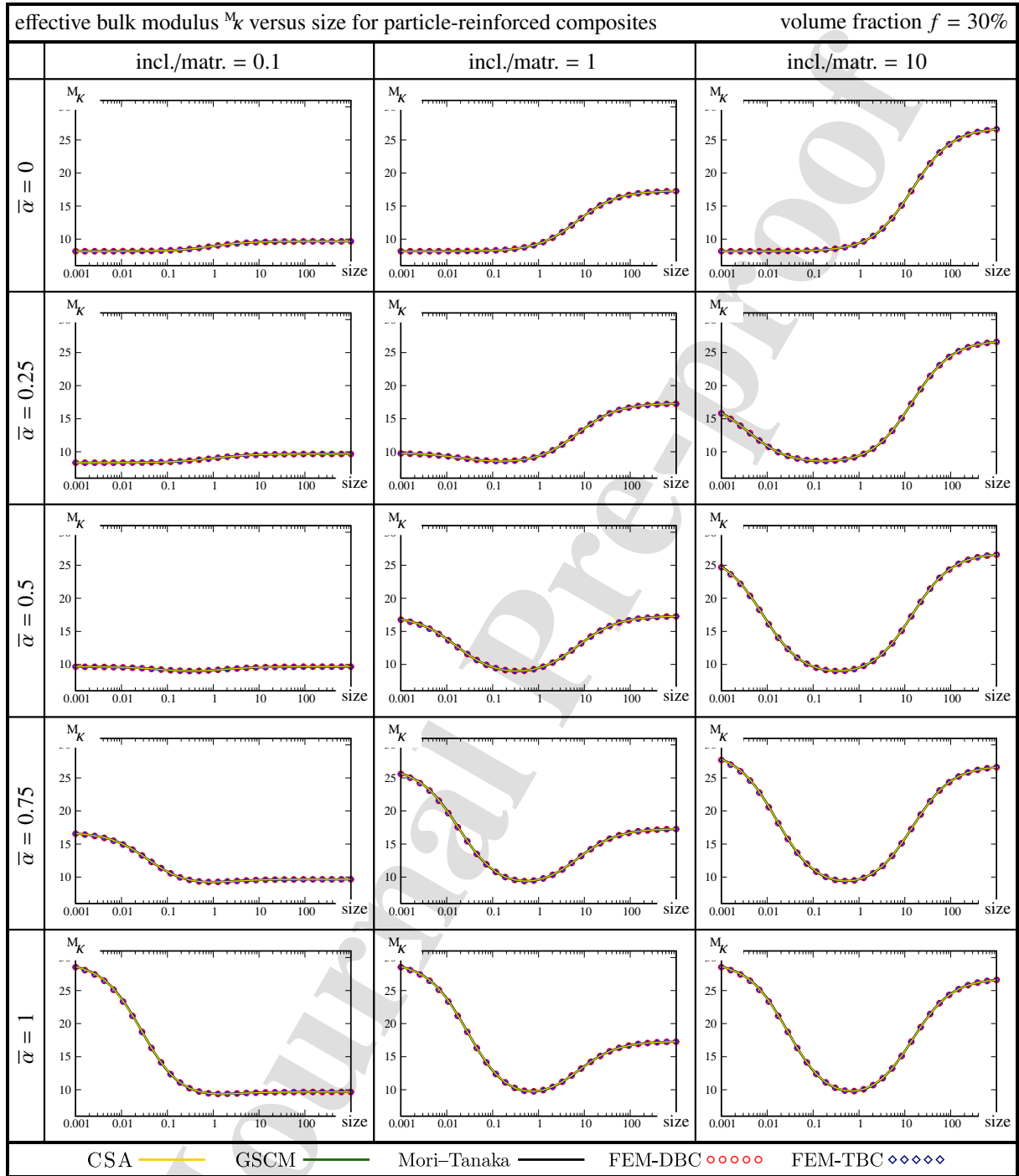


Figure 8: Overall bulk modulus versus size for particle-reinforced composites. Rows represent the interface positions and columns represent the stiffness ratio. Lines correspond to the analytical solution obtained by the Mori-Tanaka method whereas points correspond to the solutions obtained by FEM.

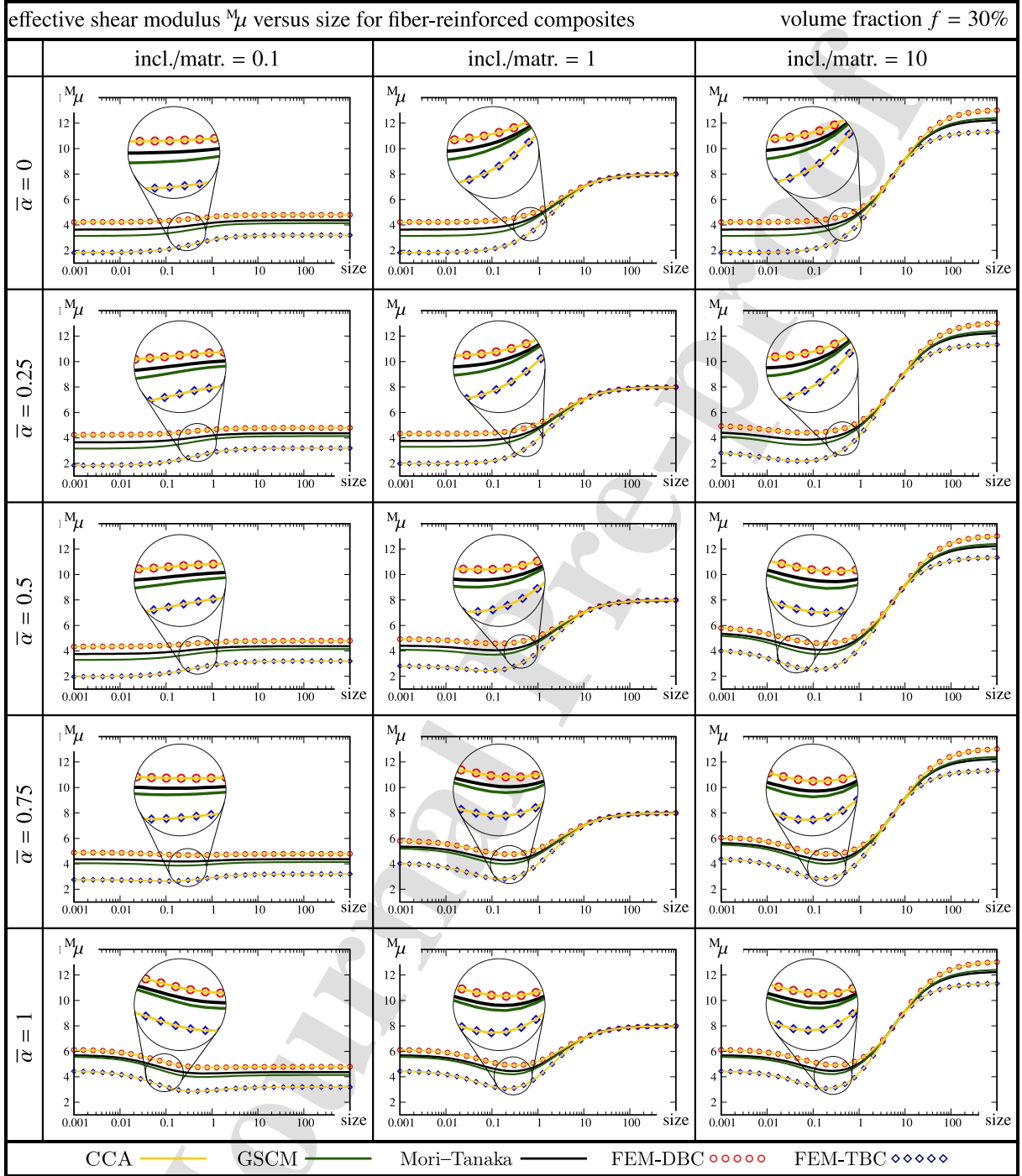


Figure 9: Overall shear modulus versus size for fiber-reinforced composites. Rows represent the interface positions and columns represent the stiffness ratio. Lines correspond to the analytical solution obtained by the Mori-Tanaka method whereas points correspond to the solutions obtained by FEM.

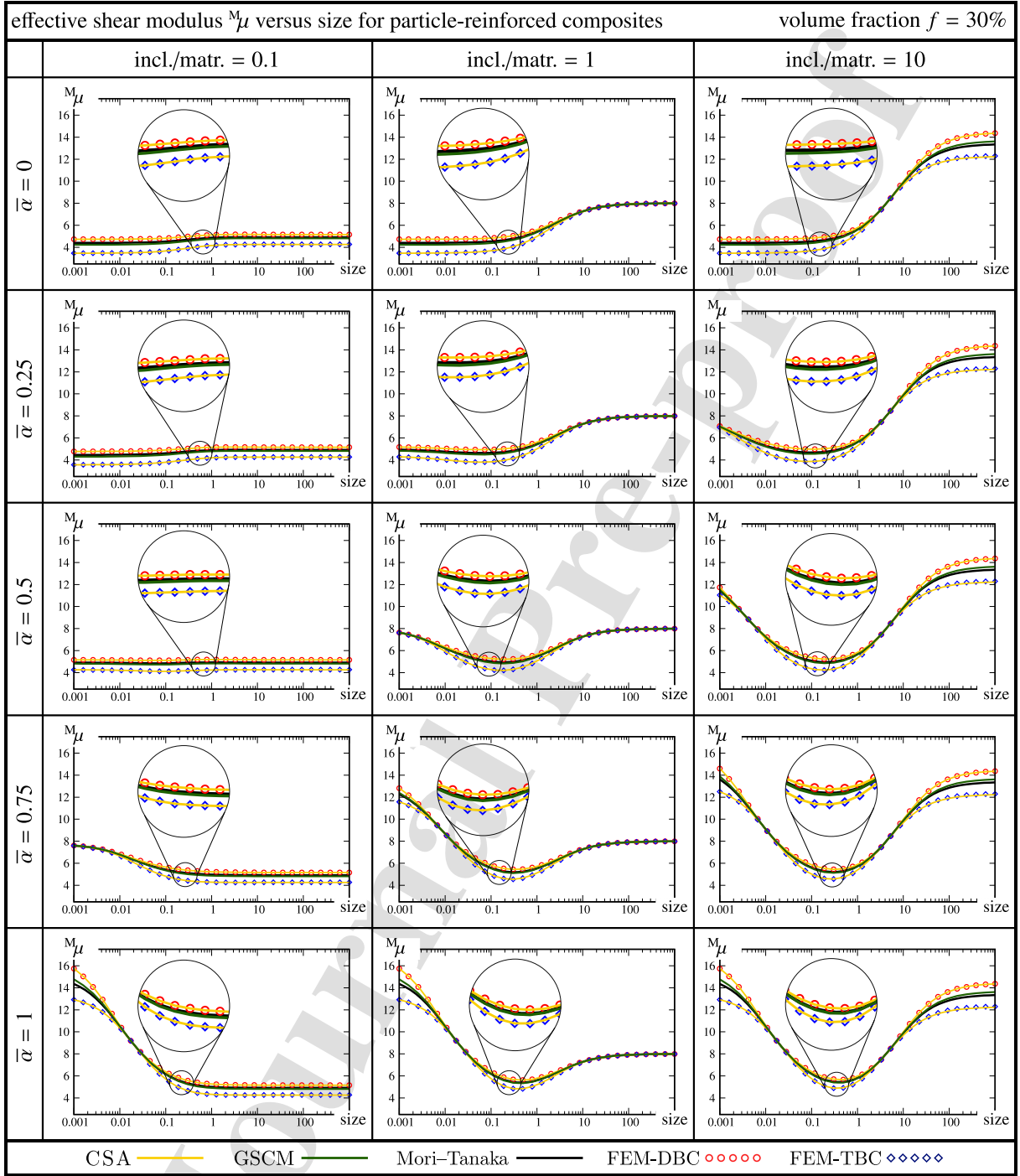


Figure 10: Overall shear modulus versus size for particle-reinforced composites. Rows represent the interface positions and columns represent the stiffness ratio. Lines correspond to the analytical solution obtained by the Mori-Tanaka method whereas points correspond to the solutions obtained by FEM.

Figures 7 and 8 depict the *overall bulk modulus* versus size for fiber- and particle-reinforced composites, respectively. Rows correspond to the interface position and columns correspond to the stiffness ratio. Lines represent the analytical solutions whereas points correspond to computational results obtained by FEM. The black line corresponds to the Mori–Tanaka method, the green line corresponds to the generalized self-consistent method and the yellow line corresponds to either composite cylinder assemblage or composite sphere assemblage. For the computational analysis, the RVE is subject to volumetric expansion under two different boundary conditions; displacement boundary condition (DBC) and traction boundary condition (TBC). These two boundary conditions normally lead to an upper bound and lower bound on the overall material response in classical homogenization. An excellent agreement between all the analytical solutions and computational results is observed. In addition, due to the RVE geometry and the symmetry of loading, the upper and lower bounds coincide. For each stiffness ratio, the overall bulk modulus remains insensitive with respect to the interface position at large sizes. This is justifiable since larger size implies diminished interface effects, thus the role of interface position in the overall material response becomes negligible. Another significant observation is that as the interface moves from the inhomogeneity towards the matrix (increasing $\bar{\alpha}$), the overall material response switches from smaller-weaker to smaller-stronger. These two particular responses were previously solely attributed to the cohesive interface model and the elastic interface model, respectively. Here, with the new developed interface model, all the ranges between the overall responses associated with these two interface models can be captured. For all interface positions, increasing the stiffness ratio yields stiffer response at large sizes. In addition, for the cases when the interface is completely attached to the inhomogeneity ($\bar{\alpha} = 0$) and to the matrix ($\bar{\alpha} = 1$), the overall response at small sizes remains insensitive with respect to the stiffness ratio. Figures 9 and 10 are the counterparts of Figs. 7 and 8 for the *overall shear modulus*. Here, the RVE is subject to simple shear which results in distinct upper and lower bounds. It is observed that the analytical solutions associated with CCA and CSA perfectly coincide with the computational results due to DBC and TBC which provide upper and lower bounds. The other two analytical solutions furnishing the effective shear modulus always remain within the bounds. For fiber-reinforced composites, when $\text{incl./matr.} = 0.1$, the bounds remain distinct and separate and the response associated with GSCM underestimates that of Mori–Tanaka. When, $\text{incl./matr.} = 1$ the bounds tend to coincide at large sizes. At small sizes, the response obtained via GSCM underestimates the Mori–Tanaka solution whereas at large sizes, they coincide all together with the bounds. When $\text{incl./matr.} = 10$, moving from small to large sizes, the bounds tend to approach until they coincide and they distance afterwards. The solution due to GSCM underestimate the Mori–Tanaka solution before the bounds coincide and it overestimate the Mori–Tanaka solution after the bounds coincide. Under simple shear loading, smaller stronger response is attainable for fiber-reinforced composites only when the stiffness ratio is 0.1. For other stiffness ratio, the material response is always stronger at large sizes. For particle-reinforced composites the behavior of the

bounds is more complicated and depending on the interface positions, various observations can be made. In contrast to fiber-reinforced composites, when $\text{incl./matr.} = 0.1$, the bounds coincide when the interface is closer to the matrix. For some cases for $\text{incl./matr.} = 1$ and $\text{incl./matr.} = 10$, the bounds coincide twice within the size range. Each coincidence switches the relative position between the solutions associated with GSCM and the Mori–Tanaka method.

As mentioned earlier, a noteworthy advantage of the Mori–Tanaka method was determining overall properties as well as average fields within the constituents of the medium. Therefore, the state of the stress and strain in both the inhomogeneity and the matrix can be estimated. In what follows a set of examples are devised to demonstrate the average fields within the constituents of fiber- and particle-reinforced composites. Figures 11 and 12 provide a thorough comparison between the numerical and analytical stress distributions for various interface positions for fiber-reinforced composites and particle-reinforced composites, respectively. For these examples, the micro-structure is subject to volumetric expansion. The stiffness ratio is set to 10 and the RVE size is 0.01. The color patterns display $[\sigma_{xx} + \sigma_{yy}]/2$ for the two dimensional case and $[\sigma_{xx} + \sigma_{yy} + \sigma_{zz}]/3$ for the three dimensional case. This choice is made to provide meaningful stress distributions for each case. Each row represent a specific interface position and contains 5 micro-structures. In each row, the left and right pairs render the computational stress distribution due to DBC and TBC, respectively, obtained from the finite element method. The very left and very right RVEs render the local stress distributions. Since our proposed analytical approach determines the average stress in the constituents, the average of these local stresses is calculated in each phase and rendered in the RVEs next to them. Such illustration facilitates comparison with analytical stresses. The center micro-structure correspond to the analytical average stress distribution obtained by the Mori–Tanaka method. The values of the average stress in the inhomogeneity $\langle \sigma \rangle^1$ and in the matrix $\langle \sigma \rangle^2$ are shown for the sake of clarity. It is observed that a perfect agreement holds between the stress distributions predicted by our proposed Mori–Tanaka method and the average stresses obtained by FEM. For all cases, the matrix tends to undergo larger average stress as the interface moves from the inhomogeneity towards the matrix. Figures 13 and 14 are the counterparts of Figs. 11 and 12 for the simple shear loading. The stress component of interest for these examples is σ_{xy} . The difference between the local stresses and average stresses associated with FEM results is more visible in these figures. For the shear deformation various conclusions can be drawn. The overall analytical stress average within the matrix is always bounded between the computational average stresses under DBC and TBC. However, for the inhomogeneity, when $\bar{\alpha} = 0$ and $\bar{\alpha} = 1$, the average stress is lowest for DBC and highest for TBC. For the other interface positions which are $\bar{\alpha} = 0.25$ and $\bar{\alpha} = 0.5$ and $\bar{\alpha} = 0.75$, the inhomogeneity average stress is lowest for TBC. For these cases, sometimes the analytical average stress is the highest and sometimes DBC provides the highest stress.

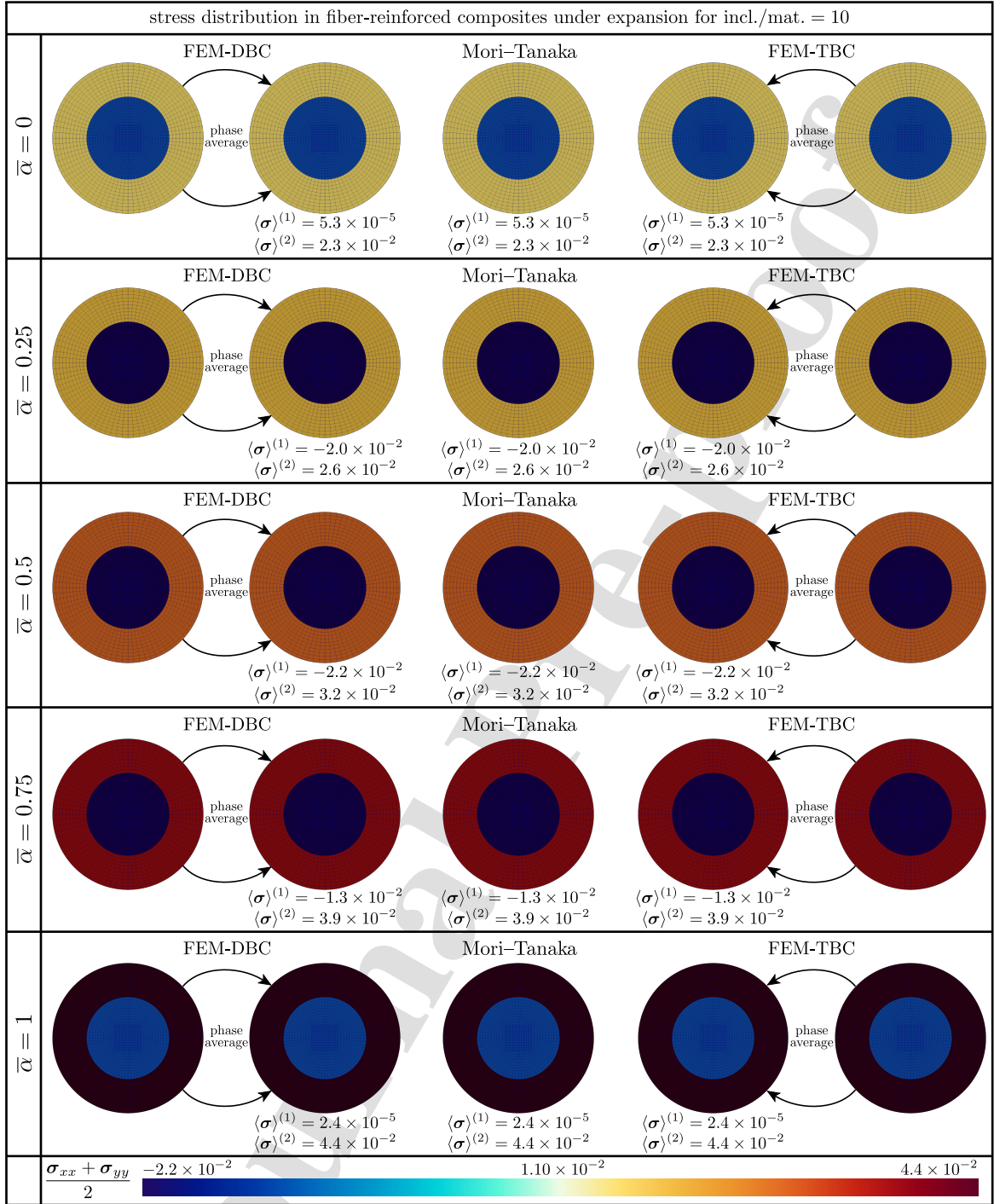


Figure 11: Stress distribution throughout the constituents of a fiber-reinforced composite under volumetric expansion for incl./matr. = 10. The left RVE pair correspond to finite element stress distribution when DBC is imposed to the RVE. The center RVE correspond to the analytical average stress obtained via the Mori-Tanaka method. The right RVE pair correspond to finite element stress distribution when TBC is imposed to the RVE. The finite element stress distributions include the local stresses together with their averages in each phase.

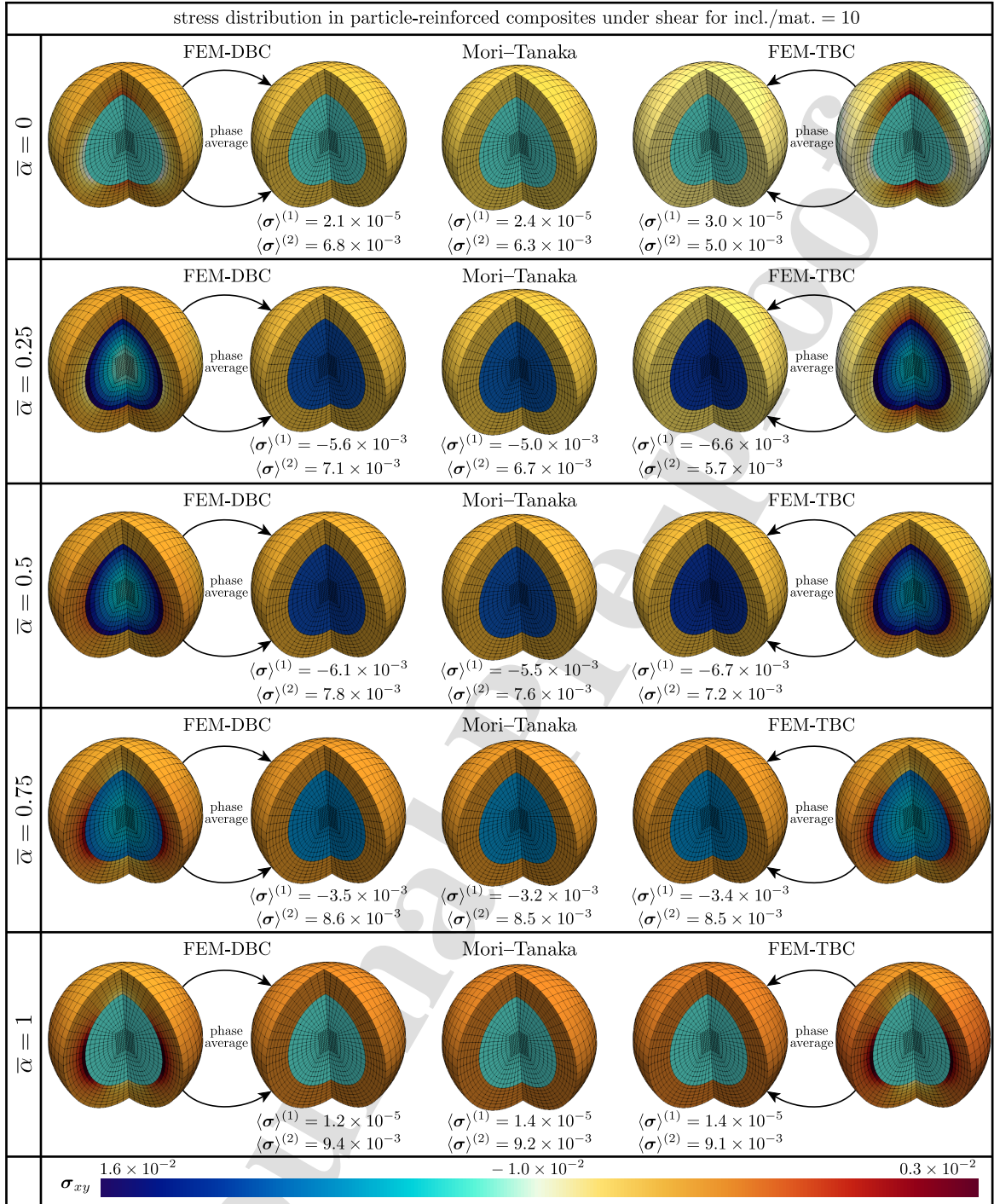


Figure 14: Stress distribution throughout the constituents of a particle-reinforced composite under simple shear for incl./matr. = 10. The left RVE pair correspond to finite element stress distribution when DBC is imposed to the RVE. The center RVE correspond to the analytical average stress obtained via the Mori-Tanaka method. The right RVE pair correspond to finite element stress distribution when TBC is imposed to the RVE. The finite element stress distributions include the local stresses together with their averages in each phase.

6. Summary and Conclusion

In summary, a comprehensive study on the mechanics of a continuum body embedding an extended general interface was carried out. A homogenization framework based on the Mori–Tanaka method was established and the significant influence of arbitrary interface positions on the material response was studied in detail. The advantage of the proposed Mori–Tanaka approach is that in addition to providing estimates on the overall properties, it is capable of determining the average stresses and strains within the constituents of the medium. Closed-form, explicit expressions for the effective bulk modulus and effective shear modulus of fiber-reinforced and particle-reinforced composites were obtained as a function of the interface position. Computational analysis was carried out to evaluate the performance of the analytical approaches and an outstanding agreement between the results was observed. It turns out that under volumetric expansion, CCA, CSA, GSCM and the Mori–Tanaka method all yield the same overall material response. However, under simple shear, CCA and CSA provide bounds on the material response for fiber- and particle-reinforced composites with the GSCM and the Mori–Tanaka solution lying within the bounds consistently. The same observations relatively hold between the average stresses estimated by the Mori–Tanaka method and the average stresses obtained by FEM. Moreover, we observed that the choice of interface position can lead to any of smaller-stronger or smaller-weaker responses which were previously attributed to the elastic and cohesive interface models, respectively. Our methodology sheds light on some counter-intuitive behaviors observed in composites embedding general interfaces originating from the trivial assumption of the interface coinciding with the mid-plane. The newly developed extended general interface model can be considered as the most generic existing interface model since it involves all the characteristics of the classical general interface, elastic interface and cohesive interface models. We believe that this manuscript deepens our understanding of various interface effects and the size-dependent behavior of composites which paves the way towards computational design of metamaterials.

Acknowledgment

A. Javili gratefully acknowledge the support provided by Scientific and Technological Research Council of Turkey (TÜBİTAK) Career Development Program, grant number 218M700.

References

- [1] G. C. Papanicolaou, S. A. Paipetis, P. S. Theocaris, The concept of boundary interphase in composite mechanics, *Colloid and Polymer Science* 256 (1978) 625–630.
- [2] G. C. Papanicolaou, P. S. Theocaris, Thermal properties and volume fraction of the boundary interphase in metal-filled epoxies, *Colloid and Polymer Science* 257 (1979) 239–246.

- [3] L. J. Walpole, A coated inclusion in an elastic medium, *Mathematical Proceedings of the Cambridge Philosophical Society* 83 (1978) 495–506.
- [4] P. S. Theocaris, G. C. Papanicolaou, The effect of the boundary interphase on the thermomechanical behaviour of composites reinforced with short fibres, *Fibre Science and Technology* 12 (1979) 421–433.
- [5] B. W. Rosen, Mechanics of composite strengthening, in: *Fibre Composite Materials*, American Society for Metals, 1965, pp. 37–75.
- [6] H. A. Luo, G. J. Weng, On Eshelby's inclusion problem in a three-phase spherically concentric solid, and a modification of Mori-Tanaka's method, *Mechanics of Materials* 6 (1987) 347–361.
- [7] H. A. Lou, G. J. Weng, On Eshelby's S-tensor in a three-phase cylindrically concentric solid, and the elastic moduli of fiber-reinforced composites, *Mechanics of Materials* 8 (1989) 77–88.
- [8] Y. Benveniste, G. J. Dvorak, T. Chen, Stress fields in composites with coated inclusions, *Mechanics of Materials* 7 (1989) 305–317.
- [9] Y. Benveniste, G. J. Dvorak, T. Chen, On effective properties of composites with coated cylindrically orthotropic fibers, *Mechanics of Materials* 12 (1991) 289–297.
- [10] H. L. Duan, J. Wang, Z. P. Huang, Y. Zhong, Stress fields of a spheroidal inhomogeneity with an interphase in an infinite medium under remote loadings, *Proceedings of the Royal Society A* 461 (2005) 1055–1080.
- [11] Y. P. Qiu, G. J. Weng, Elastic moduli of thickly coated particle and fiber-reinforced composites, *Journal of Applied Mechanics* 58 (1991) 388–398.
- [12] M. Cherkaoui, H. Sabar, M. Berveiller, Elastic composites with coated reinforcements: A micromechanical approach for nonhomothetic topology, *International Journal of Engineering Science* 33 (1995) 829–843.
- [13] M. El Mouden, M. Cherkaoui, A. Molinari, M. Berveiller, The overall elastic response of materials containing coated inclusions in a periodic array, *International Journal of Engineering Science* 36 (1998) 813–829.
- [14] L. Nazarenko, H. Stolarski, H. Altenbach, Thermo-elastic properties of random particulate nano-materials for various models of interphase, *International Journal of Mechanical Sciences* 126 (2017) 130–141.
- [15] F. Lebon, R. Rizzoni, Asymptotic behavior of a hard thin linear elastic interphase: An energy approach, *International Journal of Solids and Structures* 48 (2011) 441–449.
- [16] G. C. Papanicolaou, P. S. Theocaris, G. D. Spathis, Adhesion efficiency between phases in fibre-reinforced polymers by means of the concept of boundary interphase, *Colloid and Polymer Science* 258 (1980) 1231–1237.
- [17] M. Ostoja-Starzewski, I. Jasiuk, W. Wang, K. Alzebedeh, Composites with functionally graded interphases: Mesocontinuum concept and effective transverse conductivity, *Acta Materialia* 44 (1996) 2057–2066.
- [18] P. S. Theocaris, G. Spathis, E. Sideridis, Elastic and viscoelastic properties of fibre-reinforced composite materials, *Fibre Science and Technology* 17 (1982) 169–181.
- [19] P. S. Theocaris, E. P. Sideridis, G. C. Papanicolaou, The elastic longitudinal modulus and Poisson's ratio of fiber composites, *Journal of Reinforced Plastics and Composites* 4 (1985) 396–418.
- [20] A. Dasgupta, S. M. Bhandarkar, A generalized self-consistent Mori-Tanaka scheme for fiber-composites with multiple interphases, *Mechanics of Materials* 14 (1992) 67–82.
- [21] Y. M. Shabana, A micromechanical model for composites containing multi-layered interphases, *Composite Structures* 101 (2013) 265–273.
- [22] E. Herve, A. Zaoui, n-Layered inclusion-based micromechanical modelling, *International Journal of Engineering Science* 31 (1993) 1–10.
- [23] S. Berbenni, M. Cherkaoui, Homogenization of multicoated inclusion-reinforced linear elastic composites with eigenstrains: Application to thermoelastic behavior, *Philosophical Magazine* 90 (2010) 3003–3026.
- [24] I. Jasiuk, M. W. Kouider, The effect of an inhomogeneous interphase on the elastic constants of transversely isotropic composites, *Mechanics*

- of Materials 15 (1993) 53–63.
- [25] Y. M. Wu, Z. P. Huang, Y. Zhong, J. Wang, Effective moduli of particle-filled composite with inhomogeneous interphase: Part I - bounds, Composites Science and Technology 64 (2004) 1345–1351.
- [26] Y. Zhong, J. Wang, Y. M. Wu, Z. P. Huang, Effective moduli of particle-filled composite with inhomogeneous interphase: Part II - mapping method and evaluation, Composites Science and Technology 64 (2004) 1353–1362.
- [27] M. P. Lutz, R. W. Zimmerman, Effect of the interphase zone on the conductivity or diffusivity of a particulate composite using Maxwell's homogenization method, International Journal of Engineering Science 98 (2016) 51–59.
- [28] W. Xu, Y. Wu, X. Gou, Effective elastic moduli of nonspherical particle-reinforced composites with inhomogeneous interphase considering graded evolutions of elastic modulus and porosity, Computer Methods in Applied Mechanics and Engineering 350 (2019) 535–553.
- [29] E. Sanchez-Palencia, Comportement limite d'un probleme de transmission travers une plaque faiblement conductrice, Comptes Rendus Mathematique Academie des Sciences 270 (1970) 1026–1028.
- [30] H. Pham Huy, E. Sanchez-Palencia, Phénomènes de transmission à travers des couches minces de conductivité élevée, Journal of Mathematical Analysis and Applications 47 (1974) 284–309.
- [31] Y. Benveniste, The effective mechanical behaviour of composite materials with imperfect contact between the constituents, Mechanics of Materials 4 (1985) 197–208.
- [32] Y. Benveniste, T. Miloh, Imperfect soft and stiff interfaces in two-dimensional elasticity, Mechanics of Materials 33 (2001) 309–323.
- [33] A. Klarbring, A. B. Movchan, Asymptotic modelling of adhesive joints, Mechanics of Materials 28 (1998) 137–145.
- [34] A. Klarbring, Derivation of a model of adhesively bonded joints by the asymptotic expansion method, International Journal of Engineering Science 29 (1991) 493–512.
- [35] Z. Hashin, Thermoelastic properties of particulate composites with imperfect interface, Journal of the Mechanics and Physics of Solids 39 (1991) 745–762.
- [36] Z. Hashin, Thermoelastic properties of fiber composites with imperfect interface, Mechanics of Materials 8 (1990) 333–348.
- [37] Z. Hashin, The spherical inclusion with imperfect interface, Journal of Applied Mechanics 58 (1991) 444–449.
- [38] P. Bövik, On the modelling of thin interface layers in elastic and acoustic scattering problems, Quarterly Journal of Mechanics and Applied Mathematics 47 (1994) 17–42.
- [39] S. Baranova, S. G. Mogilevskaya, V. Mantić, S. Jiménez-Alfaro, Analysis of the Antiplane Problem with an Embedded Zero Thickness Layer Described by the Gurtin-Murdoch Model, Journal of Elasticity 140 (2020) 171–195.
- [40] S. Baranova, S. G. Mogilevskaya, T. H. Nguyen, D. Schilling, Higher-order imperfect interface modeling via complex variables based asymptotic analysis, International Journal of Engineering Science 157 (2020) 103399.
- [41] Y. Benveniste, O. Berdichevsky, On two models of arbitrarily curved three-dimensional thin interphases in elasticity, International Journal of Solids and Structures 47 (2010) 1899–1915.
- [42] D. Bigoni, S. K. Serkov, M. Valentini, A. B. Movchan, Asymptotic models of dilute composites with imperfectly bonded inclusions, International Journal of Solids and Structures (35) (1998) 3239–3258.
- [43] R. Rizzoni, S. Dumont, F. Lebon, E. Sacco, Higher order model for soft and hard elastic interfaces, International Journal of Solids and Structures 51 (2014) 4137–4148.
- [44] F. Lebon, R. Rizzoni, Asymptotic behavior of a hard thin linear elastic interphase: An energy approach, International Journal of Solids and Structures 48 (2011) 441–449.
- [45] F. Lebon, R. Rizzoni, Asymptotic analysis of a thin interface: The case involving similar rigidity, International Journal of Engineering Science 48 (2010) 473–486.

- [46] M. Serpilli, R. Rizzoni, F. Lebon, S. Dumont, An asymptotic derivation of a general imperfect interface law for linear multiphysics composites, *International Journal of Solids and Structures* 180-181 (2019) 97–107.
- [47] R. Rizzoni, F. Lebon, Imperfect interfaces as asymptotic models of thin curved elastic adhesive interphases, *Mechanics Research Communications* 51 (2013) 39–50.
- [48] M. Serpilli, R. Rizzoni, S. Dumont, F. Lebon, Higher order interface conditions for piezoelectric spherical hollow composites: asymptotic approach and transfer matrix homogenization method, *Composite Structures* 279 (2022) 114760.
- [49] S. Baranova, S. G. Mogilevskaya, On the Bökvik – Benveniste methodology and related approaches for modelling thin layers *Subject Areas*, *Mathematics and mechan* 380 (2022) 20210420.
- [50] V. I. Kushch, S. G. Mogilevskaya, On modeling of elastic interface layers in particle composites, *International Journal of Engineering Science* 176 (2022) 103697.
- [51] M. E. Gurtin, A. I. Murdoch, A continuum theory of elastic material surfaces, *Archive for Rational Mechanics and Analysis* 57 (1975) 291–323.
- [52] M. E. Gurtin, A. I. Murdoch, Surface stress in solids, *International Journal of Solids and Structures* 14 (1978) 431–440.
- [53] D. J. Steigmann, R. W. Ogden, Elastic surface – substrate interactions, *Proceedings of the Royal Society of London A* 455 (1999) 437–474.
- [54] D. S. Dugdale, Yielding of steel sheets containing slits, *Journal of the Mechanics and Physics of Solids* 8 (1960) 100–104.
- [55] G. I. Barenblatt, The mathematical theory of equilibrium cracks in brittle fracture, *Advances in Applied Mechanics* 7 (1962) 55–129.
- [56] A. Needleman, A continuum model for void nucleation by inclusion debonding, *Journal of Applied Mechanics* 54 (1987) 525–531.
- [57] Z. Hashin, Thin interphase/imperfect interface in elasticity with application to coated fiber composites, *Journal of the Mechanics and Physics of Solids* 50 (2002) 2509–2537.
- [58] Y. Benveniste, A general interface model for a three-dimensional curved thin anisotropic interphase between two anisotropic media, *Journal of the Mechanics and Physics of Solids* 54 (2006) 708–734.
- [59] N. D. Sharma, C. M. Landis, P. Sharma, Piezoelectric thin-film superlattices without using piezoelectric materials, *Journal of Applied Physics* 108 (2010) 024304.
- [60] W. H. Qi, Size effect on melting temperature of nanosolids, *Physica B: Condensed Matter* 368 (2005) 46–50.
- [61] G. I. Barenblatt, The formation of equilibrium cracks during brittle fracture. General ideas and hypotheses. Axially-symmetric cracks, *Journal of Applied Mathematics and Mechanics* 23 (1959) 434–444.
- [62] A. K. Mal, S. K. Bose, Dynamic elastic moduli of a suspension of imperfectly bonded spheres, *Mathematical Proceedings of the Cambridge Philosophical Society* 76 (1974) 587–600.
- [63] P. S. Theocaris, S. A. Paipetis, C. A. Stassinakis, Effect of geometry and imperfect bonding in composite systems with limiting shear properties, *Fibre Science and Technology* 11 (1978) 335–352.
- [64] Y. Benveniste, T. Miloh, The effective conductivity of multiphase composites with imperfect thermal contact at constituent interfaces, *International Journal of Engineering Science* 24 (1986) 1537–1552.
- [65] J. Aboudi, Constitutive equations for elastoplastic composites with imperfect bonding, *International Journal of Plasticity* 4 (1988) 103–125.
- [66] J. Aboudi, Damage in composites-Modeling of imperfect bonding, *International Journal of Engineering Science* 28 (1987) 103–128.
- [67] Z. Hashin, Extremum principles for elastic heterogeneous media with imperfect interfaces and their application to bounding of effective moduli, *Journal of the Mechanics and Physics of Solids* 40 (1992) 767–781.
- [68] Z. Hashin, Composite materials with interphase: thermoelastic and inelastic effects, in: *Inelastic deformation of composite materials*, Springer-Verlag, 1991, pp. 3–34.
- [69] R. Lipton, B. Vernescu, Variational methods, size effects and extremal microgeometries for elastic composites with imperfect interface,

- Mathematical Models and Methods in Applied Sciences 5 (1995) 1139–1173.
- [70] Z. Gao, Circular inclusion with imperfect interface: Eshelby's tensor and related problems, *Journal of Applied Mechanics* 62 (1995) 860–866.
- [71] Y. H. Zhao, G. J. Weng, Transversely isotropic moduli of two partially debonded composites, *International Journal of Solids and Structures* 34 (1997) 493–507.
- [72] H. L. Duan, J. Wang, Z. P. Huang, Z. Y. Luo, Stress concentration tensors of inhomogeneities with interface effects, *Mechanics of Materials* 37 (2005) 723–736.
- [73] H. L. Duan, X. Yi, Z. P. Huang, J. Wang, A unified scheme for prediction of effective moduli of multiphase composites with interface effects. Part I: Theoretical framework, *Mechanics of Materials* 39 (2007) 81–93.
- [74] H. L. Duan, X. Yi, Z. P. Huang, J. Wang, A unified scheme for prediction of effective moduli of multiphase composites with interface effects: Part II-Application and scaling laws, *Mechanics of Materials* 39 (2007) 94–103.
- [75] C. Q. Ru, Interface design of neutral elastic inclusions, *International Journal of Solids and Structures* 35 (1998) 559–572.
- [76] C. Q. Ru, A circular inclusion with circumferentially inhomogeneous sliding interface in plane elastostatics, *Journal of Applied Mechanics* 65 (1998) 30–38.
- [77] T. Mura, I. Jasiuk, B. Tsuchida, The stress field of a sliding inclusion, *International Journal of Solids and Structures* 21 (1985) 1165–1179.
- [78] I. Jasiuk, E. Tsuchida, T. Mura, The sliding inclusion under shear, *International Journal of Solids and Structures* 23 (1987) 1373–1385.
- [79] Z. Zhong, S. A. Meguid, On the elastic field of a spherical inhomogeneity with an imperfectly bonded interface, *Journal of Elasticity* 46 (1997) 91–113.
- [80] J. H. Huang, R. Furuhashi, T. Mura, Frictional sliding inclusions, *Journal of the Mechanics and Physics of Solids* 41 (1993) 247–265.
- [81] M. Lee, I. Jasiuk, E. Tsuchida, The sliding circular inclusion in an elastic half-plane, *Journal of Applied Mechanics* 59 (1992) S57–S64.
- [82] Y. Benveniste, J. Aboudi, A continuum model for fiber reinforced materials with debonding, *International Journal of Solids and Structures* 20 (1984) 935–951.
- [83] I. Jasiuk, J. Chen, M. F. Thorpe, Elastic moduli of composites with rigid sliding inclusions, *Journal of the Mechanics and Physics of Solids* 40 (1992) 373–391.
- [84] S. Jun, I. Jasiuk, Elastic moduli of two-dimensional composites with sliding inclusions-A comparison of effective medium theories, *International Journal of Solids and Structures* 30 (1993) 2501–2523.
- [85] M. Königsberger, B. Pichler, C. Hellmich, Micromechanics of ITZ-aggregate interaction in concrete part I: Stress concentration, *Journal of the American Ceramic Society* 97 (2014) 535–542.
- [86] M. Königsberger, B. Pichler, C. Hellmich, Micromechanics of ITZ-Aggregate Interaction in Concrete Part II: Strength Upscaling, *Journal of the American Ceramic Society* 97 (2014) 543–551.
- [87] L. H. He, J. Jiang, Transient mechanical response of laminated elastic strips with viscous interfaces in cylindrical bending, *Composites Science and Technology* 63 (2003) 821–828.
- [88] T. Qu, D. Verma, M. Shahidi, B. Pichler, C. Hellmich, V. Tomar, Mechanics of organic-inorganic biointerfaces-Implications for strength and creep properties, *MRS Bulletin* 40 (2015) 349–358.
- [89] L. H. He, Y. L. Liu, Damping behavior of fibrous composites with viscous interface under longitudinal shear loads, *Composites Science and Technology* 65 (2005) 855–860.
- [90] X. P. Xu, A. Needleman, Numerical simulations of fast crack growth in brittle solids, *Journal of the Mechanics and Physics of Solids* 42 (1994) 1397–1434.
- [91] P. Bisegna, R. Luciano, Bounds on the overall properties of composites with debonded frictionless interfaces, *Mechanics of Materials* 28

- (1998) 23–32.
- [92] P. Wriggers, G. Zavarise, T. I. Zohdi, A computational study of interfacial debonding damage in fibrous composite materials, *Computational Materials Science* 12 (1998) 39–56.
- [93] J. D. Achenbach, H. Zhu, Effect of interfacial zone on mechanical behavior and failure of fiber-reinforced composites, *Journal of the Mechanics and Physics of Solids* 37 (1989) 381–393.
- [94] J. D. Achenbach, H. Zhu, Effect of interphase on micro and macromechanical behavior of hexagonal-array fiber composites, *Journal of Applied Mechanics* 57 (1990) 956–963.
- [95] Q. Z. Zhu, S. T. Gu, J. Yvonnet, J. F. Shao, Q. C. He, Three-dimensional numerical modelling by XFEM of spring-layer imperfect curved interfaces with applications to linearly elastic composite materials, *International Journal for Numerical Methods in Engineering* 88 (2011) 307–328.
- [96] M. Ortiz, A. Pandolfi, Finite-deformation irreversible cohesive elements for three-dimensional crack-propagation analysis, *International Journal for Numerical Methods in Engineering* 44 (1999) 1267–1282.
- [97] T. C. Gasser, G. A. Holzapfel, Geometrically non-linear and consistently linearized embedded strong discontinuity models for 3D problems with an application to the dissection analysis of soft biological tissues, *Computer Methods in Applied Mechanics and Engineering* 192 (2003) 5059–5098.
- [98] J. Mergheim, P. Steinmann, A geometrically nonlinear FE approach for the simulation of strong and weak discontinuities, *Computer Methods in Applied Mechanics and Engineering* 195 (2006) 5037–5052.
- [99] A. Hansbo, P. Hansbo, An unfitted finite element method, based on Nitsche’s method, for elliptic interface problems, *Computer Methods in Applied Mechanics and Engineering* 191 (2002) 5537–5552.
- [100] A. Hansbo, P. Hansbo, A finite element method for the simulation of strong and weak discontinuities in solid mechanics, *Computer Methods in Applied Mechanics and Engineering* 193 (2004) 3523–3540.
- [101] M. J. van den Bosch, P. J. G. Schreurs, M. G. D. Geers, On the development of a 3D cohesive zone element in the presence of large deformations, *Computational Mechanics* 42 (2008) 171–180.
- [102] M. J. van den Bosch, P. J. G. Schreurs, M. G. D. Geers, An improved description of the exponential Xu and Needleman cohesive zone law for mixed-mode decohesion, *Engineering Fracture Mechanics* 73 (2006) 1220–1234.
- [103] M. J. van den Bosch, P. J. G. Schreurs, M. G. D. Geers, A cohesive zone model with a large displacement formulation accounting for interfacial fibrillation, *European Journal of Mechanics, A/Solids* 26 (2007) 1–19.
- [104] B. G. Vossen, P. J. G. Schreurs, O. van der Sluis, M. G. D. Geers, On the lack of rotational equilibrium in cohesive zone elements, *Computer Methods in Applied Mechanics and Engineering* 254 (2013) 146–153.
- [105] N. S. Ottosen, M. Ristinmaa, J. Mosler, Fundamental physical principles and cohesive zone models at finite displacements - Limitations and possibilities, *International Journal of Solids and Structures* 53 (2015) 70–79.
- [106] N. S. Ottosen, M. Ristinmaa, J. Mosler, Framework for non-coherent interface models at finite displacement jumps and finite strains, *Journal of the Mechanics and Physics of Solids* 90 (2016) 124–141.
- [107] T. Heitbreder, N. S. Ottosen, M. Ristinmaa, J. Mosler, Consistent elastoplastic cohesive zone model at finite deformations – Variational formulation, *International Journal of Solids and Structures* 106-107 (2017) 284–293.
- [108] T. Heitbreder, N. S. Ottosen, M. Ristinmaa, J. Mosler, On damage modeling of material interfaces: Numerical implementation and computational homogenization, *Computer Methods in Applied Mechanics and Engineering* 337 (2018) 1–27.
- [109] S. Ghosh, Y. Ling, B. Majumdar, R. Kim, Interfacial debonding analysis in multiple fiber reinforced composites, *Mechanics of Materials* 32 (2000) 561–591.

- [110] G. N. Wells, L. J. Sluys, A new method for modelling cohesive cracks using finite elements, *International Journal for Numerical Methods in Engineering* 50 (2001) 2667–2682.
- [111] R. Guo, H. J. Shi, Z. H. Yao, Modeling of interfacial debonding crack in particle reinforced composites using voronoi cell finite element method, *Computational Mechanics* 32 (2003) 52–59.
- [112] M. Fagerström, R. Larsson, Theory and numerics for finite deformation fracture modelling using strong discontinuities, *International Journal for Numerical Methods in Engineering* 66 (2006) 911–948.
- [113] S. Ghosh, J. Bai, P. Raghavan, Concurrent multi-level model for damage evolution in microstructurally debonding composites, *Mechanics of Materials* 39 (2007) 241–266.
- [114] M. Paggi, P. Wriggers, A nonlocal cohesive zone model for finite thickness interfaces - Part I: Mathematical formulation and validation with molecular dynamics, *Computational Materials Science* 50 (2011) 1625–1633.
- [115] M. Paggi, P. Wriggers, A nonlocal cohesive zone model for finite thickness interfaces - Part II: FE implementation and application to polycrystalline materials, *Computational Materials Science* 50 (2011) 1634–1643.
- [116] S. Rezaei, D. Jaworek, J. R. Mianroodi, S. Wulfinghoff, S. Reese, Atomistically motivated interface model to account for coupled plasticity and damage at grain boundaries, *Journal of the Mechanics and Physics of Solids* 124 (2019) 325–349.
- [117] S. Rezaei, J. R. Mianroodi, K. Khaledi, S. Reese, A nonlocal method for modeling interfaces: Numerical simulation of decohesion and sliding at grain boundaries, *Computer Methods in Applied Mechanics and Engineering* 362 (2020) 112836.
- [118] H. R. Bayat, S. Rezaei, T. Brepols, S. Reese, Locking-free interface failure modeling by a cohesive discontinuous Galerkin method for matching and nonmatching meshes, *International Journal for Numerical Methods in Engineering* 121 (2020) 1762–1790.
- [119] A. I. Murdoch, A thermodynamical theory of elastic material interfaces, *Quarterly Journal of Mechanics and Applied Mathematics* 29 (1976) 245–275.
- [120] X. Gao, Z. Huang, J. Qu, D. Fang, A curvature-dependent interfacial energy-based interface stress theory and its applications to nanostructured materials: (I) General theory, *Journal of the Mechanics and Physics of Solids* 66 (2014) 59–77.
- [121] X. Gao, Z. Huang, D. Fang, Curvature-dependent interfacial energy and its effects on the elastic properties of nanomaterials, *International Journal of Solids and Structures* 113–114 (2017) 100–107.
- [122] D. Caillerie, Sur le comportement limite d'une inclusion mince de grande rigidite, *Comptes rendus de l'Académie des sciences Série 1* 287 (1978) 675–678.
- [123] M. B. Rubin, Y. Benveniste, A Cosserat shell model for interphases in elastic media, *Journal of the Mechanics and Physics of Solids* 52 (2004) 1023–1052.
- [124] E. Fried, M. E. Gurtin, Thermomechanics of the interface between a body and its environment, *Continuum Mechanics and Thermodynamics* 19 (2007) 253–271.
- [125] R. Dingreville, J. Qu, Interfacial excess energy, excess stress and excess strain in elastic solids: Planar interfaces, *Journal of the Mechanics and Physics of Solids* 56 (2008) 1944–1954.
- [126] R. Dingreville, J. Qu, A semi-analytical method to compute surface elastic properties, *Acta Materialia* 55 (2007) 141–147.
- [127] P. Sharma, S. Ganti, N. Bhat, Effect of surfaces on the size-dependent elastic state of nano-inhomogeneities, *Applied Physics Letters* 82 (2003) 535–537.
- [128] P. Sharma, Size-dependent elastic fields of embedded inclusions in isotropic chiral solids, *International Journal of Solids and Structures* 41 (2004) 6317–6333.
- [129] F. Yang, Size-dependent effective modulus of elastic composite materials: Spherical nanocavities at dilute concentrations, *Journal of Applied Physics* 95 (2004) 3516–3520.

- [130] L. Sun, Y. Wu, Z. Huang, J. Wang, Interface effect on the effective bulk modulus of a particle-reinforced composite, *Acta Mechanica Sinica* 20 (2004) 676–679.
- [131] H. L. Duan, J. Wang, Z. P. Huang, B. L. Karihaloo, Eshelby formalism for nano-inhomogeneities, *Proceedings of the Royal Society A* 461 (2005) 3335–3353.
- [132] H. L. Duan, J. Wang, Z. P. Huang, B. L. Karihaloo, Size-dependent effective elastic constants of solids containing nano-inhomogeneities with interface stress, *Journal of the Mechanics and Physics of Solids* 53 (2005) 1574–1596.
- [133] H. L. Duan, J. Wang, B. L. Karihaloo, *Theory of elasticity at the nanoscale*, Vol. 42, Elsevier, 2009.
- [134] Z. P. Huang, J. Wang, A theory of hyperelasticity of multi-phase media with surface/interface energy effect, *Acta Mechanica* 182 (2006) 195–210.
- [135] E. Monteiro, Q. C. He, J. Yvonnet, Hyperelastic large deformations of two-phase composites with membrane-type interface, *International Journal of Engineering Science* 49 (2011) 985–1000.
- [136] Z. P. Huang, L. Sun, Size-dependent effective properties of a heterogeneous material with interface energy effect: From finite deformation theory to infinitesimal strain analysis, *Acta Mechanica* 190 (2007) 151–163.
- [137] L. H. He, Self-strain of solids with spherical nanovoids, *Applied Physics Letters* 88 (2006) 151909.
- [138] H. Le Quang, Q. C. He, Size-dependent effective thermoelastic properties of nanocomposites with spherically anisotropic phases, *Journal of the Mechanics and Physics of Solids* 55 (2007) 1899–1931.
- [139] H. Le Quang, Q. C. He, Variational principles and bounds for elastic inhomogeneous materials with coherent imperfect interfaces, *Mechanics of Materials* 40 (2008) 865–884.
- [140] H. Le Quang, Q. C. He, Estimation of the effective thermoelastic moduli of fibrous nanocomposites with cylindrically anisotropic phases, *Archive of Applied Mechanics* 79 (2009) 225–248.
- [141] S. G. Mogilevskaya, S. L. Crouch, H. K. Stolarski, Multiple interacting circular nano-inhomogeneities with surface/interface effects, *Journal of the Mechanics and Physics of Solids* 56 (2008) 2298–2327.
- [142] S. G. Mogilevskaya, S. L. Crouch, H. K. Stolarski, A. Benusiglio, Equivalent inhomogeneity method for evaluating the effective elastic properties of unidirectional multi-phase composites with surface/interface effects, *International Journal of Solids and Structures* 47 (2010) 407–418.
- [143] S. G. Mogilevskaya, S. L. Crouch, A. La Grotta, H. K. Stolarski, The effects of surface elasticity and surface tension on the transverse overall elastic behavior of unidirectional nano-composites, *Composites Science and Technology* 70 (2010) 427–434.
- [144] S. G. Mogilevskaya, H. K. Stolarski, S. L. Crouch, On Maxwells concept of equivalent inhomogeneity: When do the interactions matter?, *Journal of the Mechanics and Physics of Solids* 60 (2012) 391–417.
- [145] V. I. Kushch, S. G. Mogilevskaya, H. K. Stolarski, S. L. Crouch, Elastic interaction of spherical nanoinhomogeneities with Gurtin-Murdoch type interfaces, *Journal of the Mechanics and Physics of Solids* 59 (2011) 1702–1716.
- [146] V. I. Kushch, S. G. Mogilevskaya, H. K. Stolarski, S. L. Crouch, Elastic fields and effective moduli of particulate nanocomposites with the Gurtin-Murdoch model of interfaces, *International Journal of Solids and Structures* 50 (2013) 1141–1153.
- [147] V. I. Kushch, I. Sevostianov, V. S. Chernobai, Effective conductivity of composite with imperfect contact between elliptic fibers and matrix: Maxwell’s homogenization scheme, *International Journal of Engineering Science* 83 (2014) 146–161.
- [148] N. I. Muskhelishvili, *Some basic problems of the mathematical theory of elasticity*, Springer Science & Business Media, 2013.
- [149] V. I. Kushch, I. Sevostianov, The “rigorous” Maxwell homogenization scheme in 2D elasticity: Effective stiffness tensor of composite with elliptic inhomogeneities, *Mechanics of Materials* 103 (2016) 44–54.
- [150] Y. Benveniste, T. Miloh, Soft neutral elastic inhomogeneities with membrane-type interface conditions, *Journal of Elasticity* 88 (2007)

87–111.

- [151] V. Monchiet, D. Kondo, Semi-analytical investigation of stress interfacial effects in ductile media with nanosized spheroidal cavities, *Procedia IUTAM* 3 (2012) 228–238.
- [152] V. I. Kushch, Stress field and effective elastic moduli of periodic spheroidal particle composite with Gurtin-Murdoch interface, *International Journal of Engineering Science* 132 (2018) 79–96.
- [153] P. Sharma, L. T. Wheeler, Size-dependent elastic state of ellipsoidal nano-inclusions incorporating surface/interface tension, *Journal of Applied Mechanics* 74 (2007) 447–454.
- [154] T. Chen, G. J. Dvorak, Fibrous nanocomposites with interface stress: Hill's and Levin's connections for effective moduli, *Applied Physics Letters* 88 (2006) 211912.
- [155] H. Chen, X. Liu, G. Hu, Overall plasticity of micropolar composites with interface effect, *Mechanics of Materials* 40 (2008) 721–728.
- [156] F. D. Fischer, J. Svoboda, Stresses in hollow nanoparticles, *International Journal of Solids and Structures* 47 (2010) 2799–2805.
- [157] A. Javili, N. S. Ottosen, M. Ristinmaa, J. Mosler, Aspects of interface elasticity theory, *Mathematics and Mechanics of Solids* 23 (2018) 1004–1024.
- [158] A. Javili, *Thermomechanics of Solids Accounting for Surfaces and Interfaces*, Ph.D. thesis (2012).
- [159] L. Nazarenko, S. Bargmann, H. Stolarski, Influence of interfaces on effective properties of nanomaterials with stochastically distributed spherical inclusions, *International Journal of Solids and Structures* 51 (2014) 954–966.
- [160] G. Chatzigeorgiou, Y. Chemisky, F. Meraghni, Computational micro to macro transitions for shape memory alloy composites using periodic homogenization, *Smart Materials and Structures* 24 (2015) 035009.
- [161] L. Nazarenko, H. Stolarski, H. Altenbach, Effective properties of short-fiber composites with Gurtin-Murdoch model of interphase, *International Journal of Solids and Structures* 97_98 (2016) 75–88.
- [162] L. Nazarenko, S. Bargmann, H. Stolarski, Closed-form formulas for the effective properties of random particulate nanocomposites with complete Gurtin-Murdoch model of material surfaces, *Continuum Mechanics and Thermodynamics* 29 (2017) 77–96.
- [163] D. J. Steigmann, R. W. Ogden, Plane deformations of elastic solids with intrinsic boundary elasticity, *Proceedings of the Royal Society A* 453 (1997) 853–877.
- [164] A. Y. Zemlyanova, S. G. Mogilevskaya, On spherical inhomogeneity with Steigmann–Ogden interface, *Journal of Applied Mechanics* 85 (2018) 121009.
- [165] A. Y. Zemlyanova, S. G. Mogilevskaya, Circular inhomogeneity with Steigmann–Ogden interface: Local fields, neutrality, and Maxwell's type approximation formula, *International Journal of Solids and Structures* 135 (2018) 85–98.
- [166] Z. Han, S. G. Mogilevskaya, D. Schillinger, Local fields and overall transverse properties of unidirectional composite materials with multiple nanofibers and Steigmann–Ogden interfaces, *International Journal of Solids and Structures* 147 (2018) 166–182.
- [167] J. Yvonnet, Q. C. He, C. Toulemonde, Numerical modelling of the effective conductivities of composites with arbitrarily shaped inclusions and highly conducting interface, *Composites Science and Technology* 68 (2008) 2818–2825.
- [168] A. Javili, A. McBride, P. Steinmann, Thermomechanics of solids with lower-dimensional energetics: On the importance of surface, interface, and curve structures at the nanoscale. A unifying review, *Applied Mechanics Reviews* 65 (2013) 010802.
- [169] A. Javili, G. Chatzigeorgiou, A. T. McBride, P. Steinmann, C. Linder, Computational homogenization of nano-materials accounting for size effects via surface elasticity, *GAMM Mitteilungen* 38 (2015) 285–312.
- [170] A. Javili, A. McBride, P. Steinmann, B. D. Reddy, A unified computational framework for bulk and surface elasticity theory: A curvilinear-coordinate-based finite element methodology, *Computational Mechanics* 54 (2014) 745–762.
- [171] Y. Koutsawa, S. Tiem, W. Yu, F. Addiego, G. Giunta, A micromechanics approach for effective elastic properties of nano-composites with

- energetic surfaces/interfaces, *Composite Structures* 159 (2017) 278–287.
- [172] Y. Benveniste, Models of thin interphases with variable moduli in plane-strain elasticity, *Mathematics and Mechanics of Solids* 18 (2013) 119–134.
- [173] Y. Benveniste, Models of thin interphases and the effective medium approximation in composite media with curvilinearly anisotropic coated inclusions, *International Journal of Engineering Science* 72 (2013) 140–154.
- [174] V. Monchiet, G. Bonnet, Interfacial models in viscoplastic composites materials, *International Journal of Engineering Science* 48 (2010) 1762–1768.
- [175] S. T. Gu, Q. C. He, Interfacial discontinuity relations for coupled multifield phenomena and their application to the modeling of thin interphases as imperfect interfaces, *Journal of the Mechanics and Physics of Solids* 59 (2011) 1413–1426.
- [176] S. T. Gu, E. Monteiro, Q. C. He, Coordinate-free derivation and weak formulation of a general imperfect interface model for thermal conduction in composites, *Composites Science and Technology* 71 (2011) 1209–1216.
- [177] S. T. Gu, J. T. Liu, Q. C. He, Size-dependent effective elastic moduli of particulate composites with interfacial displacement and traction discontinuities, *International Journal of Solids and Structures* 51 (2014) 2283–2296.
- [178] M. Wang, W. Ye, Size-dependent elastic field of nano-inhomogeneity: from interface effect to interphase effect, *Archive of Applied Mechanics* 90 (2020) 2319–2333.
- [179] Y. Xu, Q. C. He, S. T. Gu, Effective elastic moduli of fiber-reinforced composites with interfacial displacement and stress jumps, *International Journal of Solids and Structures* 80 (2016) 146–157.
- [180] S. Firooz, G. Chatzigeorgiou, F. Meraghni, A. Javili, Homogenization accounting for size effects in particulate composites due to general interfaces, *Mechanics of Materials* 139 (2019) 103204.
- [181] S. Firooz, G. Chatzigeorgiou, F. Meraghni, A. Javili, Bounds on size effects in composites via homogenization accounting for general interfaces, *Continuum Mechanics and Thermodynamics* 32 (2020) 173–206.
- [182] G. Chatzigeorgiou, F. Meraghni, A. Javili, Generalized interfacial energy and size effects in composites, *Journal of the Mechanics and Physics of Solids* 106 (2017) 257–282.
- [183] S. T. Gu, J. T. Liu, Q. C. He, The strong and weak forms of a general imperfect interface model for linear coupled multifield phenomena, *International Journal of Engineering Science* 85 (2014) 31–46.
- [184] A. Javili, P. Steinmann, J. Mosler, Micro-to-macro transition accounting for general imperfect interfaces, *Computer Methods in Applied Mechanics and Engineering* 317 (2017) 274–317.
- [185] A. Javili, S. Kaessmair, P. Steinmann, General imperfect interfaces, *Computer Methods in Applied Mechanics and Engineering* 275 (2014) 76–97.
- [186] S. Kaessmair, A. Javili, P. Steinmann, Thermomechanics of solids with general imperfect coherent interfaces, *Archive of Applied Mechanics* 84 (2014) 1409–1426.
- [187] A. Javili, Variational formulation of generalized interfaces for finite deformation elasticity, *Mathematics and Mechanics of Solids* 23 (2018) 1303–1322.
- [188] S. Saeb, P. Steinmann, A. Javili, Designing tunable composites with general interfaces, *International Journal of Solids and Structures* 171 (2019) 181–188.
- [189] S. Saeb, P. Steinmann, A. Javili, Bounds on size-dependent behaviour of composites, *Philosophical Magazine* 98 (2018) 437–463.
- [190] S. Saeb, P. Steinmann, A. Javili, On effective behavior of microstructures embedding general interfaces with damage, *Computational Mechanics* 64 (2019) 1473–1494.
- [191] K. Pham, A. Maurel, J.-J. Marigo, Revisiting imperfect interface laws for two-dimensional elastodynamics, *Proceedings of the Royal Society*

- A 477 (2245) (2021) 20200519.
- [192] S. Firooz, A. Javili, Understanding the role of general interfaces in the overall behavior of composites and size effects, *Computational Materials Science* 162 (2019) 245–254.
- [193] S. Firooz, Homogenization of composites embedding general imperfect interfaces, Master's thesis, Bilkent University (2019).
- [194] W. Xu, H. Ma, S. Ji, H. Chen, Analytical effective elastic properties of particulate composites with soft interfaces around anisotropic particles, *Composites Science and Technology* 129 (2016) 10–18.
- [195] S. Firooz, S. Saeb, G. Chatzigeorgiou, F. Meraghni, P. Steinmann, A. Javili, Systematic study of homogenization and the utility of circular simplified representative volume element, *Mathematics and Mechanics of Solids* 24 (2019) 2961–2985.
- [196] S. Saeb, S. Firooz, P. Steinmann, A. Javili, Generalized interfaces via weighted averages for application to graded interphases at large deformations, *Journal of the Mechanics and Physics of Solids* 149 (2021) 104234.
- [197] S. Firooz, P. Steinmann, A. Javili, Homogenization of composites with extended general interfaces: Comprehensive review and unified modeling, *Applied Mechanics Reviews* (2021).
- [198] Z. F. Khisaeva, M. Ostoj-Starzewski, On the size of RVE in finite elasticity of random composites, *Journal of Elasticity* 85 (2006) 153–173.
- [199] I. Temizer, T. I. Zohdi, A numerical method for homogenization in non-linear elasticity, *Computational Mechanics* 40 (2007) 281–298.
- [200] I. M. Gitman, H. Askes, E. C. Aifantis, The representative volume size in static and dynamic micro-macro transitions, *International Journal of Fracture* 135 (2005) 3–9.
- [201] S. Saeb, P. Steinmann, A. Javili, Aspects of computational homogenization at finite deformations: A unifying review from Reuss' to Voigt's Bound, *Applied Mechanics Reviews* 68 (2016) 050801.
- [202] N. Charalambakis, G. Chatzigeorgiou, Y. Chemisky, F. Meraghni, Mathematical homogenization of inelastic dissipative materials: a survey and recent progress, *Continuum Mechanics and Thermodynamics* 30 (2018) 1–51.
- [203] K. Matous, M. G. D. Geers, V. G. Kouznetsova, A. Gillman, A review of predictive nonlinear theories for multiscale modeling of heterogeneous materials, *Journal of Computational Physics* 330 (2017) 192–220.
- [204] M. J. Pindera, H. Khatam, A. S. Drago, Y. Bansal, Micromechanics of spatially uniform heterogeneous media : A critical review and emerging approaches, *Composites Part B* 40 (2009) 349–378.
- [205] G. Chatzigeorgiou, A. Javili, P. Steinmann, Multiscale modelling for composites with energetic interfaces at the micro- or nanoscale, *Mathematics and Mechanics of Solids* 20 (2015) 1130–1145.
- [206] H. L. Duan, B. L. Karihaloo, Effective thermal conductivities of heterogeneous media containing multiple imperfectly bonded inclusions, *Physical Review B* 75 (2007) 064206.
- [207] Z. Wang, R. J. Oelkers, K. C. Lee, F. T. Fisher, Annular Coated Inclusion model and applications for polymer nanocomposites – Part II: Cylindrical inclusions, *Mechanics of Materials* 101 (2016) 50–60.
- [208] Z. Wang, R. J. Oelkers, K. C. Lee, F. T. Fisher, Annular Coated Inclusion model and applications for polymer nanocomposites – Part I: Spherical inclusions, *Mechanics of Materials* 101 (2016) 170–184.
- [209] G. Wang, M. J. Pindera, Locally-exact homogenization theory for transversely isotropic unidirectional composites, *Mechanics Research Communications* 78 (2016) 2–14.
- [210] G. Wang, Q. Chen, Z. He, M. J. Pindera, Homogenized moduli and local stress fields of unidirectional nano-composites, *Composites Part B* 138 (2018) 265–277.
- [211] J. D. Eshelby, The determination of the elastic field of an ellipsoidal inclusion, and related problems, *Proceedings of the Royal Society of London. Series A* 241 (1957) 376–396.
- [212] P. B. Entchev, D. C. Lagoudas, Modeling porous shape memory alloys using micromechanical averaging techniques, *Mechanics of Materials*

34 (2002) 1–24.

[213] Z. Hashin, B. W. Rosen, The elastic moduli of fiber-reinforced materials, *Journal of Applied Mechanics* 31 (1964) 223–232.

[214] Z. Hashin, S. Shtrikman, A variational approach to the theory of the elastic behaviour of polycrystals, *Journal of the Mechanics and Physics of Solids* 10 (1962) 343–352.

[215] P. Wriggers, *Nonlinear finite element methods*, Springer Science & Business Media, 2008.

[216] T. J. R. Hughes, *The finite element method: linear static and dynamic finite element analysis*, Courier Corporation, 2012.

Journal Pre-proof

Declaration of interests

The authors declare that they have no known competing financial interests or personal relationships that could have appeared to influence the work reported in this paper.

The authors declare the following financial interests/personal relationships which may be considered as potential competing interests:

Journal Pre-proof